Title
Diverse Reactivity of Rhenium β-Diketiminates

Author
Lohrey, Trevor D.

Publication Date
2019

Peer reviewed|Thesis/dissertation

Diverse Reactivity of Rhenium β-Diketiminates

By

Trevor D. Lohrey

A dissertation submitted in partial satisfaction of the

requirements for the degree of

Doctor of Philosophy

in

Chemistry

in the

Graduate Division

of the

University of California, Berkeley

Committee in charge:

Professor John Arnold, Chair

Professor Robert G. Bergman

Professor T. Don Tilley

Professor Alexander Katz

Summer 2019

Abstract

Diverse Reactivity of Rhenium β-Diketiminates

By

Trevor D. Lohrey

Doctor of Philosophy in Chemistry

University of California, Berkeley

Professor John Arnold, Chair

Chapter 1. Previous work with group 5 imido β-diketiminates and rhenium terminal oxo complexes is summarized, which in combination provide the theoretical basis for the subsequent chapters. The overarching hypothesis and goals of this work are stated.

Chapter 2. Synthetic access to the first rhenium oxo β-diketiminate is achieved. Subsequently, the oxygen atom transfer (OAT) reactivity of this complex is gauged. It is determined that OAT from this complex is limited to trialkylphosphines of a moderate steric profile (e.g. PEt_3), as small trialkylphosphines (e.g. PMe_3) bind strongly to the metal center, and larger phosphines (e.g. PPh_3) are kinetically limited due to the encumbering β-diketiminate ligand. Nitrene transfer from the β-diketiminate ligand to the metal is also observed, implying an ancillary limitation of this ligand in low valent rhenium complexes at high temperatures.

Chapter 3. Attempts to incorporate a cyclopentadienyl ligand into the rhenium oxo β-diketiminate system using NaCp led to the isolation of an olefin-supported rhenium(III) terminal oxo complex. It was found that using $SnCp_2$ rather than NaCp leads to the intended rhenium(V) oxo Cp complex. The reactivity of this rhenium(V) complex suggested that both the Cp ligand and oxo ligand are susceptible to nucleophilic attack, yielding a variety of rhenium(III) complexes. Computational studies suggest some degree of metal-ligand conjugation ("π-loading") exists between the Cp and oxo ligands in the starting rhenium(V) complex, which supports the observations made during reactivity studies.

Chapter 4. The oxygen atom transfer reactivity of a rhenium(III) terminal oxo β-diketiminate complex is evaluated. It is shown that this compound will only transfer its oxo ligand to electrophilic reagents (e.g. isocyanides and CO) rather than nucleophilic ones (e.g. PMe_3). A number of rhenium(I) isocyanide and carbonyl complexes are isolated as products of the oxygen atom transfer process. In all, the results suggest that the oxo moiety of the starting rhenium(III) complex behaves as a nucleophile, and has no demonstrable electrophilic character.

Chapter 5. Reduction of a cationic rhenium(V) oxo Cp β-diketiminate with metallic sodium yields an anionic rhenium(I) complex that is both strongly reducing and basic. Accordingly, the corresponding neutral rhenium(II) and rhenium(III) hydride complexes are isolated following oxidation and protonation, respectively, of the anionic compound. Combination of the anionic rhenium(I) compound with $ZnCl_2$ formed a tetrametallic Re(I)-Zn(I)-Zn(I)-Re(I) complex where the four metal centers are arranged in a nearly linear fashion. This compound is the first example of a Zn(I) compound to be supported exclusively by bonding to other metal centers. Computational and reactivity studies of this tetrametallic compound are also presented.

Diverse Reactivity of Rhenium β-Diketiminates

Table of Contents

Acknowledgements

At this juncture I feel as though there are too many people deserving of more kind words than I can reasonably fit into this section. That said, I am grateful to a great number of people that have helped me along the path to satisfying my childhood dream of becoming a Ph.D., and I will take the opportunity presented here to do my best to thank them.

I will start by thanking my parents. If I were not raised with the level of education they were insistent upon, or the freedom to follow the goals I set for myself so long as I worked hard, there are many junctures that could have prevented me from attending both Reed and subsequently UC Berkeley. Despite knowing little about science, my parents have never faltered in their support, and I am could not have asked for better guidance as I found and walked down my own path.

Next I would like to thank my Ph.D. advisor, Prof. John Arnold. John welcomed me into his group rather informally in summer 2013, before my senior year at Reed, when I was a novice laboratory chemist who sorely needed an opportunity to develop their hands while thinking on their feet. I was happy to be able to return to his group for the long haul the following year, and I the experience has been nothing short of formative. I am grateful for the environment John cultivates in his group, and the freedom I was allowed to make graduate school everything I wanted it to be. I thank John for his pragmatism, coupled with his frequent encouragement to shoot for the moon.

Prof. Robert G. Bergman, while not a formal advisor of mine, has also had a significant influence on my development as a chemist and researcher. Bob has always been a great resource to discuss complex kinetic and labeling experiments, and has helped me learn that research is not only about satisfying one's own curiosities but is a matter that requires the constant practice of due diligence. I have now seen firsthand that the most interesting results tend to stem from what may at first seem like dismissible anomalies.

Beyond familial and professorial support, graduate school would hardly be possible without the friends you make along the way. While the ordering of the subsequent acknowledgements is sure to be put under a microscope, I will proceed to thank some of the wonderful people I have met in my time here.

For the past 5 years, Ash Ward has been a perpetual source of sage advice and true friendship. Beyond my time in lab, I have changed in many ways for the better as a person, owing in a major part to her guidance and at times baffling tolerance of my quirks. Thanks to our experiences together I know more about myself than I thought there was to know, and have never felt better about how I experience the world around me. I am happy to have her in my corner.

Michael Boreen has also been one of my best comrades throughout the graduate school experience. I thank him for his constant willingness to hear out my wildest ideas and unhindered instinct to bring me back down to Earth. I like to think we have made each other better chemists throughout the years in lab together, though he might not ever admit it has gone both ways. It is a rarity to find someone you can collaborate with on both esoteric multimetallic molecules, as well as a 12-pack of Coors Light.

I would also like to thank Jessica Ziegler for her role in helping me through graduate school in its most unsure of stages. Our shared instinct to immediately think the worst has come to pass was fortunately complemented by our mutual ability to talk the other off the ledge. In our microcosm of transition metal chemistry in the Arnold Group, we talked through many of the most difficult and pressing problems that each of us had to face on the path to a Ph.D. An ardent planner, Jessica is also someone I knew I could rely on day-to-day to keep me on track (as annoying as I am sure that was).

A final specific shout out goes to Benjamin Kriegel, my Benpai. While several years my senior, I am glad that he noticed me, and was here to pass along knowledge that only comes from several years of grinding away at the same project. I appreciate Ben's guidance in my early days as a Ph.D. student, and I credit him for helping me figure out the most efficient ways to get reactions done and compounds isolated.

I would like to thank all of the other members of the Arnold Group throughout my time here, old and new. This includes (in a vague, illogical order): Bernard Parker, Jade Fostvedt, Mary Garner, Alison Altman, Nick Settineri, Mark Straub, Clément Camp, Stephan Hohloch, Alex Oanta, Brighton Skeel, Alex Brown, Angela Shiau, Max Bernbeck, Dan Kellenberger, Leah Rubin, Heather Buckley, Erik Ouellette, Joe Brackbill, Thomas Gianetti, Michael Nechayev, Brendon McNicholas, Lauren Grant, Anne-Christine Kick, Lara Naested, and Martin Lichtenthaler, among others. Thank you all for making this group a lively, engaging, wonderful place to learn and collaborate. While many of you have already gone on to great places, many more are still on the way upwards, and I wish you all the best. To Jade and Erik specifically, it has been a joy to watch you both begin graduate school. I am leaving confident you both will do great chemistry and keep the rhenium boat afloat.

To conclude I would like to look backwards, and thank a few people who made my time at Berkeley possible. The most important of these people is one of my professors from Reed, my thesis advisor Prof. Margret Geselbracht. Maggie, who passed in 2014 shortly after I started graduate school, was an avid educator who, in my experience, remains unparalleled as a champion for her students and their potential. It was Maggie who first suggested I pursue a summer research position with John, and if it were not for her encouragement, it is very doubtful I would have had that crucial opportunity to get outside the Reed bubble and end up here.

I also would like to thank all of my professors at Reed, and for the rigors and enthusiasm they all brought to my time there, which provided me with a strong basis for thinking critically about everything I do. Prof. Alan Shusterman and Prof. Arthur Glasfeld in particular are thanked for passing on many key ideas I find myself referring to often. Dr. Aaron Nilsen, while only at Reed for one year, is also thanked for his willingness to bring me into his lab despite his already hectic schedule, allowing me to have a crucial first research experience before I came to Berkeley in the summer of 2013.

I have surely excluded many others by name, and for that I apologize for the brevity of this section. However, if you are reading this and have any doubts about any role you might have played, feel free to request a blurb of your own from me. I would be happy to pass it along.

Chapter 1

Motivations for the Study of Rhenium β-Diketiminates

Related Previous Work with Niobium and Tantalum Imido β-Diketiminates

Metal complexes of the β-diketiminate (BDI, or "NacNac") ligand have been frequent targets and subjects of study in synthetic inorganic chemistry for over two decades (Scheme 1.1).[1-3] The ease of synthesis and facile steric and electronic tunability of the BDI framework make it a pragmatic choice of ancillary ligand.[1] Additionally, the BDI ligand, in its most basic and commonly-used forms (such as that with 2,6-diisopropylphenyl groups on the chelating N atoms), only occupies two metal coordination sites while providing ample kinetic stability to the bound metal center. For example, while many transition metals can bind three equivalents of the similarly bidentate acetylacetonate ("acac") ligand, it is uncommon to observe a transition metal bind more than one equivalent of a BDI ligand unless the N-substituent is very small (i.e. methyl, ethyl, H). While non-innocent behavior of BDI ligands has been widely observed with elements across the periodic table, a number of significant and otherwise unknown moieties and compounds have been accessed thanks to this versatile framework.[1,2]

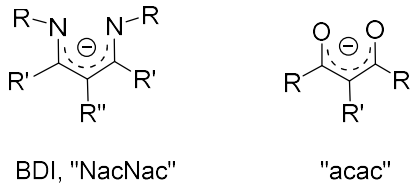

Scheme 1.1 Generalized depictions of the BDI and "acac" ligands, which share a similar conjugated, monoanionic electronic structure, in conjuction with N or O groups that most often lead to bidentate binding to metal centers. R denotes the potential sites of various substituents.

For approximately the past decade, the Arnold and Bergman groups have undertaken the study of group 5 BDI complexes featuring terminal imido ligands.[3] These studies were initiated with the hope of accessing new modes of early transition metal-ligand multiple bond reactivity: a subject first broached in seminal work in Bergman's group (concurrently with similar work in the lab of Prof. Peter Wolczanski) on the behavior of the first known zirconium terminal imido species.[4,5] These studies in the labs of Arnold and Bergman, summarized below, demonstrate both the general utility of BDI as an ancillary ligand as well as the intriguing chemistry that can be accessed by the underlying metal fragments of its complexes.

One major group of studies from Arnold and Bergman involves the reactivity of niobium(III) and tantalum(III) imido BDI complexes. It was found that depending on the synthetic pathway, the niobium(III) dicarbonyl complex **1.1** and the niobium(III) arene complex **1.2** could be readily obtained (Scheme 1.2).[6,7] Low valent complexes of niobium are typically reducing and difficult to stabilize, which is why beyond the kinetic stabilization provided by the BDI ligand, the electron-accepting CO and arene ligands in **1.1** and **1.2** are also necessary to stabilize these isolable compounds. By a similar route, the tantalum analog of **1.1**, namely **1.3**, could also be accessed.[8] It was found that the dicarbonyl **1.1** is a competent catalyst for the *Z*-selective semi-hydrogenation of methylphenylacetylene, with the reaction requiring a CO/H_2 mixture, as opposed to a pure H_2 atmosphere, to proceed cleanly.[9] Complexes **1.1** and **1.3** were also found to be suitable reagents for the activation of P_4 to yield the dinuclear *cyclo*-P_4 complexes **1.4** and **1.5**, respectively.[10]

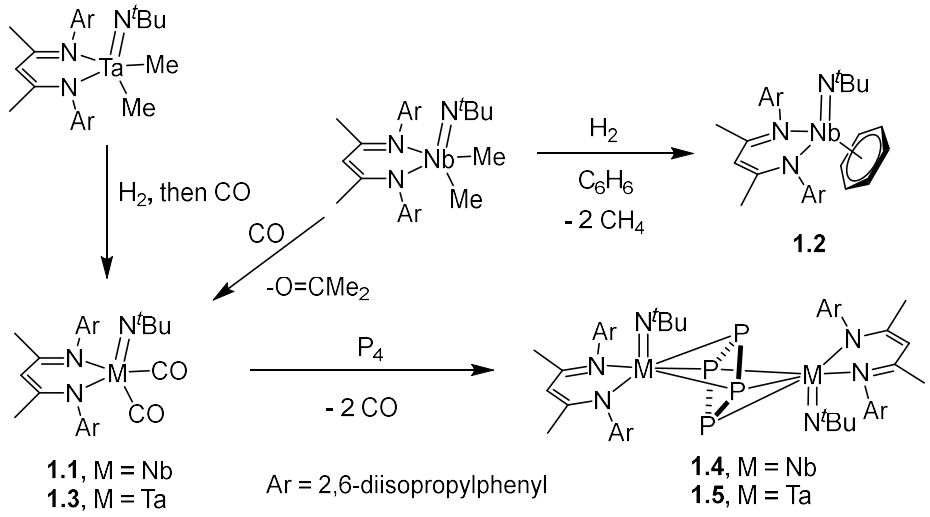

Scheme 1.2 Routes to low valent Nb and Ta imido BDI complexes and the formation of *cyclo*-P_4 compounds.

The niobium(III) arene complex **1.2** proved to be a competent catalyst for the hydrodefluorination of aryl fluorides (Scheme 1.3).[11] These reactions involve the direct oxidative addition of a C-F bond to a Nb(III) center as a key step. The aryl C-F bond is among the strongest single bonds in organic chemistry; however, the combination of oxophilicity and reducing power found in the Nb center of **1.2** proved to be sufficient to directly activate C-F bonds to form niobium(V) aryl fluoride complexes (**1.6**). Addition of silanes to these reactions led to fluoride-hydride exchange to yield silyl fluorides and transient niobium(V) aryl hydride species (**1.7**) that undergo C-H reductive elimination to form arene complexes akin to **1.2**, which can then go on to restart the catalytic cycle. Benzylic CF_3 groups are also subject to C-F activation by **1.2**; however the reaction of **1.2** with α,α,α-trifluorotoluene proceeds to completely disassemble this moiety and insert a benzyl fragment into the metal-imido bond, forming the complex **1.8**.[12]

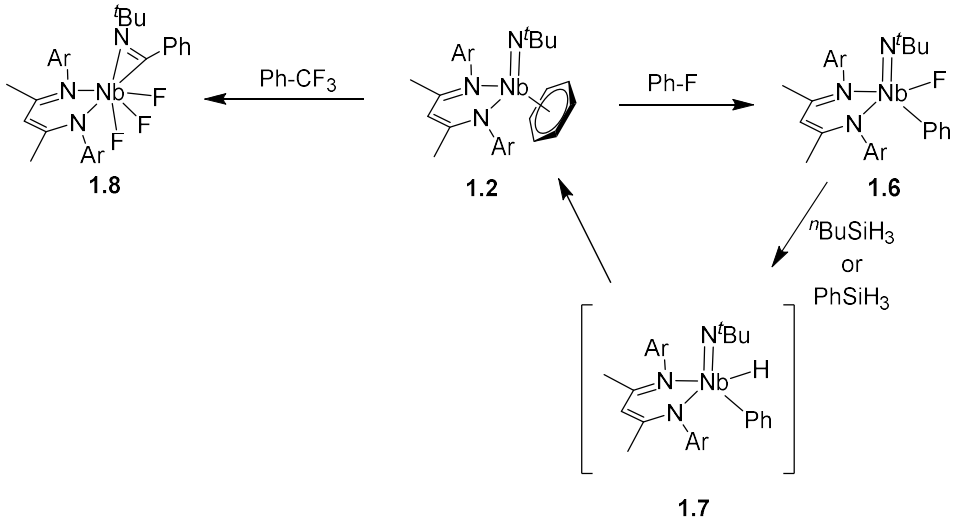

Scheme 1.3 Overview of C-F bond activation processes.

Complex **1.2** was also found to display intriguing solution behavior, forming the dinuclear inverse sandwich complex **1.9** irreversibly at room temperature. Kinetic investigations showed that **1.9** forms by a dissociative mechanism, forming the intermediate **1.10** in solution (Scheme 1.4).[7] While **1.9** is largely inert, one-electron oxidation to form the cationic, mixed valent, Nb(III)/Nb(IV) complex **1.11** leads to lower hapticity binding of the arene ligand to each metal center.[13] As a result, **1.11** was found to display a variety of reactivity modes that led to displacement of the arene ligand.

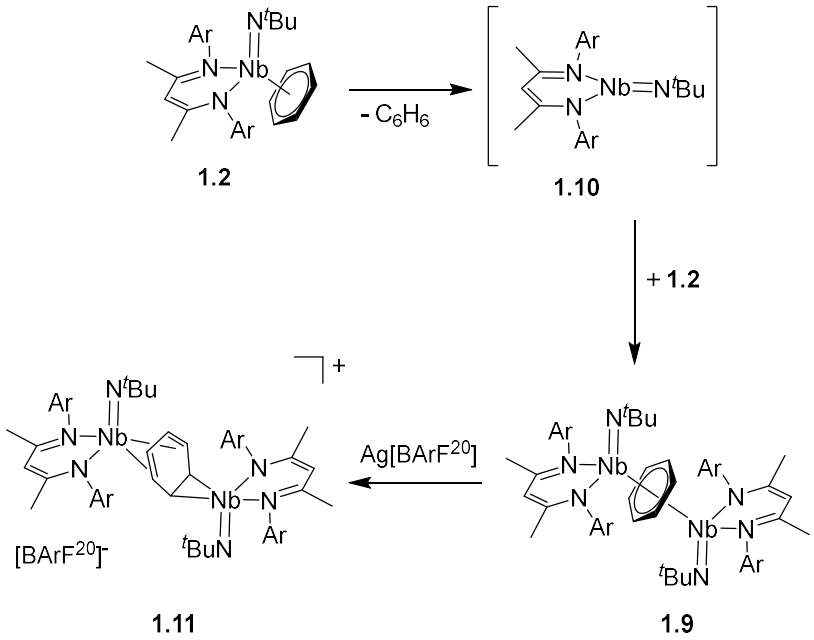

Scheme 1.4 Formation and oxidation of an inverse sandwich complex.

The niobium BDI system has also proved capable of supporting high valent Nb bis(imido) complexes that display high reactivity at the metal-ligand multiple bonds. For example, it was found that the bis(imido) complex **1.12**, which is readily formed from **1.2** by its oxidative reaction with ^{t}BuN$_3$, catalyzes nitrene transfer to alkyl isocyanides to form asymmetric carbodiimides (Scheme 1.5).[14] These catalytic reactions work best with electron-rich alkyl isocyanides in the presence of a vast excess of ^{t}BuN$_3$, as otherwise undesired side products readily form. Aryl isocyanides in combination with **1.12** do not form carbodiimides, but rather lead to nitrene exchange between the Nb and isocyanide carbon, forming complexes of the formulation **1.13**.

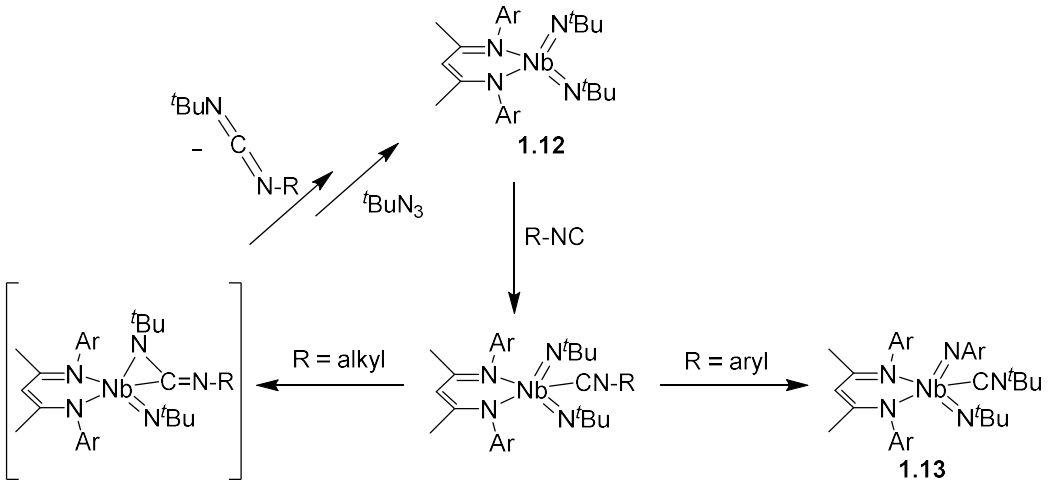

Scheme 1.5 Catalytic nitrene transfer to alkyl isocyanides forms asymmetric carbodiimides, while aryl isocyanides lead to stoichiometric nitrene exchange.

Considering the range of chemistry observed with group 5 imido BDI complexes, this body of work provides a good rationale for incorporating a new, multiply-bonded metal-ligand fragment into the BDI framework. Along these lines, the rhenium oxo moiety as first glance appeared to be an ideal candidate; however a broader survey of the literature was required to fully understand the implications of this choice.

The Reactivity and Electronic Nature of Rhenium Oxo Moieties

Perrhenate (ReO_4^-) salts and various rhenium oxides have long been studied for their use as oxidants and catalysts, particularly for olefin metathesis.[15] Additionally, owing to the low oxophilicity (and ease of handling) of rhenium as compared to the early transition metals, it was among the first metals studied in the field of synthetic organometallic chemistry.[16] Accordingly, since at least the 1950s there has been an uninterrupted stream of fundamental studies focused on homogeneous rhenium complexes that continues to this day. Studies of rhenium terminal oxo complexes have led to a variety of novel behaviors, and a complete summary of this subject could occupy an entire encyclopedic volume. Below are summarized some studies in this area that bear direct relevance to the research presented in this work.

One mode of reactivity commonly observed and gauged in rhenium terminal oxo complexes (and those of other transition metals, most prominently molybdenum and tungsten) is oxygen atom transfer (OAT), whereby an incoming acceptor removes a terminal oxo ligand via a redox process, where the metal (the OAT donor) is reduced by two electrons by the formal loss of an oxygen atom. Typically these reactions are most favorable when the added acceptor is electron-rich and a strong Lewis base, such as with small trialkylphosphines (e.g. PMe_3). Sometimes, the reduced metal species can be isolated following OAT, and in other cases, the reduced fragment is too reactive to isolate but can be utilized *in situ*. For example, in one work from Mayer and coworkers, a cationic rhenium(V) terminal oxo complex, **1.14**, and its corresponding rhenium(III) analog (**1.15**, without an oxo ligand) were each evaluated for their OAT donor and acceptor abilities, and this was only enabled by the stability of each species (Scheme 1.6).[17]

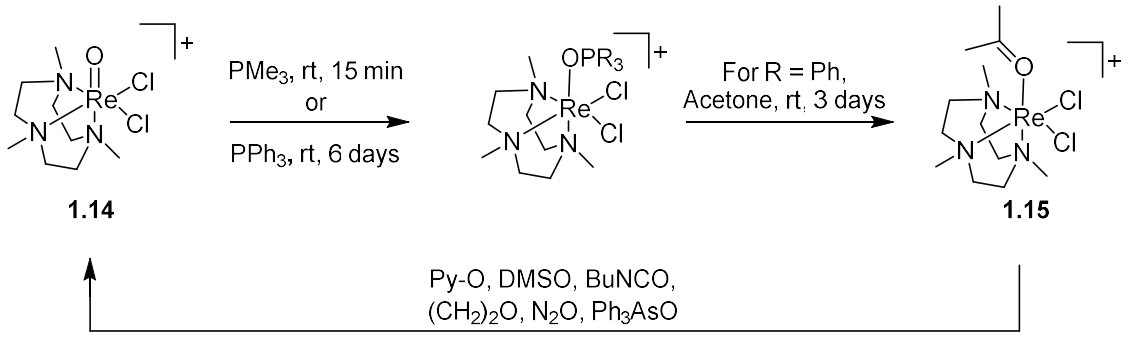

Scheme 1.6 OAT donor and acceptor reactions of cationic rhenium(V) and rhenium(III) complexes.

In contrast, the thoroughly studied rhenium(VII) complex methyltrioxorhenium (MTO, **1.16**) readily donate an oxygen atom to triphenylphosphine, generating a unisolable intermediate, the dioxo compound **1.17**, which will readily bind alkynes (forming **1.18**) or condense with glycols and polyols to form rhenium(V) glycolate complexes (**1.19**, Scheme 1.7).[18] These glycolate complexes undergo a thermal cycloreversion to eject olefins and reform the MTO starting material, and this process is at the forefront of current efforts to catalytically deoxygenate biomass to yield carbon neutral liquid fuels.[19] In all, oxygen atom transfer is one of the primary means of assessing the relative reactivity and behavior of a rhenium terminal oxo complex, and this method has led to a number of fruitful fundamental and applied studies.

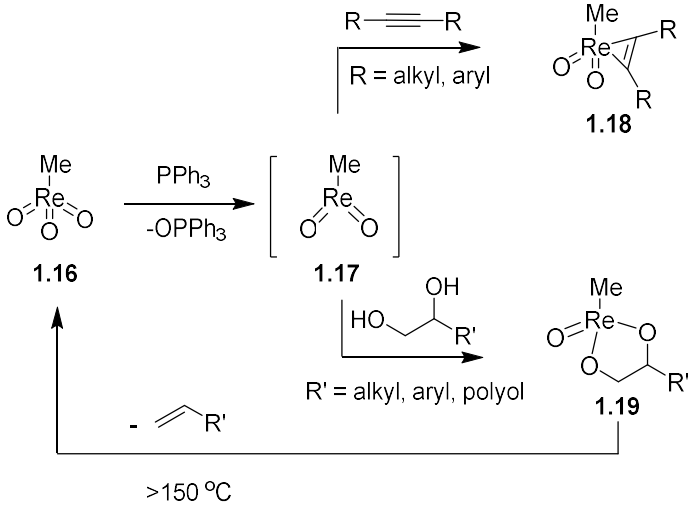

Scheme 1.7 Reactivity of a transient intermediate generated by OAT from MTO.

Rhenium terminal oxo groups have also been present in compounds that challenged the classical notions of metal-ligand multiple bonding in terms of their chemical behavior and electronic structure. The most well-known examples of this are the acetylene-supported rhenium(III) and rhenium(I) terminal oxo complexes **1.20** and **1.21** studied extensively by Mayer and coworkers (Scheme 1.8).[20-22] Prior to these works, no transition metal oxo complex with an electronic configuration of d^4 or greater had been isolated. The observation that such species could be accessed rationally, but still contained robust and persistent metal oxo groups, was striking: the

majority of reactions with this complexes occurred at the metal rather than at the multiply-bonded ligand. Classically, terminal oxo groups are only found in transition metal complexes with high valent metals with 2 or less *d* electrons residing on the metal (provided there is tetragonal symmetry in its coordination sphere).[23] These studies by Mayer and coworkers demonstrated that lower valent terminal oxo complexes could be rationally accessed in lower symmetry transition metal complexes, and these works have informed a number of subsequent studies of d^4 and d^5 terminal oxo species.[24-26]

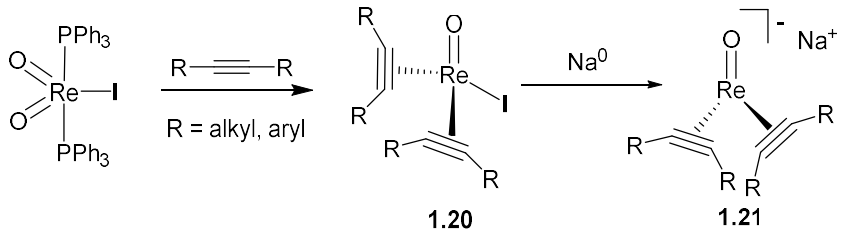

Scheme 1.8 Synthesis and structure of rhenium(III) and rhenium(I) terminal oxo complexes.

In more recent work from the group of Elon Ison, a rhenium(V) terminal oxo complex in an electron-rich coordination environment (**1.22**) demonstrated both electrophilic and nucleophilic behavior at the terminal oxo ligand, yielding the complexes **1.23** and **1.24**, respectively (Scheme 1.9).[27] While electrophilic and nucleophilic terminal oxo complexes are both well precedented, Ison's work showed that metal oxo species (perhaps especially those of rhenium) are subject to a precise degree of electronic tuning that has a direct influence on their behavior. The electronic tuning of metal oxides, more often of the first row transition elements, is targeted towards the use of these groups in C-H activation chemistry.[28]

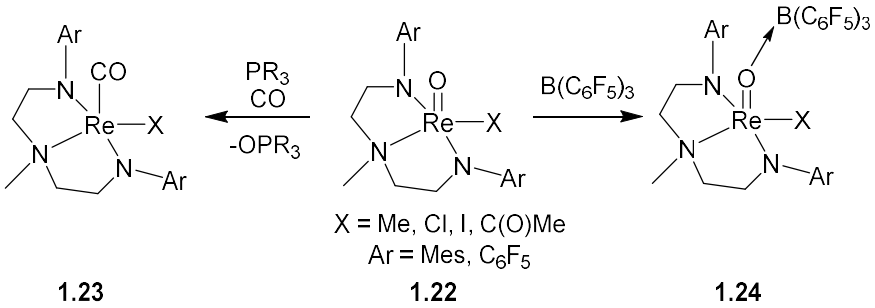

Scheme 1.9 Electrophilic and nucleophilic reactivity in the same rhenium(V) oxo complex.

The field of homogeneous rhenium oxo chemistry has been a persistent source of important fundamental results, and informed developments in other areas of synthetic inorganic chemistry and catalysis. This precedent provided an ample theoretical basis to justify the synthesis of the first rhenium oxo β-diketiminates.

Guiding Hypothesis, and Entry into the Rhenium β-Diketiminate System

The hypothesis driving this work is as follows: given the proven capability of the BDI ligand to support uniquely reactive group 5 imido species in both high and low valent forms, as well as the proven ability of the rhenium oxo moiety to display a wide range of reactivity in

multiple oxidation states, it was postulated that similarly novel compounds and behaviors will be observed upon the synthesis and study of the first rhenium oxo BDI complexes. While this work is generally focused on studying reactivity of the rhenium oxo moiety, species not containing an oxo ligand were also accessed, and their reactivity was subsequently assessed. Cumulatively, this work in one part highlights the utility of the BDI ligand as a versatile ancillary framework, but more largely demonstrates a number of novel behaviors of rhenium oxo complexes, and in some cases, of transition metal complexes in general.

Prior to this work, there were only a handful of preexisting examples of rhenium BDI complexes, reported in a single article.[29] These complexes were exclusively based on rhenium(I) carbonyl fragments (**1.25**), and their reported reactivity was limited to the non-innocent behavior of the BDI ligand, and its reversible addition to metal-bound nitriles (Scheme 1.10). In this study, the neutral, protonated BDI ligand was used directly in the rhenium complexation reactions; however, the primary targets of this work were high valent oxo complexes, which bear little resemblance to the reported series of rhenium carbonyl BDI complexes. Therefore, it was apparent a different means of BDI metalation, such as salt metathesis, would need to be employed in this work. In summary, this work was initiated with little to no direct guidance from the literature, and the subsequent chapters are likely to provide a meaningful precedent for all future studies of rhenium BDI complexes.

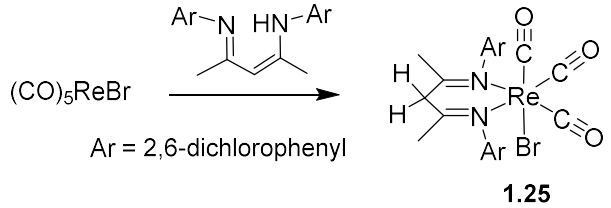

1.25

Scheme 1.10 Representative example of a rhenium BDI complex that predates this work.

Notes and References

(1) Bourget-Merle, L.; Lappert, M. F.; Severn, J. R. *Chem. Rev.* **2002**, *102*, 3031.
(2) Camp, C.; Arnold J. *Dalton Trans.* **2016**, *45*, 14462.
(3) Hohloch, S.; Kriegel, B. M.; Bergman, R. G.; Arnold, J. *Dalton Trans.* **2016**, *45*, 15725.
(4) Walsh, P. J.; Hollander, F. J.; Bergman, R. G. *J. Am. Chem. Soc.* **1988**, *110*, 8729.
(5) Cummins, C. C.; Baxter, S. M.; Wolczanski, P. T. *J. Am. Chem. Soc.* **1988**, *110*, 8731.
(6) Tomson, N. C.; Yan, A.; Arnold, J.; Bergman, R. G. *J. Am. Chem. Soc.* **2008**, *130*, 11262.
(7) Gianetti, T. L.; Nocton, G.; Minasian, S. G.; Tomson, N. C.; Kilcoyne, A. L. D.; Kozimor, S. A.; Shuh, D. K.; Tyliszczak, T.; Bergman, R. G.; Arnold. J. *J. Am. Chem. Soc.* **2013**, *135*, 3224.
(8) Kriegel, B. M.; Bergman, R. G.; Arnold, J. *Dalton Trans.* **2014**, *43*, 10046.
(9) Gianetti, T. L.; Tomson, N. C.; Arnold, J.; Bergman R. G. *J. Am. Chem. Soc.* **2011**, *133*, 14904.
(10) Camp, C.; Maron, L.; Bergman, R. G.; Arnold, J. *J. Am. Chem. Soc.* **2014**, *136*, 17652.
(11) Gianetti, T. L.; Bergman, R. G.; Arnold, J. *Chem. Sci.* **2014**, *5*, 2517.
(12) Gianetti, T. L.; Bergman, R. G.; Arnold, J. *J. Am. Chem. Soc.* **2013**, *135*, 3771.

(13) Gianetti, T. L.; Nocton, G.; Minasian, S. G.; Kaltsoyannis, N.; Kilcoyne, A. L. D.; Kozimor, S. A.; Shuh, D. K.; Tyliszczak, T.; Bergman, R. G.; Arnold, J. *Chem. Sci.* **2015**, *6*, 993.
(14) Kriegel, B. M.; Bergman, R. G.; Arnold, J. *J. Am. Chem. Soc.* **2016**, *138*, 52.
(15) Chabanas, M.; Baudoin, A.; Copéret, C.; Basset, J.-M. *J. Am. Chem. Soc.* **2001**, *123*, 2062.
(16) Wilkinson, G.; Birmingham, J. M. *J. Am. Chem. Soc.* **1955**, *77*, 3421.
(17) Conry, R. R.; Mayer, J. M. *Inorg. Chem.* **1990**, *29*, 4862.
(18) Raju, S.; Moret, M.; Klein Gebbink, R. J. M. *ACS Catal.* **2015**, *5*(1), 281.
(19) Shiramizu, M.; Toste, F. D. *Angew. Chem. Int. Ed.* **2013**, *52*, 12905.
(20) Mayer, J. M.; Tulip, T. H. *J. Am. Chem. Soc.* **1984**, *106*, 3878.
(21) Mayer, J. M.; Tulip, T. H.; Calabrese, J. C.; Valencia, E. *J. Am. Chem. Soc.* **1987**, *109*, 157.
(22) Spaltenstein, E.; Conry, R. R.; Critchlow, S. C.; Mayer, J. M. *J. Am. Chem. Soc.* **1989**, *111*, 8741.
(23) Nugent, W. A.; Mayer, J. M. *Metal-ligand Multiple bonds*. John Wiley & Sons: New York, 1988.
(24) MacBeth, C. E.; Golombek, A. P.; Young Jr., V. G.; Yang, C.; Kuczera, K.; Hendrich, M. P.; Borovik, A. S. *Science*, **2000**, *289*, 938.
(25) Poverenov, E.; Efremenko, I.; Frenkel, A. I.; Ben-David, Y.; Shimon, L. J. W.; Leitus, G.; Konstantinovski, L.; Martin, J. M. L.; Milstein, D. *Nature* **2008**, *455*, 1093.
(26) Hong, S.; Lee, Y.-M.; Sankaralingam, M.; Vardhaman, A. K.; Park, Y. J.; Cho, K.-B.; Ogura, T.; Sarangi, R.; Fukuzumi, S.; Nam, W. *J. Am. Chem. Soc.* **2016**, *138*, 8523.
(27) Smeltz, J. L.; Lilly, C. P.; Boyle, P. D.; Ison, E. A. *J. Am. Chem. Soc.* **2013**, *135*, 9433.
(28) Gunay, A.; Theopold, K. H. *Chem. Rev.* **2010**, *110*, 1060.
(29) Yempally, V.; Fan, W. Y.; Arndtsen, B. A.; Bengali, A. A. *Inorg. Chem.* **2015**, *54*, 11441.

Chapter 2

Oxygen Atom Transfer and Intramolecular Nitrene Transfer in a Rhenium β-Diketiminate Complex

Introduction

The chemistry of transition metal oxo complexes is a diverse and extensively studied area of research due to its relevance to enzymatic processes and catalytic applications.[1-4] Of consistent interest are rhenium terminal oxo complexes, due to their proven ability to catalyze a plethora of transformations, including deoxygenations, didehydroxylations, hydrosilylations, C-C and C-O bond forming reactions, as well as numerous organic oxidations.[5-14] The reactivity of metal oxo complexes, including those of rhenium, have been found to be highly variable depending upon the specific electronic and steric properties of the ancillary ligands they contain.[15] For example, while many rhenium oxo moieties display electrophilic reactivity, the use of a proper ancillary framework can lead to nucleophilic reactivity as well.[16-19] This high degree of variability has stimulated our interest in investigating the effects of unexplored ligand frameworks on the rhenium oxo fragment with the hope of creating an environment suitable for the observation of novel modes of reactivity and the stabilization of new structural motifs.

One popular ancillary framework that has not been applied to oxo rhenium chemistry is the β-diketiminate (BDI) ligand. This anionic, sterically encumbering framework has previously allowed for the synthesis and isolation of highly reactive inorganic fragments, such as those bearing low valent alkaline earth metal and main group element centers, as well as those containing early and late transition metals.[20-25] Previously, the BDI framework has also been used to support a variety of Re(I) carbonyl complexes that have been observed to undergo intramolecular C-H addition across organic nitriles.[26] A major research effort in our group has been the study of the properties and reactivity of niobium and tantalum imido complexes supported by the BDI ligand.[27-39] These complexes have demonstrated numerous modes of stoichiometric and catalytic reactivity previously unobserved in Group 5 imido complexes.

The target for this work was the synthesis of the first oxo rhenium BDI complexes for the purpose of determining their unique reactivity and properties. As a guide for future studies, we also sought to probe some of the ancillary limitations of the BDI framework for rhenium oxo complexes to establish what conditions may lead to non-innocent or degradative reactivity.

Results and Discussion

We have developed a facile, scalable synthesis of the first oxo rhenium BDI complex, $OReCl_2$(BDI) (**2.1**), which utilizes the easily accessed precursors $OReCl_3(PPh_3)_2$ and (BDI)MgCl(THF) (Scheme 2.1). Complex **2.1** can also be accessed in similar yield when $OReCl_3(SMe_2)_2$ is instead used as the rhenium source. One key advantage of using $OReCl_3(SMe_2)_2$ rather than $OReCl_3(PPh_3)_2$ is the ability to isolate **2.1** by Soxhlet extraction into hexane as opposed to crystallization from diethyl ether. Both routes yield **2.1** as dark green crystalline solids. Attempts using the common rhenium oxo precursor $OReCl_3(SMe_2)(OPPh_3)$ only gave low yields of **2.1** after a protracted workup procedure. Additionally, when the common BDI source (BDI)Li(Et_2O) was used in place of the magnesium salt, only low yields of **2.1** were obtained. It has previously been reported that the magnesium salts of PNP-pincer ligands led to much higher yields in salt metathesis reactions with rhenium oxyhalide precursors than do their lithium analogs.[40-41]

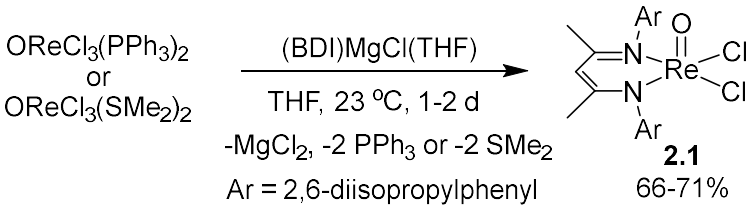

Scheme 2.1 Salt metathesis routes to yield **2.1**.

The X-ray crystal structure of **2.1** (Figure 2.1) displays distorted square pyramidal geometry, with the oxo ligand occupying the apical position. Complex **2.1** is coordinately and electronically unsaturated (5-coordinate, 16 e^-), presumably due to the high steric bulk of the BDI ligand. Another noteworthy feature in the structure of **2.1** is the relative locations of the two chloride ligands: one chloride is slightly tucked under towards the open coordination site that lies *trans* to the oxo ligand. This difference is highlighted in the measurements of the O-Re-Cl bond angles of 104.17(9)° and 111.70(9)°.

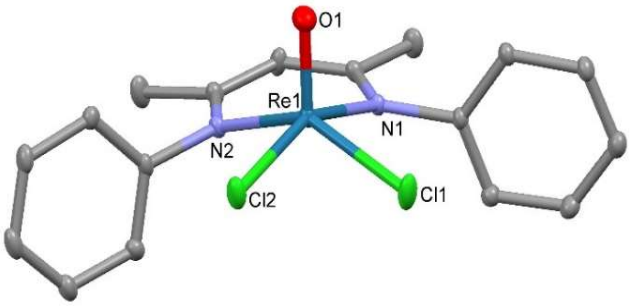

Figure 2.1 X-ray crystal structure of **2.1** with thermal ellipsoids set to 50% probability. Solvent, BDI isopropyl, and hydrogen atoms have been removed for clarity. Selected bond distances (Å): N(1)-Re(1) 2.064(2), N(2)-Re(1) 2.030(3), O(1)-Re(1) 1.670(2), Cl(1)-Re(1) 2.3310(10), Cl(2)-Re(1) 2.3436(10).

In most cases, the chemistry of **2.1** is dominated by its tendency to form octahedral adducts with small σ-donors. Red adducts of **2.1** with phosphines, isonitriles, and pyridines all form within seconds at room temperature, as demonstrated by the synthesis and isolation of the complexes $OReCl_2(BDI)(PEt_3)$ (**2.2a**), $OReCl_2(BDI)(XylNC)$ (**2.2b**) (XylNC = 2,6-dimethylphenylisocyanide), and $OReCl_2(BDI)(DMAP)$ (**2.2c**) (DMAP = 4-dimethylaminopyridine) (See Scheme 2.2). All of these complexes feature the dative ligand binding *cis* to the oxo group, as confirmed by the solid state structures of **2.2a** and **2.2c** as well as the apparent symmetry displayed in the ^{1}H NMR spectrum of **2.2b**. An adduct of **2.1** with acetonitrile (MeCN) is also observed to form, as a dark red solution is obtained when **2.1** is dissolved in this solvent. However, it was found that **2.2d** was too labile to remain intact during workup, leading only to the recovery of starting material (see Experimental). No adducts of **2.1** were observed to form with ethylene, various alkynes, or carbon monoxide, implying that **2.1** will not readily form π-backbonding interactions despite the d^2 electron configuration of its Re(V) center.

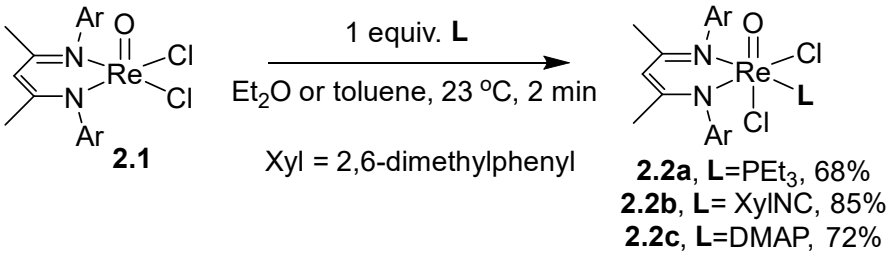

Scheme 2.2 Formation of isolable adducts of **2.1** with strong σ-donor ligands.

The solid state structures of **2.2a** and **2.2c** bear high resemblance to one another (Figure 2.2). Both exhibit distorted octahedral geometries with no differences between the analogous bonding parameters to the metal center (excluding those for PEt_3 or DMAP themselves) exceeding 0.036(6) Å. Both DMAP and PEt_3 force the BDI framework to bind in an asymmetric manner, with the *cis* N atom being pushed further away from the metal due to the steric clash between the BDI aryl group and the adducting ligand. This effect is slightly more pronounced in **2.2c**, where the *cis* N atom is 0.099(6) Å further from the metal than the *trans* N atom of the BDI ligand. In **2.2a** this difference is only 0.079(6) Å, likely because in these complexes PEt_3 binds much further away from the metal center than does DMAP, which lessens its steric repulsion on the binding of the BDI framework. For example, the Re-L distance is 2.5471(13) Å in **2.2a** versus only 2.219(5) Å in **2.2c**. The distorted octahedral geometry of these complexes is apparent in the non-ideal bonding angles of the oxo ligand; the angles between it and the *trans* chloride ligand noticeably deviate from linearity (O-Re-Cl = 166.65(11)° in **2.2a** and 165.78(12)° in **2.2c**). In addition to this distortion, a measureable *trans*-influence due to the oxo ligand is also observed in the rhenium to chloride bond distances. This *trans*-influence appears to be much larger in **2.2a** than in **2.2c**, with *trans*-Cl bond lengths exceeding the *cis*-Cl bond lengths by 0.074(2) Å and 0.023(2) Å, respectively.

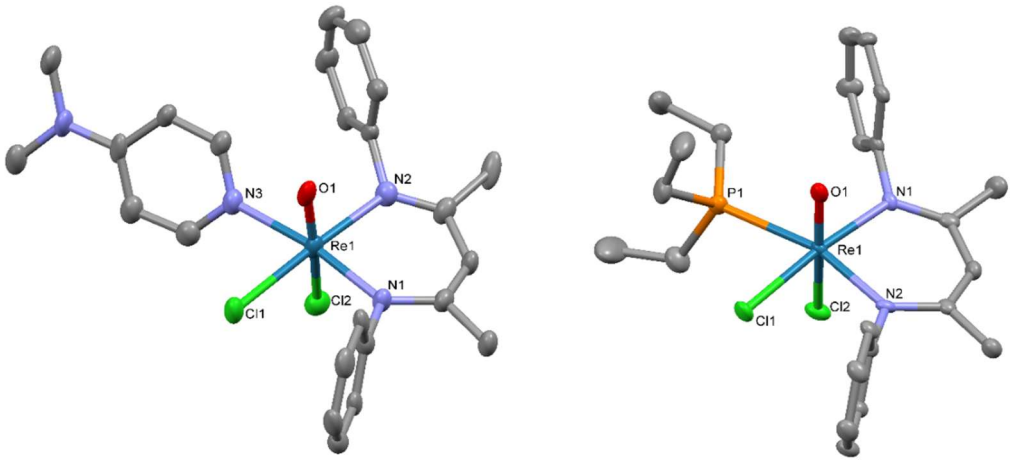

Figure 2.2 X-ray crystal structures of **2.2c** (left) and **2.2a** (right) with thermal ellipsoids set to 50% probability. Solvent, BDI isopropyl, and hydrogen atoms have been removed for clarity. Selected bond distances (Å) for **2.2c**: N(1)-Re(1) 2.046(4), N(2)-Re(1) 2.143(4), N(3)-Re(1) 2.219(5), O(1)-Re(1) 1.672(4), Cl(1)-Re(1) 2.3812(14), Cl(2)-Re(1) 2.4046(16). Selected bond distances (Å) for

2.2a: N(1)-Re(1) 2.159(4), N(2)-Re(1) 2.082(4), O(1)-Re(1) 1.684(4), P(1)-Re(1) 2.5471(13), Cl(1)-Re(1), 2.3643(12), Cl(2)-Re(1) 2.4383(13).

Of the adducts of **2.1**, only **2.2a** was selected for further study on the basis of its solid state structure, which indicated a long Re-P distance of 2.5471(13) Å, elongated from its expected value by over 0.1 Å.[42] This long bond length is presumably due to the steric clash between the ethyl groups of the phosphine and the BDI framework, potentially resulting in a weakened bond between the phosphine and the rhenium center. This hypothesis was confirmed when a solution of **2.2a** was heated to 80 ºC for several days and periodically monitored by ^{1}H and ^{31}P NMR spectroscopies. During this time the formation of multiple species was observed, including new phosphine-containing species as well as one species containing what was believed to be Re-bound triethylphosphine oxide ($OPEt_3$) (See Figure 2.3). The two new phosphine-containing and one new phosphine oxide-containing species did not undergo further conversion with additional heating. We believed that oxygen atom transfer (OAT) was taking place, leading to the formation of a phosphine-supported Re(III) BDI complex.

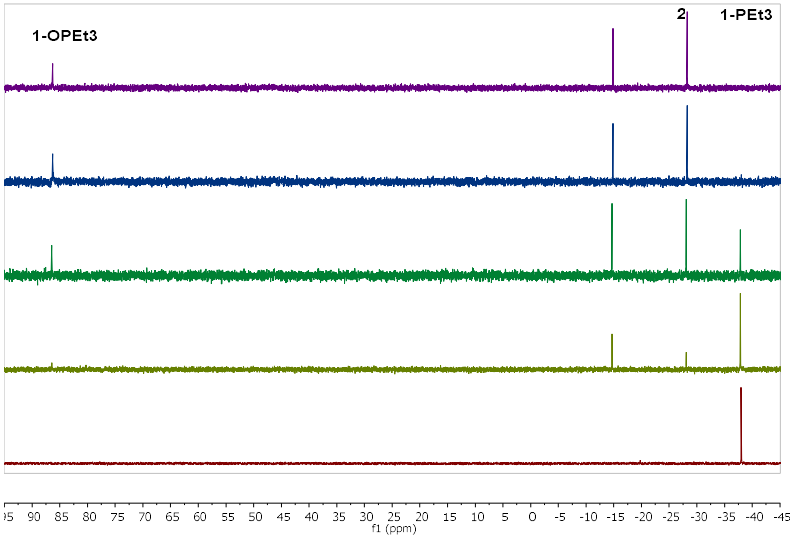

Figure 2.3 ^{31}P NMR spectra illustrating the thermal reaction of **2.2a** over several days at 80 ºC to generate **2.2e** (86.3 ppm) and two new phosphine-containing species, including compound **2.3** (-28.2 ppm). The species corresponding to the peak at -15.8 ppm could not be identified.

In order to investigate the intriguing thermolysis reactivity of **2.2a**, we attempted to identify the multiple new species whose signals were observed in the ^{31}P NMR data. We confirmed that the downfield signal observed at 86.3 ppm corresponds to the adduct $OReCl_2(BDI)(OPEt_3)$ (**2.2e**) by combining **2.1** with excess $OPEt_3$ and measuring the ^{31}P NMR spectrum of the resulting bright red solution (see Experimental). This verified that $OPEt_3$ was indeed being formed upon the thermolysis of **2.2a**, a clear indication that OAT was taking place. Since **2.2e** was observed rather than free $OPEt_3$, it was clear phosphine oxide had exchanged with PEt_3 from unreacted **2.2a**. The liberated PEt_3 then appeared to play a role in trapping or reacting with the species formed by OAT. Therefore, it was hypothesized that a second equivalent of phosphine was necessary to trap the product of OAT from **2.1** and bring the reaction to completion.

To test the effects of added PEt_3 on the thermal reaction of **2.2a**, two separate NMR scale reactions were conducted, where equal amounts of **2.1** were heated in toluene-d_8 at 120 ºC with either 2.3 or 10 equivalents of PEt_3. In both cases **2.2a** was the only Re-containing species observed before heating, indicating that **2.1** had bound one equivalent of the added phosphine in each reaction mixture. It was found that both reactions displayed first-order rates of consumption of **2.2a** over time, and that increased concentration of PEt_3 resulted in faster consumption of **2.2a** (see Experimental). Interestingly, in addition to increasing the rate of the reaction, a higher concentration of phosphine had a drastic effect on the product distribution. First, in both reactions no **2.2e** was observed, but rather free $OPEt_3$ was seen to form as the reaction proceeded. This indicates that the reaction to form **2.2e** only occurs when there is a lack of phosphine present to trap or react with the species arising from OAT. Second, it was found that the signal due to the major product of these reactions corresponded to the previously observed ^{31}P NMR signal at -28.2 ppm, whereas the signal seen at -15.8 ppm was greatly diminished compared to that observed for the thermolysis of **2.2a** (Figure 2.4). These observations demonstrate that the presence of free PEt_3 both allows the OAT reaction to consume all of the starting material by preventing the formation of **2.2e**, as well as yield only one major phosphine-containing product. As seen in previous experiments, there was a significant amount of protonated BDI ligand observed in the ^{1}H NMR spectra of these reaction mixtures, indicating some decomposition process was also occurring over the course of the reactions. Numerous minor peaks were also observed in the ^{31}P NMR data as a result of thermal degradation. Due to these degradative reaction pathways and the convoluted product mixture observed in this system, we determined a quantitative kinetic analysis based on these experiments would be imprudent. Regardless, the conclusion that higher concentrations of free PEt_3 both increased the rate of the reaction as well as controlled its product distribution to predominantly a single product allowed us to efficiently carry on with preparative experiments.

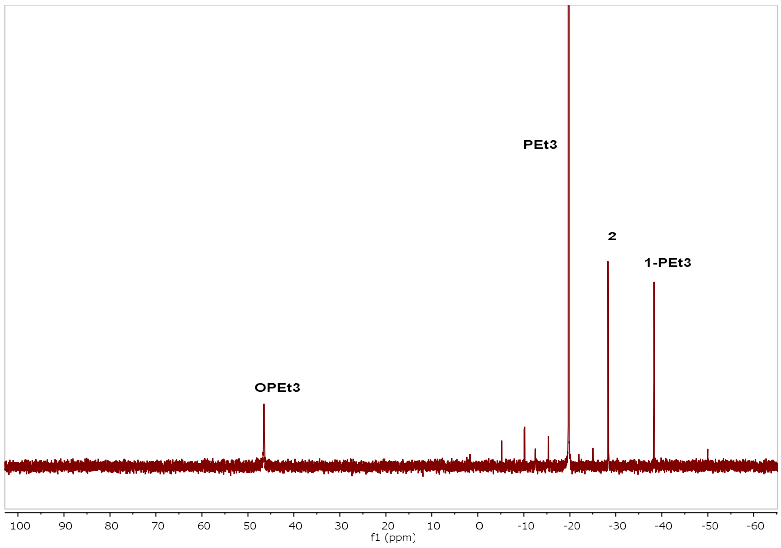

Figure 2.4 ^{31}P NMR spectrum of the reaction mixture generated from **2.1** with 10 eq. of PEt_3 after 5 h at 120 ºC.

Based on the results of the NMR spectroscopy experiments, we wished to isolate and characterize the major product of OAT in this system. Thus, **2.1** and 5 equiv. of PEt_3 were heated

in toluene at 120 ºC to yield a single isolated product, (ArN)$ReCl_2$(MAD)(PEt_3) (**2.3**) (Ar = 2,6-diisopropylphenyl, MAD = 4-((2,6-diisopropylphenyl)imino)pent-2-en-2-ide) (See Scheme 2.3). Characterization of this product by NMR spectroscopy demonstrated that it was indeed the main species observed to form from the thermal reaction of **2.2a**, with a ^{31}P NMR signal at -28.2 ppm. Complex **2.3** is formed via nitrene transfer to the metal center from the BDI ligand following OAT from **2.1**, which presumably forms an unobserved, Re(III) intermediate, "$ReCl_2$(BDI)($OPEt_3$)." This mode of cleavage of the BDI ligand has precedent in work done by our group.[43-45] The formation of complex **2.3** by this route is the first documented example of oxidative nitrene transfer to rhenium from a carbon atom. Nitrene transfer to rhenium is a known reaction using azide compounds, and this reaction has previously been studied in high-valent rhenium complexes.[46-47]

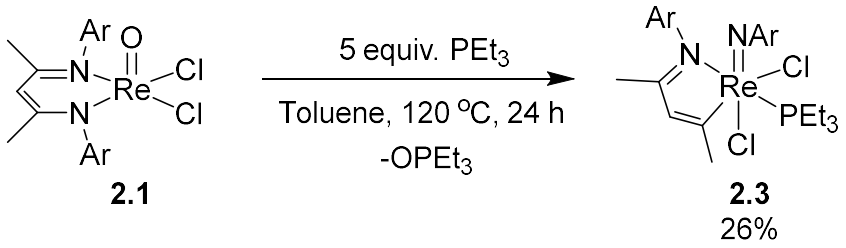

Scheme 2.3 Oxygen atom transfer from **2.1** to PEt_3 followed by intramolecular nitrene transfer from the BDI ligand to form **2.3**.

The solid-state structure of **2.3** was determined by X-ray crystallography, and it was found to crystallize in the triclinic space group P-1 with two independent molecules of **2.3** in the asymmetric unit (Figure 2.5). The geometry of **2.3** is very similar to those of **2.2a** and **2.2c**, with the PEt_3 ligand bound *cis* relative to the imido moiety. The PEt_3 in **2.3** is bound *cis* to the ligating C atom of the MAD ligand, which lacks significant bulk relative to the ligating N(Ar) group. Due to the significantly decreased steric profile of the MAD ligand relative to the BDI framework, the PEt_3 ligand in **2.3** is bound much closer to the metal center than it is in **2.2a** (Re-P = 2.4279(15) Å and 2.4293(13) Å). The diminished steric requirements for the MAD ligand are also observable in its narrow bite angles of 77.23(14)º and 77.53(14)º as measured in the crystal structure of **2**, versus the bite angles for the BDI ligand in **2.2a** and **2.2c** of 90.84(15)º and 88.78(17)º, respectively. The imido moiety in **2.3** is almost perfectly linear in geometry (Re-N-C = 176.9(3)º and 177.8(3)º) and imposes steric and electronic distortions analogous to those observed in both **2.2a** and **2.2c**, including a measureable *trans*-influence in the chloride ligands (0.0139(17) Å and 0.0179(17) Å in the two independent molecules of **2**) as well as a skewed binding angle of the imido moiety (N-Re-*trans* Cl = 170.47(12)º and 170.87(12)º).

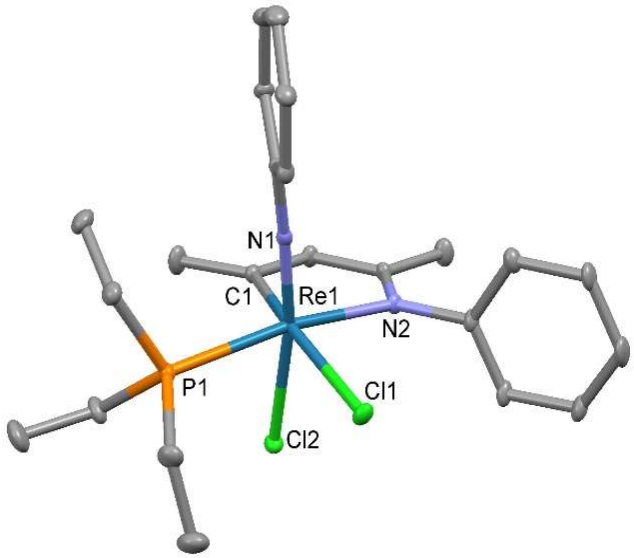

Figure 2.5 X-ray crystal structure of one of the two crystallographically independent molecules of **2.3** with thermal ellipsoids set to 50% probability. Isopropyl and hydrogen atoms have been removed for clarity. Selected bond distances (Å): N(1)-Re(1) 1.736(4), N(2)-Re(1) 2.189(4), C(1)-Re(1) 2.146(4), P(1)-Re(1) 2.4279(15), Cl(1)-Re(1) 2.4455(11), Cl(2)-Re(1) 2.4594(12).

Based on the above results, it appeared that the BDI ligand would prove incapable of supporting low-valent fragments resulting from OAT from **2.1**. Thus, the ancillary limitations of BDI in Re complexes are similar to those found in the Nb imido BDI complexes studied by our group, in which intramolecular nitrene transfer from the BDI ligand occurred when a low-coordinate Nb(III) center was generated in the presence of a dative ligand. It is unclear if a dative ligand is required for nitrene transfer to occur in the Re system under discussion, or if the thermal conditions of the reaction play a key role in this step. Interestingly, it was found that when the same OAT reaction was attempted in the presence of excess trimethylphosphine (PMe_3), only the adduct $OReCl_2(BDI)(PMe_3)$ (**2.2f**) was isolated and identified on the basis of its ^1H and ^{31}P NMR spectra. Presumably the smaller size of PMe_3 relative to PEt_3 allows it to form a stronger adduct with **2.1** that cannot be thermolyzed under similar conditions (100 ^oC) to promote OAT reactivity. Additionally, when a strong adduct, **2.2c**, was heated in the presence of PEt_3 no reaction was observed. We also found that complex **2.1** did not react or form an adduct with PPh_3, even after heating at 100 ^oC for extended periods.

These experiments demonstrate that OAT in this system can occur from **2.1** but not its adducts, and only with oxygen atom acceptors that are sterically incapable of forming a strong bond directly to the metal center. The formation of a strong bond to the metal prevents the migration or dissociation step that is necessary for OAT to take place. Also, as demonstrated by the lack of reactivity of **2.1** with PPh_3, when the oxygen atom acceptor is too bulky to form any bond directly to the metal center there is no kinetically accessible pathway to OAT. In short, because of the sterically encumbering nature of the BDI ligand, the OAT reactivity of **2.1** is tuned to phosphines that, like PEt_3, can interact with the Re center, but only to the extent that these interactions are labile upon heating.

This conclusion implies that OAT from **2.1** can proceed by one of two distinct mechanisms, which were briefly mentioned earlier. One involves an intramolecular OAT via direct migration of PEt_3 in **2.2a** from the Re center to the oxo moiety. The other mechanism would involve two steps: dissociation of PEt_3 from **2.2a** followed by intermolecular nucleophilic attack on the oxo moiety of **2.1** by free PEt_3. Based on our kinetic data alone, these two mechanisms are indistinguishable. Specifically, an increase in free phosphine concentration could increase the rate of OAT in either case, either by favoring the equilibrium to form **2.2a** (and thus the intramolecular pathway) or by increasing the rate of nucleophilic attack on the oxo moiety of free **2.1** (which would favor the intermolecular pathway). Additionally, none of our data precludes the possibility of both pathways being kinetically accessible at 120 °C (Scheme 4). In the future, a computational study using density functional theory (DFT) may help elucidate which of these pathways is more favorable.

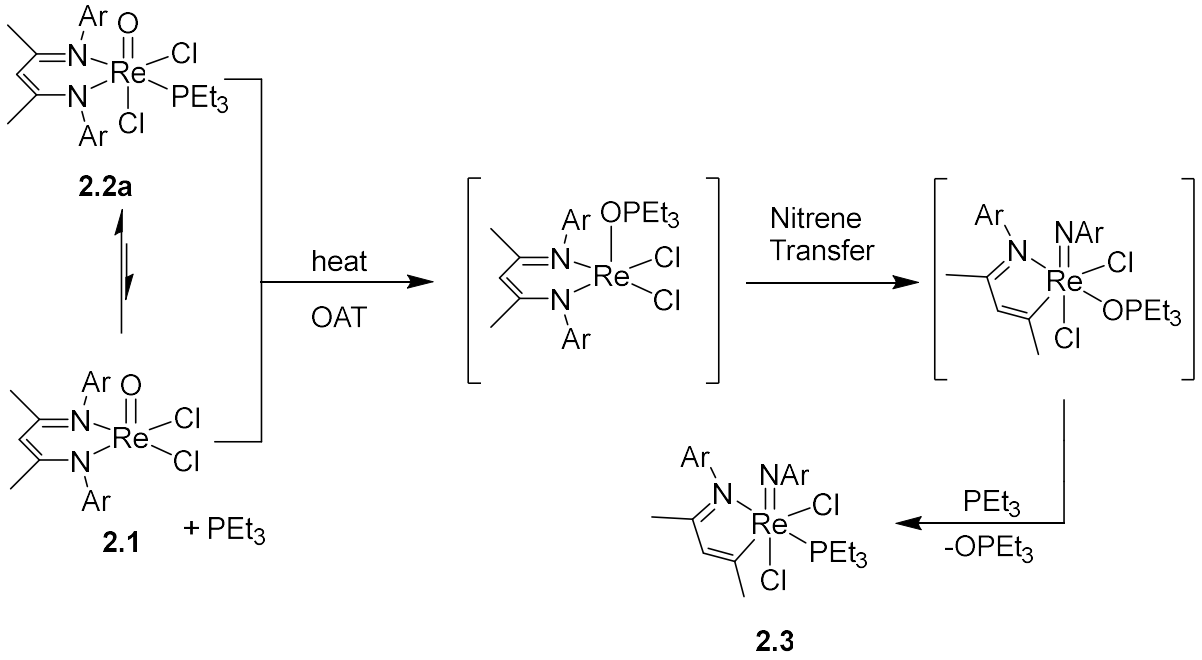

Scheme 2.4 Outline of plausible mechanistic pathways to generate **2.3**, based on the insights gained from kinetic and reactivity studies of **2.1** and **2.2a**.

Summary and Conclusions

In summary, we have reported the synthesis of the first oxo rhenium β-diketiminate complex, $OReCl_2$(BDI) (**2.1**), as well as syntheses of several Lewis base adducts of this complex with isonitriles, phosphines, and DMAP (**2.2a-c**). Complex **2.1** has been found to undergo oxygen atom transfer with PEt_3 under thermal conditions, yielding the imido monoazabutadiene complex (ArN)$ReCl_2$(MAD)(PEt_3) (**2.3**), which is generated via intramolecular nitrene transfer from the BDI ligand. This cleavage of the BDI ligand indicates an ancillary limitation of the BDI framework in rhenium complexes that will be considered in our future studies of this class of complexes.

Experimental

General Considerations: All manipulations were carried out either in an MBraun LabStar glovebox under a dry nitrogen atmosphere or on a Schlenk line using standard techniques. All solvents were dried by passage through a basic alumina column and were handled and stored in standard Strauss flasks under a dry nitrogen atmosphere. Deuterated benzene was obtained from Cambridge Isotope Labs, dried over Na/benzophenone, and transferred under vacuum prior to storage in the glovebox over 4 Å molecular sieves. DMAP and XylNC were dried under vacuum at ambient temperature overnight prior to storage in the glovebox. Trimethylphosphine and triethylphosphine were transferred to storage flasks from their commercial packaging and stored under nitrogen. The reported compounds $ORe Cl_3(PPh_3)_2$,[48] $ORe Cl_3(SMe_2)_2$,[41] and MgCl(BDI)(THF)[49] were synthesized using literature procedures. NMR spectroscopy data were obtained on Bruker AV-300, AVQ-400, AVB-400, AV-500, DRX-500, and AV-600 spectrometers. All ^1H and ^{13}C spectra were calibrated to the residual peak of the solvent used. ^{31}P NMR spectra were obtained using a proton-decoupled parameter set, and reported chemical shifts were referenced to the shifts of known compounds. Select peak assignments were corroborated with ^1H-^1H COSY and ^1H-^{13}C HSQC experiments as necessary. Infrared absorption data was obtained using a Thermo Scientific Nicolet iS10 instrument, with the sample chamber under ambient atmosphere. Samples were prepared as Nujol mulls pressed between KBr plates in the glovebox. A background IR spectrum was obtained immediately prior to data acquisition for each sample.

$ORe Cl_2$(BDI) (2.1): Route A: A solid mixture of $ORe Cl_3(SMe_2)_2$ (6.04 g, 9.54 mmol) and MgCl(BDI)(THF) (5.24 g, 9.54 mmol) was dissolved in 30 mL of THF at room temperature, giving a dark, opaque solution. After being stirred for ca. 19 h, the volatile components of the reaction mixture were removed in vacuo, leaving a dark residue. This residue was triturated with two 10 mL aliquots of hexanes prior to a Soxhlet extraction into 150 mL of hexanes for 48 h. This extraction gave a dark green solution and a sizable accumulation of dark green microcrystalline solids. After storage of this mixture overnight at -40 ºC **2.1** was collected by filtration. Yield: 4.32 g, 66%. Route B: $ORe Cl_3(PPh_3)_2$ (12.4 g, 14.9 mmol) and MgCl(BDI(THF) (8.21 g, 14.9 mmol) were combined in a 500 mL round-bottom Schlenk flask. THF (250 mL) was then added by cannula transfer to give a yellow-green suspension. This suspension was stirred vigorously for ca. 36 h over which time a dark green solution with a fine, pale precipitate was observed to form. The volatile components of the reaction mixture were removed in vacuo, and the resulting dark residue was triturated with hexane (2 x 50 mL) to remove residual THF. The residue was then extracted with ca. 800 mL of diethyl ether, with the extracts being filtered through Celite on a medium-porosity Schlenk frit. The collected extracts were concentrated in vacuo to ca. 450 mL and stored overnight at -40 ºC to give **2.1** as large, dark green needle-shaped crystals. Yield: 7.28 g, 71%. m.p.: 180 ºC (decomp.). ^1H NMR (500 MHz, C_6D_6, 298 K): 7.21 (t, 2H, Ar), 7.17 (d, 2H, Ar), 7.09 (d, 2H, Ar), 5.00 (s, 1H, C*H*(C(Me)NAr)$_2$), 2.96 (sept, 2H, C*H*Me$_2$), 2.21 (sept, 2H, C*H*Me$_2$), 1.55 (s, 6H, CH(C(*Me*)NAr)$_2$), 1.37 (d, 6H, CH*Me*$_2$), 1.17 (d, 6H, CH*Me*$_2$), 1.08 (d, 6H, CH*Me*$_2$), 0.98 (d, 6H, CH*Me*$_2$). ^{13}C NMR (150 MHz, C_6D_6, 298 K): 175.5 (CH(*C*(Me)NAr)$_2$), 151.3 (Ar), 142.6 (Ar), 142.0 (Ar), 128.4 (Ar), 125.1 (Ar), 125.0 (Ar), 123.9 (Ar), 112.8 (*C*H(C(Me)NAr)$_2$), 29.7 (*C*HMe$_2$), 28.0 (*C*HMe$_2$), 26.8 (CH(C(*Me*)NAr)$_2$), 24.5 (CH*Me*$_2$), 24.4 (CH*Me*$_2$), 24.2 (CH*Me*$_2$),

24.0 (CH*Me*$_2$). IR (Nujol): 1591, 1553, 1522, 1353, 1316, 1293, 1261, 1243, 1228, 1180, 1100w, 1057, 1015w, 936, 869, 852, 802, 764, 725, 708. Anal. Calcd for $C_{29}H_{41}N_2OCl_2Re$ (**2.1**): C, 50.42; H, 5.98; N, 4.05. Found: C, 50.52; H, 6.08; N, 4.09.

OReCl$_2$(BDI)(PEt$_3$) (2.2a): PEt$_3$ (53.3 μL, 42.8 mg, 0.362 mmol) was added to a suspension of **2.1** (250 mg, 0.362 mmol) in diethyl ether (ca. 5 mL) at room temperature with stirring, resulting in an immediate color change of the solution from dark green to dark red. The reaction mixture was allowed to stir at room temperature for 1 h, after which the volatile components were removed in vacuo. The resulting dark red residue was extracted into hexanes (2 x 4mL), and these extracts were filtered and concentrated. Storage of the concentrated extracts at -40 ºC gave the product as dark red blocks. Yield: 199 mg, 68%. m.p. 130-1 ºC ^{1}H NMR (400 MHz, C_6D_6, 298 K): 7.32 (d, 1H, Ar), 7.25 (t, 1H, Ar), 7.16 (d, 1H, Ar), 7.09 (t, 2H, Ar), 7.00 (t, 1H, Ar), 4.99 (s, 1H, C*H*(C(Me)NAr)$_2$), 3.74 (sept, 2H, C*H*Me$_2$), 3.17 (sept, 2H, C*H*Me$_2$), 1.85 (s, 3H, CH(C(*Me*)NAr)$_2$), 1.79 (sept, 4H, P(C*H*$_2$CH$_3$)$_3$), 1.73 (s, 3H, CH(C(*Me*)NAr)$_2$), 1.68 (d, 3H, CH*Me*$_2$), 1.39 (d, 3H, CH*Me*$_2$), 1.37 (d, 3H, CH*Me*$_2$), 1.32 (d, 3H, CH*Me*$_2$), 1.31 (d, 3H, CH*Me*$_2$), 1.22 (d, 3H, CH*Me*$_2$), 1.12 (sept, 2H, P(C*H*$_2$CH$_3$)$_3$), 1.11 (d, 3H, CH*Me*$_2$), 1.04 (d, 3H, CH*Me*$_2$), 0.74 (quint, 9H, P(CH$_2$C*H*$_3$)$_3$. ^{13}C NMR (100 MHz, C_6D_6, 298 K) 169.8 (HC(*C*(Me)NAr)$_2$), 157.8 (HC(*C*(Me)NAr)$_2$), 149.8 (Ar), 148.3 (Ar), 146.2 (Ar), 146.0 (Ar), 143.0 (Ar), 127.2 (Ar), 125.5 (Ar), 125.0 (Ar), 124.0 (Ar), 123.8 (Ar), 106.0 (H*C*(C(Me)NAr)$_2$), 28.1 (*C*Me$_2$), 28.0 (*C*Me$_2$), 27.8 (HC(C(*Me*)NAr)$_2$), 27.7 (HC(C(*Me*)NAr)$_2$), 27.2 (C*Me*$_2$), 26.8 (C*Me*$_2$), 26.5 (C*Me*$_2$), 26.2 (C*Me*$_2$), 25.4 (C*Me*$_2$), 25.2 (C*Me*$_2$), 24.7 (C*Me*$_2$), 23.1 (C*Me*$_2$), 15.5 (d, *J* = 26 Hz, P(*C*H$_2$CH$_3$)$_3$), 7.8 (d, *J* = 6 Hz, P(CH$_2$*C*H$_3$)$_3$). ^{31}P NMR (162 MHz, C_6D_6, 298 K): -38.0. IR (Nujol): 1585, 1541, 1530, 1415, 1314, 1260, 1165, 1098, 1045, 1034, 1020, 970, 851, 798, 768, 755, 722, 708. Anal. Calcd for $C_{35}H_{56}N_2OPCl_2Re$ (**2.2a**): C, 51.97; H, 6.98; N, 3.46. Found: C, 51.88; H, 7.04; N, 3.36.

OReCl$_2$(BDI)(XylNC) (2.2b): A toluene solution of 2,6-dimethylphenyl isocyanide (19.0 mg, 0.145 mmol in 2 mL) was added to a stirring solution of **2.1** (100 mg, 0.145 mmol) in toluene (3 mL) at room temperature, resulting in an immediate color change of the solution from dark green to very dark red. The reaction mixture was stirred for ca. 18 h after which time the volatile components were removed in vacuo. The resulting dark residue was extracted thoroughly with diethyl ether (15 mL), and the dark red extracts were filtered and concentrated prior to storage at -40 ºC. After storage overnight, the product was isolated as opaque dark blocks. ^{1}H NMR analysis of the isolated crystalline material indicated the product cocrystallizes with 1 equivalent of diethyl ether. Yield: 110 mg, 85% (based on **2.2b** • Et$_2$O). m.p.: 279-281 ºC. ^{1}H NMR (500 MHz, C_6D_6, 298 K): 7.36 (dd, 1H, BDI Ar), 7.24 (t, 1H, BDI Ar), 7.19 (dd, 1H, BDI Ar), 7.08 (dd, 1H, BDI Ar), 6.97 (dd, 1H, BDI Ar), 6.87 (t, 1H, BDI Ar), 6.54-6.43 (m, 3H, xylyl Ar), 4.88 (s, 1H, C*H*(C(Me)NAr)$_2$), 3.90 (sept, 1H, C*H*Me$_2$), 3.72 (sept, 1H, C*H*Me$_2$), 3.30-3.14 (m, 2H, C*H*Me$_2$), 2.00 (s, 6H, CH(C(*Me*)NAr)$_2$), 1.79 (s, 3H, xylyl Me), 1.76 (d, 3H, CH*Me*$_2$), 1.71 (s, 3H, xylyl Me), 1.50 (d, 3H, CH*Me*$_2$), 1.45 (d, 3H, CH*Me*$_2$), 1.31 (d, 3H, CH*Me*$_2$), 1.30 (d, 3H, CH*Me*$_2$), 1.23 (d, 3H, CH*Me*$_2$), 1.08 (d, 3H, CH*Me*$_2$), 1.06 (d, 3H, CH*Me*$_2$). ^{13}C NMR (126 MHz, C_6D_6, 298 K): 169.5 (HC(*C*(Me)NAr)$_2$), 157.6 (xylylN*C*), 147.4 (BDI Ar), 145.3 (BDI Ar), 145.2 (BDI Ar), 143.6 (BDI Ar), 136.7 (xylyl Ar), 130.4 (xylyl Ar), 128.4 (BDI Ar), 128.2 (BDI Ar), 128.0 (BDI Ar), 127.7 (BDI Ar), 127.4 (xylyl Ar), 124.9 (BDI Ar), 124.5 (BDI Ar), 124.4 (BDI Ar), 124.1 (BDI Ar), 108.0 (H*C*(C(Me)NAr)$_2$), 28.4 (H*C*Me$_2$), 28.2 (H*C*Me$_2$), 28.0 (H*C*Me$_2$), 27.9 (H*C*Me$_2$),

27.0 (xylyl Me), 26.5 (HC*Me*$_2$), 26.0 (xylyl Me), 25.7 (HC*Me*$_2$), 25.6 (HC*Me*$_2$), 25.3 (HC*Me*$_2$), 25.2 (HC*Me*$_2$), 25.0 (HC*Me*$_2$), 24.6 (HC*Me*$_2$), 23.1 (HC*Me*$_2$), 18.3 (HC(C(*Me*)NAr)$_2$). IR (nujol): 2201, 2186, 1590, 1552, 1523, 1316, 1289, 1256, 1167, 1101, 1021, 955, 858, 798, 774, 721. Anal. Calcd for $C_{42}H_{60}N_3O_2Cl_2Re$ (**2.2b** • OEt_2): C, 56.30; H, 6.75; N, 4.69. Found: C, 56.04; H, 6.66; N, 4.69.

OReCl$_2$(BDI)(DMAP) (2.2c): A toluene solution of 4-dimethylaminopyridine (DMAP) (17.7 mg, 0.145 mmol in 3 mL) was added to solid **2.1** (100 mg, 0.145 mmol) at room temperature. A color change from dark green to bright red was observed immediately. A small amount of bright red precipitate was observed to form within 2 min of the addition. After being stirred for 30 min, the volatile components of the reaction mixture were removed in vacuo, giving a bright red powder. This powder was dissolved into THF (5 mL), and the resulting solution was filtered and concentrated in vacuo. To this concentrated solution, one volume of pentane (ca. 2 mL) was added immediately prior to storage at -40 ºC. After storage overnight, the product was isolated as bright red blocks. ^{1}H NMR spectroscopy analysis of the isolated crystalline product indicated the presence of cocrystallized THF. Yield: 85 mg, 72%. m.p.: 221 ºC (decomp.). ^{1}H NMR (500 MHz, C_6D_6, 298 K) 7.43 (d, 2H, DMAP Ar), 7.29-7.21 (m, 3H, BDI Ar), 7.19-7.13 (m, 2H, BDI Ar), 7.11 (t, 1H, BDI Ar), 6.96 (d, 2H, DMAP Ar), 4.90 (s, 1H, *H*C(C(Me)NAr)$_2$), 3.97 (sept, 1H, C*H*Me$_2$), 3.88 (sept, 1H, C*H*Me$_2$), 3.41 (sept, 1H, C*H*Me$_2$), 3.23 (sept, 1H, C*H*Me$_2$), 1.98 (s, 9H, DMAP Me and CH*Me*$_2$), 1.93 (s, 3H, HC(C(*Me*)NAr)$_2$), 1.91 (s, 3H, HC(C(*Me*)NAr)$_2$), 1.67 (d, 3H, C*Me*$_2$), 1.45 (d, 3H, C*Me*$_2$), 1.41 (d, 3H, C*Me*$_2$), 1.31 (d, 3H, C*Me*$_2$), 1.20 (d, 3H, C*Me*$_2$), 1.05 (d, 3H, C*Me*$_2$), 0.61 (d, 3H, C*Me*$_2$). ^{13}C NMR (125 MHz, C_6D_6, 298 K) 172.6 (HC(*C*(Me)NAr)$_2$), 155.0 (BDI Ar), 154.5 (BDI Ar), 153.6 (DMAP Ar), 148.4 (BDI Ar), 147.0 (BDI Ar), 146.1 (BDI Ar), 143.8 (BDI Ar), 127.5 (BDI Ar), 127.4 (BDI Ar), 124.6 (DMAP Ar), 124.5 (DMAP Ar), 124.1 (BDI Ar), 123.9 (BDI Ar), 108.7 (H*C*(C(Me)NAr)$_2$), 37.8 (DMAP Me), 28.5 (*C*HMe$_2$), 28.1 (*C*HMe$_2$), 27.8 (*C*HMe$_2$), 27.6 (*C*HMe$_2$), 26.8 (CH*Me*$_2$), 26.2 (CH*Me*$_2$), 26.0 (HC(C(*Me*)NAr)$_2$), 25.8 (HC(C(*Me*)NAr)$_2$), 25.6 (CH*Me*$_2$), 25.5 (CH*Me*$_2$), 25.3 (CH*Me*$_2$), 25.2 (CH*Me*$_2$), 24.7 (CH*Me*$_2$), 23.7 (CH*Me*$_2$). IR (nujol): 1629, 1569, 1540, 1518, 1319, 1280, 1263, 1247, 1236, 1170, 1099, 1064, 1018, 957, 858, 800, 764, 722. Anal. Calcd for $C_{40}H_{59}N_4O_2Cl_2Re$ (**2.2c** • THF): C, 54.28; H, 6.72; N, 6.33. Found: C, 54.48; H, 7.01; N, 6.36.

(ArN)ReCl$_2$(MAD)(PEt$_3$) (2.3)

A solution of **2.1** (250 mg, 0.362 mmol) in toluene (10 mL) was added to a 100 mL thick-walled reaction flask equipped with a threaded Teflon seal. A solution of PEt_3 (214 mg, 1.81 mmol) in toluene (5 mL) was then added to the flask, giving a dark red solution. The flask was then sealed and the reaction mixture was heated to 120 ºC and stirred overnight. Over the course of the reaction, the solution first became a green-yellow color, and eventually turned entirely dark green. After 24 h of heating the reaction mixture was allowed to cool to room temperature. The volatile components of the reaction mixture were removed in vacuo, and the residue was triturated with hexane (2 x 5 mL) before being washed with hexane (5 mL). The remaining emerald green residue was extracted into 40 mL of diethyl ether. These extracts were transferred to a 100 mL Schlenk tube, concentrated in vacuo, and stored at -40 ºC overnight to give complex **2.3** as emerald green crystals. Yield: 73 mg, 26%. m.p.: 184-5 ºC. ^{1}H NMR (500 MHz, C_6D_6, 298 K) 7.31 (d, 1H, Ar),

7.12-7.02 (m, 3H, Ar), 6.83 (d, 1H, Ar), 6.77 (s, 1H, MAD CH), 4.21 (sept, 1H, C*H*Me$_2$), 3.90 (sept, 1H, C*H*Me$_2$), 3.18 (sept, 1H, C*H*Me$_2$), 3.14 (s, 3H, MAD Me), 2.46 (sept, 1H, C*H*Me$_2$), 2.17-1.99 (m, 6H, P(C*H*$_2$CH$_3$)$_3$), 1.91 (s, 3H, MAD Me), 1.80 (d, 3H, CHMe$_2$), 1.17 (d, 3H, CHMe$_2$), 1.15 (d, 3H, CHMe$_2$), 1.11 (d, 3H, CHMe$_2$), 1.09 (d, 3H, CHMe$_2$), 1.05 (d, 3H, CHMe$_2$), 0.97 (quint, 9H, P(CH$_2$C*H*$_3$)$_3$), 0.84 (d, 3H, CHMe$_2$), 0.52 (d, 3H, CHMe$_2$). ^{13}C NMR (150 MHz, C_6D_6, 298 K) 189.54 (HC(*C*)NAr(Me)), 146.65 (Ar), 145.75 (Ar), 145.28 (Ar), 143.32 (Me(C)*C*H(C)NAr(Me)), 142.18 (Ar), 141.10 (Ar), 127.51 (Ar), 127.08 (Ar), 126.18 (Ar), 124.96 (Ar), 124.84 (Ar), 122.97 (Ar), 42.46 (*Me*(C)CH(C)NAr(Me)), 33.24 (Me(*C*)CH(C)NAr(Me)), 28.41 (*C*H(Me)$_2$), 28.35 (*C*H(Me)$_2$), 27.49 (*C*H(Me)$_2$), 26.89 (*C*H(Me)$_2$), 26.65 (CH(*Me*)$_2$), 26.21 (CH(*Me*)$_2$), 26.16 (CH(*Me*)$_2$), 25.41 (CH(*Me*)$_2$), 24.14 (CH(*Me*)$_2$), 23.57 (CH(*Me*)$_2$), 23.37 (CH(*Me*)$_2$), 22.54 (CH(*Me*)$_2$), 21.65 (Me(C)CH(C)NAr(*Me*)), 19.37 (d, P(*C*H$_2$CH$_3$)$_3$, J = 30.7 Hz), 8.73 (d, P(CH$_2$*C*H$_3$)$_3$, J = 4.8 Hz). ^{31}P NMR (162 MHz, C_6D_6, 298 K): -28.2. IR (Nujol): 1585, 1558, 1510, 1261, 1098, 1036, 796, 760. Anal. Cald for $C_{35}H_{56}N_2PCl_2Re$ (**2.3**): C, 53.02; H, 7.12; N, 3.53. Found: C, 52.83; H, 7.18; N, 3.61.

Observation of OReCl$_2$(BDI)(MeCN) (2.2d): In the glovebox, 15 mg of **2.1** was placed in a standard NMR tube. The NMR tube was then removed from the glovebox and, making no efforts to exclude air or water, ca. 0.75 mL of *d3*-MeCN was added to the tube. Dissolution of **2.1** immediately gave a dark red solution that could be characterized by ^{1}H NMR spectroscopy, revealing a single BDI-containing product, which was inferred to be **2.2d**. ^{1}H NMR (500 MHz, D_3CCN, 298 K): 7.25-7.29 (m, 2H, BDI Ar), 7.21-7.24 (m, 4H, BDI Ar), 5.50 (s, 1H, C*H*(C(Me)NAr)$_2$), 2.94-3.09 (bm, 2H, C*H*Me$_2$), 2.72, (sept, 2H, J = 6.7 Hz, C*H*Me$_2$), 2.00 (s, 6H, CH(C(*Me*)NAr)$_2$), 1.06-1.24 (m, 24H, CH*Me*$_2$).

Observation of OReCl$_2$(BDI)(OPEt$_3$) (2.2e): A solution of OPEt$_3$ (3.5 mg, 1.75 equiv.) in ca. 0.5 mL of C_6D_6 was added to an NMR tube containing solid **2.1** (10.0 mg, 1 equiv.), upon which a bright red solution was obtained, which was a clear indicator of adduct formation. NMR spectroscopic data were obtained for this solution. The ^{1}H NMR spectrum was found to be broad and of little diagnostic value, though the ^{31}P NMR spectrum was found to contain a single, sharp peak (in addition to that observed for excess OPEt$_3$) which corresponded to an identical shift observed in other experiments. ^{31}P NMR (162 MHz, C_6D_6, 298 K): 86.3.

OReCl$_2$(BDI)(PMe$_3$) (2.2f): In order to verify the identity of this compound after it was isolated following our attempts at observing OAT between **2.1** and PMe$_3$ in conditions analogous to those used for the NMR experiments with PEt$_3$, a targeted, room temperature preparation was conducted as follows: To a solution of **2.1** (50.0 mg, 0.0724 mmol) in toluene (8 mL) was added PMe$_3$ (ca. 0.1 mL, ca. 1 mmol) to immediately give a dark red solution. The solution was stirred for 10 minutes, after which time the volatile components of the reaction mixture were removed in vacuo. The residue was extracted into Et$_2$O (10 mL) and these extracts were filtered through Celite. Concentration of the filtered extracts to approx. 2 mL and storage at -40 ^{o}C yielded **2.2f** as a bright red powder. Yield: 22.4 mg, 40%. m.p.: 141-142 ^{o}C. ^{1}H NMR (500 MHz, C_6D_6, 298 K): 7.31 (dd, 1H, J = 1.1, 7.3 Hz, BDI Ar), 7.24 (t, 1H, J = 7.5 Hz, BDI Ar), 7.18 (dd, 1H, J = 1.2, 7.6 Hz, BDI Ar), 7.08 (dd, 1H, J = 1.4, 7.5 Hz, BDI Ar), 7.01 (dd, 1H, J = 1.5, 7.7 Hz, BDI Ar), 6.96 (t, 1H, J = 7.8 Hz, BDI Ar), 5.06 (s, 1H, C*H*(C(Me)NAr)$_2$), 3.72 (sept, 1H, J = 6.5 Hz, C*H*Me$_2$), 3.61 (sept,

1H, *J* = 6.5 Hz, C*H*Me$_2$), 3.13 (sept, 1H, *J* = 6.6 Hz, C*H*Me$_2$), 3.08 (sept, 1H, *J* = 6.6 Hz, C*H*Me$_2$), 1.83 (s, 3H, CH(C(*Me*)NAr)$_2$), 1.69 (s, 3H, CH(C(*Me*)NAr)$_2$), 1.66 (d, 3H, *J* = 6.6 Hz, CH*Me*$_2$), 1.44 (d, 3H, *J* = 6.6 Hz, CH*Me*$_2$), 1.29 (d, 3H, *J* = 6.5 Hz, CH*Me*$_2$), 1.27 (d, 3H, *J* = 6.1 Hz, CH*Me*$_2$), 1.26 (d, 3H, *J* = 6.1 Hz, CH*Me*$_2$), 1.19 (d, 3H, *J* = 6.8 Hz, CH*Me*$_2$), 1.07 (d, 3H, *J* = 6.7 Hz, CH*Me*$_2$), 1.00 (d, 3H, *J* = 6.8 Hz, CH*Me*$_2$), 0.87 (d, 9H, *J* = 10.4 Hz, P*Me*$_3$). ^{31}P NMR (162 MHz, C_6D_6, 298 K): -48.0.

X-Ray Crystallographic Methods: X-ray diffraction data for **2.2a** and **2.2c** were collected at CheXray, Berkeley, CA, using a Bruker APEX II QUAZAR instrument outfitted with a monochromated Mo-K_α radiation source (λ = 0.71073 Å). Diffraction data for **2.1** and **2.3** were obtained at the Advanced Light Source (ALS), (Lawrence-Berkeley National Laboratory, Berkeley, CA) station 11.3.1 using a silicon monochromated beam of 16 keV (λ = 0.7749 Å) radiation. All data collections were conducted at 100 K. Absorption corrections were carried out by a multi-scan method, utilizing the SADABS program.[50] Bruker APEX2 (CheXray) and APEX3 (ALS) software were used for the data collection, while Bruker SAINT V8.34A (CheXray) and V8.37A (ALS) software conducted the cell refinement and data reduction procedures.[51] Initial structure solutions were found using direct methods (SHELXT) and were refined by SHELXL-2014.[52-53] The structure for **2.2c** required use of the SQUEEZE protocol in PLATON to remove disordered, partial occupancy solvent (THF/pentane) from the cell that could not otherwise be modelled.[54] Structures have been deposited to the CCDC, with numbers 1502206 (**2.1**), 1502207 (**2.3**), 1502208 (**2.2c**), and 1502209 (**2.2a**).

Table 2.1. Crystallographic details for compounds **2.1**, **2.2a**, **2.2c**, and **2.3**.

	2.1 · Et_2O	**2.2a**	**2.2c**	**2.3**
Chemical formula	$C_{33}H_{51}N_2O_2Cl_2Re$	$C_{38}H_{63}N_2OPCl_2Re$	$C_{36}H_{51}N_4OCl_2Re$	$C_{35}H_{56}N_2PCl_2Re$
Formula weight	764.89	851.97	812.90	792.88
Color, habit	Green, plate	Red, plate	Orange, plate	Green, block
Temperature (K)	100(2)	100(2)	100(2)	100(2)
Crystal system	Orthorhombic	Monoclinic	Monoclinic	Triclinic
Space group	P $2_12_12_1$	P $2_1/n$	P $2_1/n$	P -1
a (Å)	8.874(4)	9.8643(7)	10.3198(4)	12.029(2)
b (Å)	18.951(9)	22.9718(19)	19.0859(7)	14.262(3)
c (Å)	20.467(9)	17.4389(14)	22.2086(9)	22.800(5)
α (°)	90	90	90	107.39(3)
β (°)	90	93.440(4)	100.516(2)	105.24(3)
γ (°)	90	90	90	90.02(3)
V ($Å^3$)	3442(3)	3944.5(5)	4300.8(3)	3588.0(15)
Z	4	4	4	4
Density (Mg m^{-3})	1.476	1.435	1.255	1.468
F(000)	1552	1748	1648	1616
Radiation Type	Synchrotron	MoK_α	MoK_α	Synchrotron
μ (mm^{-1})	4.542	3.287	2.977	4.409
Crystal size	0.090 x 0.040 x 0.010	0.140 x 0.080 x 0.030	0.100 x 0.030 x 0.020	0.040 x 0.030 x 0.020
Meas. Refl.	61894	57346	80266	62468
Indep. Refl.	16389	7263	7941	33584
R(int)	0.0399	0.0915	0.1057	0.0492
Final R indices	R = 0.0255	R = 0.0378	R = 0.0417	R = 0.0495
[I > 2σ(I)]	R_w = 0.0583	R_w = 0.0808	R_w = 0.778	R_w = 0.1494
Goodness-of-fit	1.071	1.029	1.021	1.160
$\Delta\rho_{max}$, $\Delta\rho_{min}$ (e $Å^{-3}$)	3.824, -1.605	1.686, -1.423	1.216, -0.724	3.648, -5.814
Flack parameter	0.056(3)	n/a	n/a	n/a

General Procedure for Kinetic Experiments: For each reaction conducted for the kinetic studies, a solid mixture of **2.1** (10.1 mg, 0.0145 mmol) combined with 1,3,5-trimethoxybenzene (1-1.5 mg) was dissolved into ca. 0.5 mL of toluene-*d*8. To this solution was then added a varying amount of neat PEt_3 (either approx. 2.3 eq. or 10 eq. as determined by ^1H NMR spectra of the unheated reaction mixtures). These additions immediately caused a change in color of the solution from dark green to dark red, indicative of the quantitative formation of **2.2a** (which was also verified by ^1H NMR spectroscopy). The reaction mixtures were then heated in an aluminum heating block at 120 °C, and their progress was monitored twice over the proceeding ~5 hours, which clearly showed the consumption of **2.2a**, as well as the production of protonated ligand, H(BDI), and the formation

of complex **2.3**. While a quantitative kinetic analysis was precluded by the complex mixture of products observed, these experiments demonstrated that the rate of OAT from **2.1** has some clear dependence on [PEt_3].

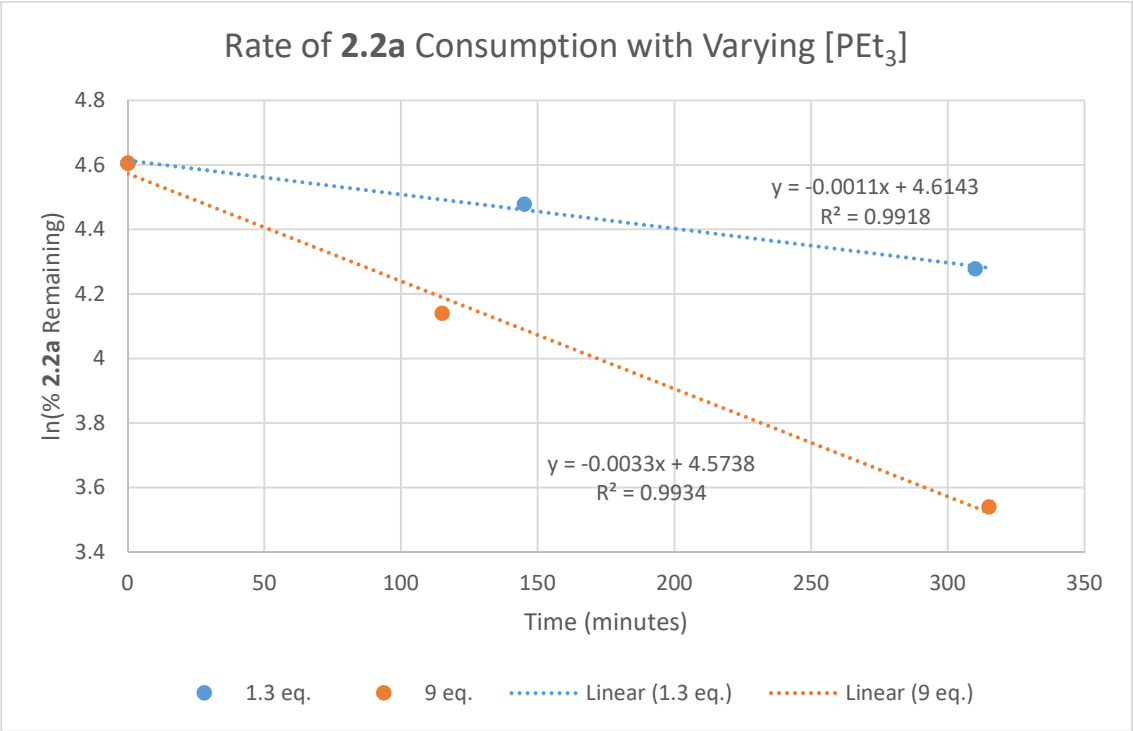

Figure 2.6 Plot of the consumption of **2.2a** versus time for the kinetic experiments with varying amounts of free PEt_3. The vertical axis shows values for ln(% **2.2a**) remaining. The distinct difference in rate is apparent in the differing slopes of the linear best fit lines for each of the reactions.

Notes and References

(1) Nugent, W. A.; Mayer, J. M. *Metal-Ligand Multiple Bonds*; Wiley: New York, 1988.
(2) Mayer, J. M. *Acc. Chem. Res.* **1998**, *31*, 441.
(3) Shaik, S.; Chen, H.; Janardanan, D. *Nat. Chem.* **2011**, *3*, 19.
(4) Hohenberger, J.; Ray, K.; Meyer, K. *Nat. Commun.* **2012**, *3*, 720.
(5) Sousa, S. C. A.; Fernandes A. C. *Coord. Chem. Rev.* **2015**, *284*, 67.
(6) Raju, S.; Moret, M.; Klein Gebbnik, R. J. M. *ACS Catal.* **2015**, *5*(1), 281.
(7) Shiramizu, M.; Toste, F. D. *Angew. Chem. Int. Ed.* **2013**, *52*, 12905.
(8) Cook, G. K.; Andrews, M. A. *J. Am. Chem. Soc.* **1996**, *118*, 9448.
(9) Nolin, K. A.; Ahn, R. W.; Toste, F. D. *J. Am. Chem. Soc.* **2005**, *127*, 12462.
(10) Ison, E. A.; Trivedi, E. R.; Corbin, R. A.; Abu-Omar, M. M. *J. Am. Chem. Soc.* **2005**, *127*, 15374.
(11) Sherry, B. D.; Radosevich, A. T.; Toste, F. D. *J. Am. Chem. Soc.* **2003**, *125*, 6076.
(12) Kennedy-Smith, J. J.; Nolin, K. A.; Gunterman, H.P.; Toste, F. D. *J. Am. Chem. Soc.* **2003**, *125*, 4056.

(13) Raju, S.; van Slagmaat, C. A. M. R.; Li, J.; Lutz, M.; Jastrzebski, J. T. B. H.; Moret, M.-E.; Klein Gebbnik, R. J. M. *Organometallics* **2015**, *35*, 2178.
(14) Kasner, G. R.; Boucher-Jacobs, C.; McClain II, J. M.; Nicholas, K. M. *Chem. Commun.* **2016**, *52*, 7257.
(15) Betley, T. A.; Wu, Q.; Voorhis, T. V.; Nocera, D. G. *Inorg. Chem.* **2008**, *47* (6), 1849.
(16) Mayer, J. M.; Thorn, D. L.; Tulip, T. H. *J. Am. Chem. Soc.* **1985**, *107*, 7454.
(17) Spaltenstein, E.; Conry, R. R.; Critchlow, S. C.; Mayer, J. M. *J. Am. Chem. Soc.* **1989**, *111*, 8741.
(18) Cundari, T. R., Conry, R. R.; Spaltenstein, E.; Critchlow, S. C.; Hall, K. A.; Tahmassebi, S. K.; Mayer, J. M. *Organometallics* **1994**, *13*, 322.
(19) Smeltz, J. L.; Lilly, C. P.; Boyle, P. D.; Ison E. A. *J. Am. Chem. Soc.* **2013**, *135* (25), 9433.
(20) Green, S. P.; Jones, C.; Stach, *Science* **2007**, *318*, 1754.
(21) Cui, C.; Roesky, H. W.; Schmidt, H.-G.; Noltemeyer, M.; Hao, H.; Cimpoesu, F. *Angew. Chem. Int. Ed.* **2000**, *39*, 4274.
(22) Bourget-Merle, L.; Lappert, M. F.; Severn, J. R. *Chem. Rev.* **2002**, *102*, 3031.
(23) Basuli, F.; Bailey, B. C.; Brown, D.; Tomaszewski, J.; Huffman, J. C.; Baik, M.-H.; Mindiola, D. J. *J. Am Chem. Soc.* **2004**, *126*, 10506.
(24) Cowley, R. E.; Eckert, N. A.; Vaddadi, S.; Figg, T. M.; Cundari, T. R.; Holland, P. L. *J. Am. Chem. Soc.* **2011**, *133*, 9796.
(25) Hohloch, S.; Kriegel, B. M.; Bergman, R. G.; Arnold, J. *Dalton Trans.* **2016**, *45*, 15725.
(26) Yempally, V.; Fan, W. Y.; Arndtsen, B. A.; Bengali, A. A. *Inorg. Chem.* **2015**, *54* (23), 11441.
(27) Tomson, N. C.; Arnold, J.; Bergman R. G. *Organometallics* **2010**, *29*, 2926.
(28) Tomson, N. C.; Arnold, J.; Bergman R. G. *Dalton Trans.* **2011**, *40*, 7718.
(29) Gianetti, T. L.; Tomson, N. C.; Arnold, J.; Bergman R. G. *J. Am. Chem. Soc.* **2011**, *133*, 14904.
(30) Gianetti, T. L.; Bergman, R. G.; Arnold, J. *J. Am. Chem. Soc.* **2013**, *135*, 8145.
(31) Gianetti, T. L.; Bergman, R. G.; Arnold, J. *Chem. Sci.* **2014**, *5*, 2517.
(32) Kriegel, B. M.; Bergman, R. G.; Arnold, J. *Dalton Trans.* **2014**, *43*, 10046.
(33) Gianetti, T. L.; Bergman, R. G.; Arnold, J. *Polyhedron* **2014**, *84*, 19.
(34) Nechayev, M.; Kriegel, B. M.; Gianetti, T. L.; Bergman, R. G.; Arnold, J. *Inorg. Chim. Acta* **2014**, *422*, 114.
(35) Camp, C.; Maron, L.; Bergman, R. G.; Arnold, J. *J. Am. Chem. Soc.* **2014**, *136*, 17652.
(36) Nechayev, M.; Gianetti, T. L.; Bergman, R. G.; Arnold, J. *Dalton Trans.*, **2015**, *44*, 19494.
(37) Kriegel, B. M.; Bergman, R. G.; Arnold, J. *J. Am. Chem. Soc.* **2016**, *138*, 52.
(38) Camp, C.; Grant, L. N.; Bergman, R. G.; Arnold, J. *Chem. Commun.* **2016**, *52*, 5538.
(39) Ziegler, J. A.; Bergman, R. G.; Arnold, J. *Dalton Trans.* **2016**, *45*, 12661.
(40) Ozerov, O. V.; Gerard, H. F.; Watson, L. A.; Huffman, J. C.; Caulton, K. G. *Inorg. Chem.* **2002**, *41*, 5615.
(41) Ozerov, O. V.; Watson, L. A.; Pink, M.; Caulton, K. G. *J. Am. Chem. Soc.* **2004**, *126* (20), 6363.
(42) Harris, S. E.; Orpen, A. G.; Bruno, I. J.; Taylor, R. *J. Chem. Inf. Model.* **2005**, *45* (6), 1727.

(43) Obenhuber, A. H.; Gianetti, T. L.; Berrebi, X.; Bergman, R. G.; Arnold, J. *J. Am. Chem. Soc.* **2014**, *136* (8), 2994.
(44) Obenhuber, A. H.; Gianetti, T. L.; Bergman, R. G.; Arnold, J. *Chem. Commun.* **2015**, *51*, 1278.
(45) For a recent review of all known modes of non-innocent reactivity of the BDI ligand see: Camp, C.; Arnold J. *Dalton Trans.* **2016**, *45*, 14462.
(46) Ison, E. A.; Cessarich, J. E.; Travia, N. E.; Fanwick, P. E.; Abu-Omar, M. M. *J. Am. Chem. Soc.* **2007**, *129* (5), 1167.
(47) Travia, N. E.; Xu, Z.; Keith, J. M.; Ison, E. A.; Fanwick, P. E.; Hall, M. B.; Abu-Omar, M. M. *Inorg. Chem.* **2011**, *50* (20), 10505.
(48) Parshall, G. W.; Shive, L. W.; Cotton, F. A. *Inorg. Synth.* **1977**, *17*, 110.
(49) Smith, J. M.; Lachicotte, R. J.; Holland, P. L. *Chem. Commun.* **2001**, *17*, 1542.
(50) Bruker. SADABS. Bruker AXS Inc., Madison, Wisconsin, USA.
(51) Bruker. APEX2, APEX3, and SAINT. Bruker AXS Inc., Madison, Wisconsin, USA.
(52) Sheldrick, G. M. A Short History of *SHELX*. *Acta Cryst.* **2008**, A**64**, 112.
(53) Farrugia, L. J. *J. Appl. Cryst.* **2012**, *45*, 849.
(54) Spek, A. L. *Acta Cryst.* **2009**, D**65**, 148.

Chapter 3

Olefin-Supported Rhenium(III) Terminal Oxo Complexes Generated by Nucleophilic Addition to a Cyclopentadienyl Ligand

Introduction

Transition metal oxo complexes have been a long-standing area of research due to their highly variable reactivity and their implication in numerous catalytic and enzymatic transformations.[1-4] While nearly all stable oxo complexes contain transition metal centers with electron configurations of d^2 or less, some examples of terminal oxo complexes containing metal centers with configurations of d^3 and greater have also been accessed, both as isolable complexes[5-19] and as species that can only be characterized in solution prior to their decomposition.[8-10] The scarcity of such compounds is mainly due to their instability, as well as a lack of reliable synthetic routes to access them. Previous work by Mayer and coworkers uncovered a facile route to robust d^4 terminal oxo complexes of Re(III) supported by π-accepting acetylene moieties.[11-17] Here, we present a route to a new Oooooclass of thermally-stable, olefin-supported d^4 Re(III) terminal oxo complexes containing a sterically encumbering β-diketiminate ligand. Furthermore, we demonstrate this route exploits the uncommon electrophilic behavior of a bound cyclopentadienide (Cp) ligand.

Results and Discussion

We have reported the synthesis of the oxo rhenium N,N'-bis(2,6-diisopropylphenyl)-2,4-dimethyl-β-diketiminate (BDI) complex, $OReCl_2(BDI)$.[20] Subsequently, we became interested in functionalizing this complex with carbanion ligands by salt metathesis. While the reactions of metal alkyl reagents with $OReCl_2(BDI)$ gave intractable mixtures of products, it was found that the reaction of $OReCl_2(BDI)$ with diphenylmagnesium ($MgPh_2$) forms the diphenyl complex $OrePh_2(BDI)$ (**3.1**; Scheme 3.1). The structure of **3.1** was confirmed by X-ray crystallography (See Experimental). Preliminary experiments indicated **3.1** is a relatively inert compound poorly suited for reactivity studies. For example, no reaction between **3.1** and triethylphosphine or H_2 was observed even at elevated temperatures. Thus, with the hope of forming a more reactive compound, we shifted our focus to functionalizing $OReCl_2(BDI)$ with the Cp ligand.

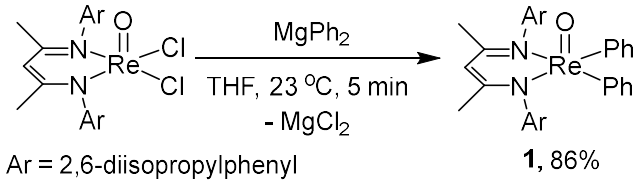

Scheme 3.1 Synthesis of complex **3.1** by a salt metathesis route.

The reaction of $OReCl_2(BDI)$ with NaCp was hypothesized to yield a κ^1-BDI complex similar to that described in an analogous niobium imido system.[21] However, we instead found that this reaction gave the dark green, terminal oxo complex $ORe(\eta^2\text{-DHF})(BDI)$ (**3.2**; DHF = dihydrofulvalene; Scheme 3.2). Complex **3.2** was also isolated after $OReCl_2(BDI)$ was stirred in THF with excess TlCp for one week. A scalable route to **3.2** was developed, which utilizes an excess of NaCp and a short reaction time.

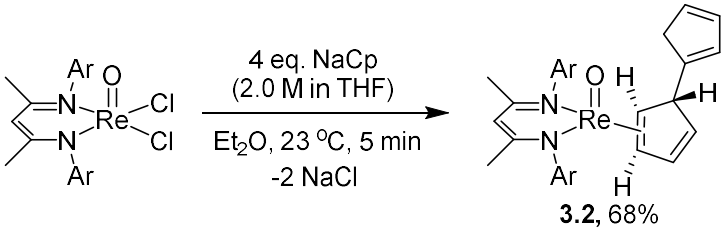

Scheme 3.2 Coupling of cyclopentadienide anions leads to reduction of rhenium to form the d^4 terminal oxo complex **3.2**.

Complex **3.2** is an intriguing compound on several fronts. First, it represents a rare instance of an oxo olefin complex.[22-25] Second, **3.2** is a very uncommon example of a terminal oxo complex of a d^4 Re(III) center.[11-19] Similar examples of NaCp acting as a sequential reductant and trapping agent can be found in the literature.[26,27] In one canonical report by Wilkinson and coworkers, it was found that the reaction of $ReCl_5$ with NaCp led to the formation of the Re(III) complex Cp_2ReH, as well as, presumably, an equivalent of coupled Cp (i.e. DHF).[28]

The X-ray crystal structure of **3.2** shows approximate tetrahedral geometry about the metal center, with nearly symmetric binding to the two carbons atoms of the bound olefin (Figure 3.1). The rhenium oxo bond length is slightly extended from that observed in $OReCl_2$(BDI) (1.692(3) Å vs. 1.670(2) Å).[20] Also, the C-C bond length of the bound olefin is 1.462(6) Å, which is expected as a high degree of π-backbonding likely forms the basis of its interaction with Re.

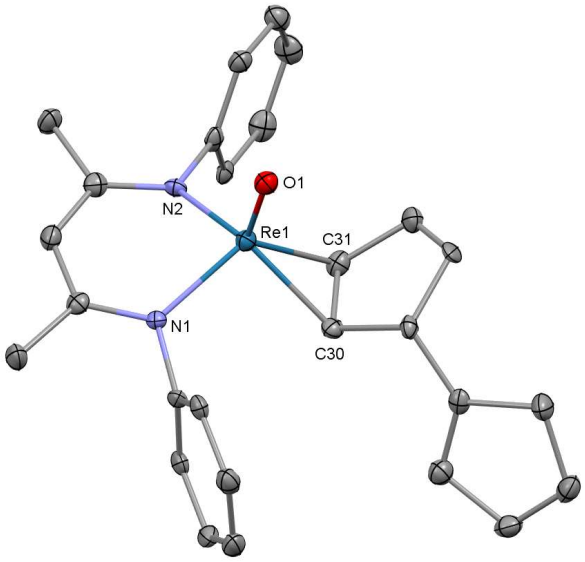

Figure 3.1 Crystal structure of **2** with 50% probability ellipsoids. H atoms and isopropyl groups are excluded for clarity. Selected distances (Å) and angles (°): Re1-O1 = 1.692(3), Re1-N1 = 2.028(4), Re1-N2 = 2.054(4), Re1-C30 = 2.101(6), Re1-C31 = 2.111(5), C30-C31 = 1.462(6), N1-Re1-N2 = 87.48(15).

While single crystals of **3.2** studied by X-ray diffraction were found to contain a single isomer of the DHF fragment, tautomerization results in a second set of signals in the ^{1}H NMR spectrum. As synthesized, samples of **3.2** can contain both tautomers, though one has been found to predominate in crystallized samples. Heating solutions of **3.2** eventually led to an approximate 1:1 ratio of the two tautomers, as observed by ^{1}H NMR spectroscopy. The presence of this second tautomer in samples of **3.2** does not affect the results of elemental analyses. It is worth noting that the facile tautomerization of DHF is a well-known phenomenon.[29]

The ^{1}H NMR spectrum of **3.2** indicates the complex is diamagnetic, though a high degree of fluxionality was observed in the DHF fragment: an extremely broad feature spans the entirety of the vinyl and methine regions. Upon cooling a toluene-*d8* solution of **3.2** to -50 °C, the ^{1}H NMR spectrum greatly resolves and all resonances of the DHF fragment can be observed. Fortunately, the apparent symmetry of the BDI ligand and the several signals from the bound DHF observed in the room temperature ^{1}H NMR data are sufficient for determining the purity of samples of **3.2**.

In order to model the electronic structure of **3.2**, density functional theory (DFT) calculations were conducted using *Gaussian09*.[30] In the optimized gas-phase structure of **3.2**, the HOMO-1 has π-backbonding character between the a rhenium 5*d* orbital and the olefin π^* orbital (Figure 3.2). This molecular orbital also appears to have some amount of lone pair density localized on the oxo moiety. After establishing the nature of the bonding between Re and DHF in **3.2**, we turned back to synthetic experiments in hope of better understanding the reaction that leads to this interesting complex.

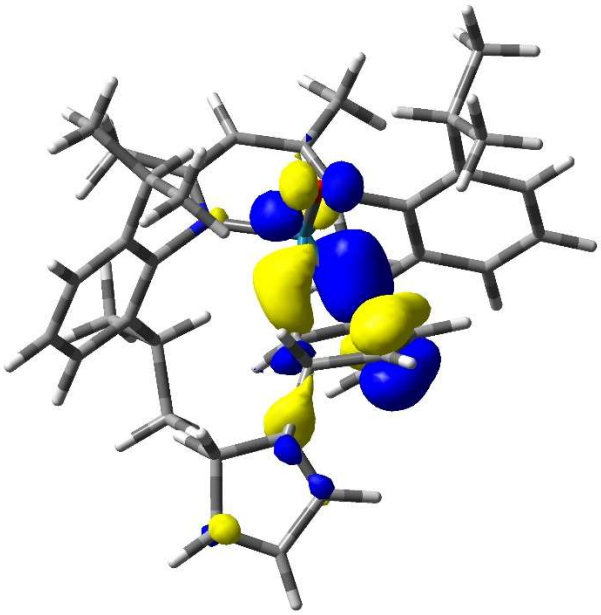

Figure 3.2 DFT-optimized gas-phase structure of **3.2** with its calculated HOMO-1 surface (isovalue = 0.05).

We sought to determine if the coupling reactivity that presumably leads to the DHF ligand in **3.2** could extend to other carbanions, which required the synthesis of an intermediate in the

reaction that leads to **3.2**. In pursuit of this intermediate, $OReCl_2(BDI)$ was combined with stannocene ($SnCp_2$), a non-polar Cp source, in toluene. The reaction formed a dark red precipitate, which was determined to be the salt $[ORe(\eta^5\text{-}Cp)(BDI)][SnCl_3]$ (**3.3a**; Figure 3.3). It was hypothesized that the Lewis acidity and open coordination site of Sn(II) are what abate the coupling reaction to form DHF, and that $[ORe(\eta^5\text{-}Cp)(BDI)]^+$ (**3.3**$^+$) was an intermediate along the pathway to **3.2**. We found that **3.3a** is best prepared on a larger scale using a combination of $SnCp_2$ and $SnCl_2$ in Et_2O (Scheme 3.3). Considering the reactive nature of the $SnCl_3^-$ anion, we pursued a route to salts of **3.3**$^+$ that contain other anions. The reaction of **3.3a** with $Ag(PF_6)$ readily gave $[ORe(\eta^5\text{-}Cp)(BDI)][PF_6]$ (**3.3b**, see Experimental). We were also able to efficiently access a new salt of **3.3**$^+$ with a two-pot procedure, involving salt metathesis of the starting material $OReCl_2(BDI)$ with Ag(OTf) (OTf = trifluoromethanesulfonate) prior to its reaction with $SnCp_2$ to give $[ORe(\eta^5\text{-}Cp)(BDI)][OTf]$ (**3.3c**).

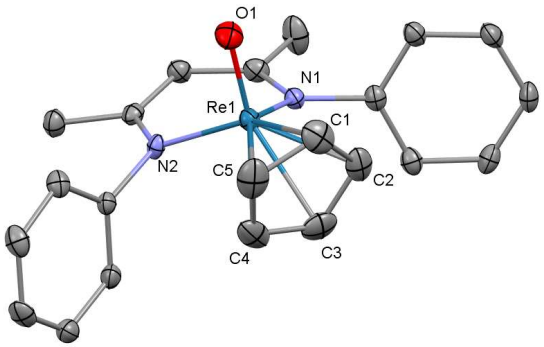

Figure 3. Crystal structure of **3.3**$^+$ as found in **3.3a** with 50% probability ellipsoids. The $SnCl_3^-$ anion, BDI isopropyl groups, and H atoms are excluded for clarity. Selected distances (Å) and angles (°): Re1-O1 = 1.693(2), Re1-N1 = 2.040(3), Re1-N2 = 2.033(3), Re1-Cp(centroid) = 2.008(2), N1-Re1-N2 = 85.39(10).

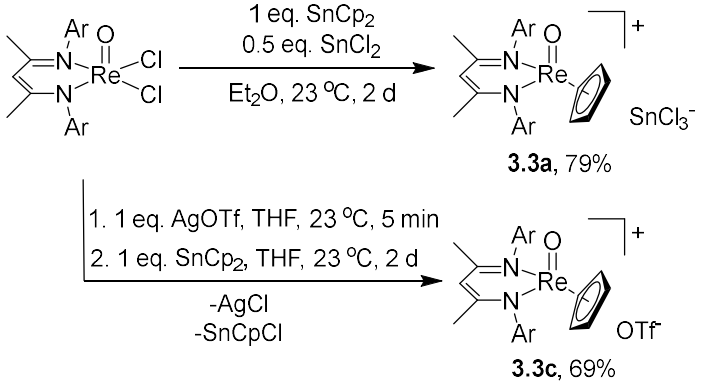

Scheme 3.3 Routes to salts of the cation **3.3**$^+$ using stannocene ($SnCp_2$) as a transfer agent.

The ability to synthesize **3.3c** allowed us to study the reactivity of **3**$^+$. We found the reaction of NaCp with **3.3c** readily gave **3.2**, as confirmed by ^{1}H NMR spectroscopy. Furthermore, we found that the reactions of **3.3c** with fluorenyl potassium (Fl-K) or Cp*K (Cp* = pentamethylcyclopentadienide) resulted in coupling to the bound Cp ligand of **3.3**$^+$ to form

ORe(η^2-Cp-Fl)(BDI) (**3.4**; Cp-Fl = (9-fluorenyl)cyclopentadiene), and ORe(η^2-Cp-Cp*)(BDI) (**3.5**; Cp-Cp* = pentamethylcyclopentadienyl cyclopentadiene) respectively (Scheme 3.4). While **3.4** could be isolated by crystallization from Et_2O, the extremely high solubility of **3.5**, even in hexamethyldisiloxane (HMDSO), only led to the isolation of impure crystalline material, from which single crystals of **5** could be selected for analysis.

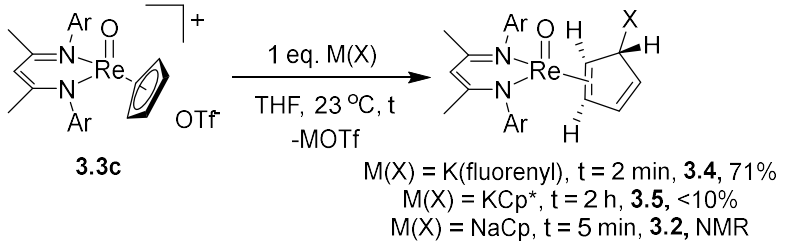

Scheme 3.4 Reactions of **3.3c** with aromatic anion salts yields a series of olefin-supported rhenium(III) terminal oxo complexes.

The successful formation of **3.2**, **3.4**, and **3.5** from **3.3c** by salt metathesis provided insight into the formation of **3.2** from $OReCl_2(BDI)$ using NaCp. Namely, **3.3**$^+$ likely forms transiently in solution with chloride as a counterion after the reaction of $OReCl_2(BDI)$ with one equivalent of NaCp. Subsequently the counterion to **3.3**$^+$ is removed by the added alkali cation as a salt, leaving an unstable ion pair (the nucleophilic Cp anion and the electrophilic **3.3**$^+$ cation) in solution, which then combine to form the neutral Re(III) oxo complex **3.2**. Thus, in the syntheses of **3.4** and **3.5**, K(Fl) and KCp* are simply acting as the second equivalent of NaCp would in our initial syntheses of **3.2**.

We also studied the reactivity of **3.3c** with other nucleophiles, and found that the use of PMe_3 (trimethylphosphine) led to the formation of the Re(III) oxo complex, [ORe(η^2-Cp-PMe_3)(BDI)][OTf] (**3.6**; Cp-PMe_3 = cyclopentadienyltrimethylphosphonium, Scheme 3.5). This result aligns with previous studies of electrophilic Cp complexes.[31] Likewise, harder nucleophiles, like organolithium or magnesium reagents, led to intractable mixtures of products in which some amounts of **3.2** could be identified. We found **3.3c** also reacted readily with both $NaBH_4$ and NaN_3, but the high solubility of the products prevented their purification and full characterization.

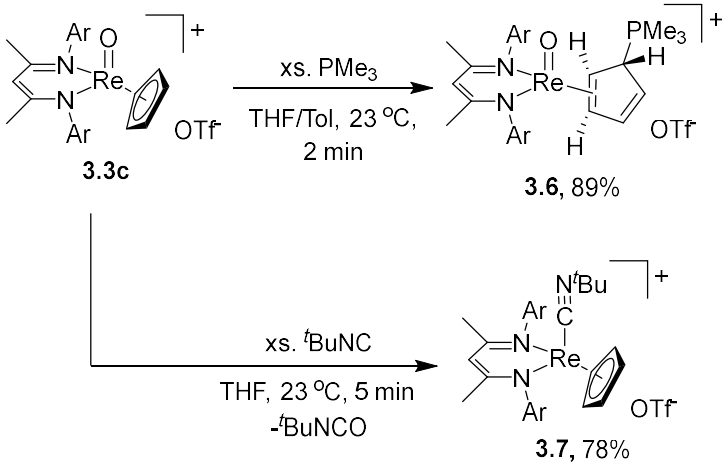

Scheme 3.5 Divergent reactivity of **3.3c** with neutral nucleophiles.

Structural determination of **3.4**, **3.5**, and **3.6** by X-ray crystallography revealed that identically to **3.2**, these complexes contain a Re center bound to one of the olefin moieties of a neutral, substituted Cp ring (Figure 3.4, see Experimental). As observed in canonical examples of nucleophilic addition to unsaturated hydrocarbon ligands, only *exo* isomers of the substituted Cp ligand were observed.[32]

In contrast, we found that rather than attack at the bound Cp ligand of **3.3**$^+$, ^{t}BuNC (*tert*-butylisocyanide) reacted at the oxo moiety, producing an equivalent of ^{t}BuNCO (*tert*-butylisocyanate) by oxygen atom transfer (OAT) prior to coordination of a second equivalent of ^{t}BuNC to give the Re(III) salt [Re(η^5-Cp)(^{t}BuNC)(BDI)][OTf] (**3.7**, Scheme 3.5). The structure of **3.7** was confirmed by X-ray crystallography, and a distinct IR absorbance at 2109 cm^{-1} for the bound isocyanide was also measured. The formation of **3.7** is intriguing in that no OAT was observed in the reaction of **3.3c** with PMe_3, a potent oxygen atom acceptor, whereas ^{t}BuNC has an entirely different selectivity. Previous examples of electrophilic Cp complexes did not contain oxo moieties, nor was their reactivity with isocyanides probed. However, OAT from reactive metal oxo species to isocyanides is a known reaction.[33] OAT from **3.3c** to CO was not observed, even with prolonged heating. Regardless, the divergent reactivity of **3.3c** to generate **3.6** and **3.7** indicates that the frontier orbitals of **3.3**$^+$ likely contain character from both the oxo and the Cp moieties. In order to test this hypothesis, we again turned to DFT calculations.

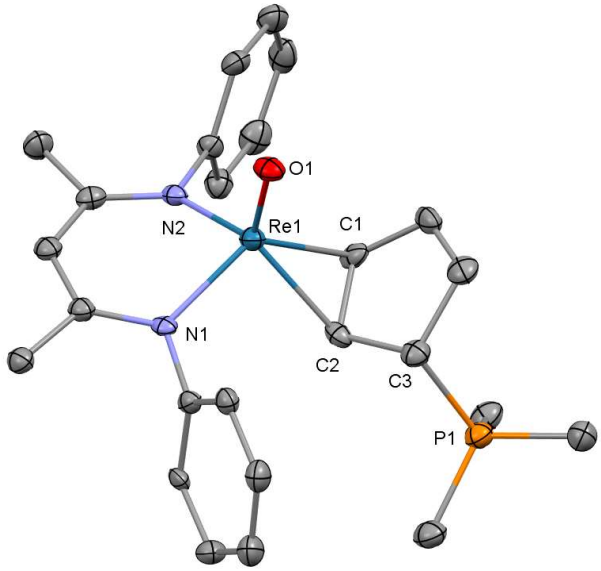

Figure 3.4 Crystal structure of the cationic portion of **3.6** with 50% probability ellipsoids. Anion, solvent, isopropyl, and H atoms have been excluded for clarity. Selected distances (Å) and angles (°): Re1-O1 = 1.685(5), Re1-N1 = 2.041(5), Re1-N2 = 2.032(3), Re1-C1 = 2.094(6), Re1-C2 = 2.125(7), C1-C2 = 1.490(9), C2-C3 = 1.529(7), C3-P1 = 1.830(8), N1-Re1-N2 = 89.02(17).

A DFT-optimized gas phase structure of **3.3**$^+$ was obtained (as was done for **3.2**) using *Gaussian09*, and surfaces for the frontier molecular orbitals of this structure were calculated (Figure 3.5).[30] We found that both the HOMO and LUMO of **3.3**$^+$ contain significant contributions from the oxo moiety, the Cp ligand, and the Re center. The HOMO is an archetypal example of

”π-loading” in that both π-donating ligands are interacting with the same metal orbital simultaneously, which should lead to enhanced reactivity of the involved metal-ligand π bonds.[34] The topic of ”π-loading” and its effect on the reactivity of metal-ligand multiple bonds has been explored previously in our groups, most notably in d^0 group 5 bis(imido) systems.[35-38]

The calculated LUMO of **3.3**$^+$ further helped to rationalize the behavior of this complex. This orbital is antibonding with respect to the oxo ligand and Re center, while the Cp ligand is forming some bonding interaction to the metal at two of its carbon atoms, and the remainder of the ligand is either antibonding or nonbonding with respect to Re. The presence of metal-ligand antibonding interactions in the LUMO of **3.3**$^+$ involving both the oxo and Cp ligands aligns with our experimental observation that both groups can readily undergo nucleophilic attack, resulting in a loss of or decrease in coordination to the metal. However, future DFT studies will be necessary to discern why one nucleophile attacks preferentially at one ligand over the other.

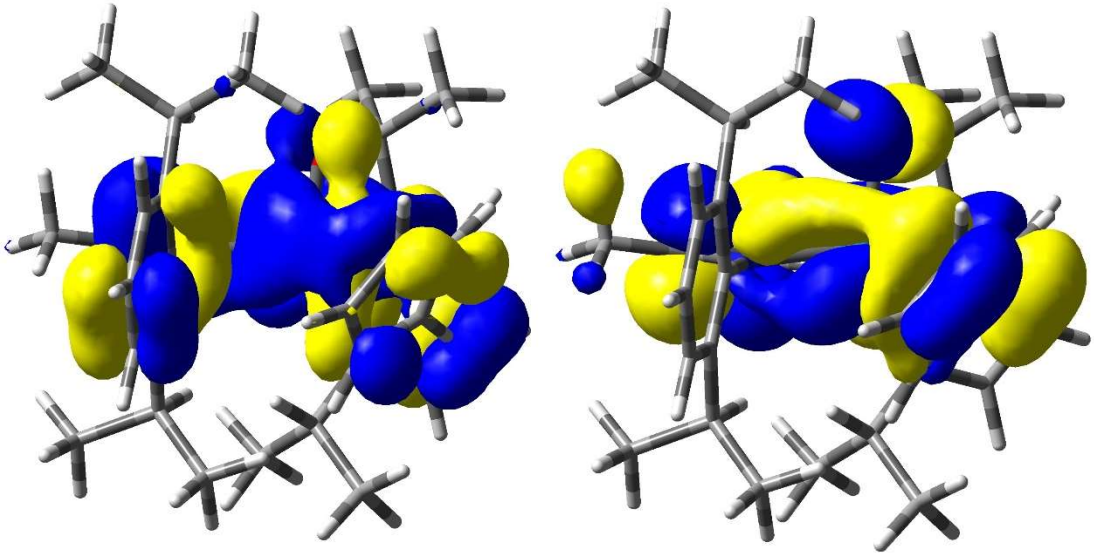

Figure 3.5 DFT-optimized gas-phase structure of **3**$^+$ with its calculated HOMO (left) and LUMO (right) surfaces (isovalue = 0.05). The oxo ligand is oriented upwards, with the Cp ligand to the right. Hydrogen atoms have been excluded for clarity.

Summary and Conclusions

In summary, we report the synthesis of a new class of low-valent terminal oxo complexes of Re(III) supported by an olefin group as well as an encumbering BDI ligand. Reactivity studies have demonstrated the Cp ligand of **3**$^+$ acts as an electrophile, allowing for a variety of nucleophiles to trigger the reduction of Re(V) to Re(III). Additionally, the divergent reactivity of **3.3c** with PMe_3 and ^{t}BuNC, along with DFT studies of **3.3**$^+$, indicated simultaneous contribution of the oxo and Cp ligands to the frontier orbitals of this cationic species. The ability of **3.3**$^+$ to display regioselectivity in its reactions with nucleophiles is particularly unique in light of its “π-loaded” nature. Further studies of **3.2** and **3.3**$^+$ will be the subject of future reports.

Experimental

General Considerations: All manipulations were carried out either in an MBraun LabStar glovebox under a dry nitrogen atmosphere or on a Schlenk line using standard inert atmosphere techniques. All solvents were dried by passage through a basic alumina column and were handled and stored in standard Strauss flasks or in the glovebox under a dry nitrogen atmosphere. Deuterated benzene and chloroform were obtained from Cambridge Isotope Labs, dried over an appropriate reagent (Na/benzophenone for C_6D_6, CaH_2 for $CDCl_3$), and transferred under vacuum prior to storage in the glovebox over 4 Å molecular sieves. Anhydrous tin(II) chloride, sodium cyclopentadienide (2.0 M in THF), silver trifluoromethanesulfonate, trimethylphosphine (1.0 M in toluene), and *tert*-butylisocyanide were obtained from commercial sources and used without further purification. The reported compounds $ORe Cl_2$(BDI),[20] cyclopentadienyl sodium (solid),[39] bis(cyclopentadienyl)tin,[40] diphenylmagnesium,[41] fluorenyl potassium,[42] and (pentamethyl)cyclopentadienyl potassium[43,44] were synthesized using known procedures. NMR spectroscopy data were obtained on Bruker AVQ-400, AV-500, and AV-600 instruments. All ^{1}H and ^{13}C spectra were calibrated to the residual peak of the solvent used. Select peak assignments were corroborated with ^{1}H-^{1}H COSY and ^{1}H-^{13}C HSQC experiments as necessary. Unless noted otherwise, "room temperature" and "ambient temperature" both refer to approx. 23 ºC. Infrared absorption data were obtained using a Thermo Scientific Nicolet iS10 instrument, with the sample chamber under ambient atmosphere. Samples were prepared as Nujol mulls pressed between KBr plates in the glovebox. A background IR spectrum was obtained immediately prior to data acquisition for each sample.

$ORePh_2$(BDI) (3.1): In the glovebox, THF (3 mL) was added to a solid mixture of $ORe Cl_2$(BDI) (100 mg, 0.145 mmol) and $MgPh_2$ (25.9 mg, 0.145 mmol) at ambient temperature. Within seconds a color change from dark green to dark red-orange was observed. After the reaction mixture was stirred for 5 minutes, its volatile components were removed in vacuo. The solid residue was extracted with hexane (12 mL), and these extracts were filtered through diatomaceous earth to give a clear orange solution. The volatile components of this solution were removed in vacuo to give beige, analytically pure, crystalline **3.1** (98 mg, 86% yield). Single crystals suitable for X-ray diffraction were obtained from a concentrated HMDSO solution stored at -40 ºC. m.p.: 200-201 ºC. ^{1}H NMR (500 MHz, C_6D_6, 298 K): 6.98 (t, 2H, BDI Ar, J = 7.6 Hz), 6.94 (dd, 2H, BDI Ar, J = 7.5, 1.1 Hz), 6.89 (dd, 2H, BDI Ar, J = 7.4, 1.1 Hz), 6.81 (t, 4H, Ph, J = 7.6 Hz), 6.44 (broad s, 4H, Ph), 6.27 (t, 2H, Ph, J = 7.3 Hz), 5.22 (s, 1H, *H*C[MeC(NAr)]$_2$), 3.59 (sept, 2H, BDI C*H*(Me)$_2$, J = 6.6 Hz), 2.36 (sept, 2H, BDI C*H*(Me)$_2$, J = 6.8 Hz), 1.74 (s, 6H, HC[*Me*C(NAr)]$_2$), 1.27 (d, 6H, BDI CH(*Me*)$_2$, J = 6.0 Hz), 1.26 (d, 6H, BDI CH(*Me*)$_2$, J = 6.1 Hz), 1.18 (d, 6H, BDI CH(*Me*)$_2$, J = 6.7 Hz), 0.98 (d, 6H, BDI CH(*Me*)$_2$, J = 6.7 Hz). ^{13}C NMR (151 MHz, C_6D_6, 298 K): 178.62 (HC[Me*C*(NAr)]$_2$), 173.36 (Ph), 149.58 (Ph), 142.43 (BDI Ar), 141.88 (BDI Ar), 127.49 (BDI Ar), 126.09 (Ph), 125.42 (BDI Ar), 123.37 (BDI Ar), 123.18 (Ph), 108.82 (H*C*[MeC(NAr)]$_2$), 29.54 (BDI *C*H(Me)$_2$), 28.05 (BDI *C*H(Me)$_2$), 26.92 (HC[*Me*C(NAr)]$_2$), 25.64 (BDI CH(*Me*)$_2$), 25.16 (BDI CH(*Me*)$_2$), 24.20 (BDI CH(*Me*)$_2$), 23.98 (BDI CH(*Me*)$_2$). Anal. Cald for $C_{41}H_{51}N_2ORe$ (**3.1**): C, 63.62; H, 6.64; N, 3.62%. Found: C, 63.80; H, 6.78; N, 3.50%.

ORe(DHF)(BDI) (3.2): A 2.0 M solution of NaCp in THF (1.4 mL, 2.8 mmol, 4 eq.) was added by syringe to a stirred solution of $OReCl_2$(BDI) (0.500 g, 0.724 mmol) in diethyl ether (40 mL) at ambient temperature. A substantial amount of pale precipitate was observed to form over the following 2-3 min, along with a subtle change in color of the solution to a deeper shade of green. After stirring the reaction mixture for a total of 5 min, its volatile components were removed in vacuo. The solid residue was extracted with hexane (60 mL). These extracts were filtered into a new flask through a glass filter tipped cannula and then they were concentrated in vacuo prior to storage at -40 °C. After several hours **3.2** was isolated as dark green crystalline solids (367 mg, 68%). Single crystals suitable for X-ray diffraction were obtained by storing a concentrated hexane solution of **3.2** at -40 °C. m.p. 178-179 °C (decomp). ^{1}H NMR (500 MHz, C_6D_6, 298 K): 7.30 (d, 2H, Ar, *J* = 7.6 Hz), 7.16 (t, 2H, Ar, *J* = 7.6 Hz), 7.09 (d, 2H, *J* = 7.6 Hz), 6.44 (d, 1H, Cp-Cp, *J* = 3.5 Hz), 6.24 (d, 1H, Cp-Cp, *J* = 5.1 Hz), 6.11 (s, 1H, Cp-Cp), 5.32 (s, 1H, *H*C[MeC(NAr)]$_2$), 4.05 (s, 1H, Cp-Cp), 3.71 (m, 2H, C*H*(Me)$_2$), 2.70 (s, 2H, Cp-Cp), 1.92 (s, 6H, HC[*Me*C(NAr)]$_2$), 1.49 (d, 8H, CH(*Me*)$_2$ and C*H*(Me)$_2$ (overlapped), *J* = 6.3 Hz), 1.27 (d, 6H, CH(*Me*)$_2$, *J* = 6.7 Hz), 0.91 (d, 6H, CH(*Me*)$_2$, *J* = 6.6 Hz), 0.84 (d, 6H, CH(*Me*)$_2$, *J* = 6.6 Hz). ^{13}C NMR (151 MHz, C_6D_6, 298 K): 172.37 (HC[Me*C*(NAr)]$_2$), 155.23 (BDI Ar), 152.12 (BDI Ar), 141.36 (BDI Ar), 140.54 (BDI Ar). 133.03 (Cp-Cp), 130.57 (Cp-Cp), 126.93 (Ar), 126.03 (Ar), 125.72 (Cp-Cp), 123.30 (BDI Ar), 107.31 ((H*C*[Me*C*(NAr)]$_2$), 58.74 (Cp-Cp), 41.78 (Cp-Cp), 28.48 (*C*H(Me)$_2$), 28.03 (*C*H(Me)$_2$), 25.35 (CH(*Me*)$_2$), 24.80 (CH(*Me*)$_2$), 24.67 (CH(*Me*)$_2$), 24.64 (CH(*Me*)$_2$), 24.31 (HC[*Me*C(NAr)]$_2$). Some of the bound dihydrofulvalene resonances could not be found in the room temperature NMR spectra. Anal. Cald for $C_{39}H_{51}N_2ORe$ (**3.2**): C, 62.45; H, 6.85; N, 3.73%. Found: C, 62.31; H, 6.85; N, 3.62%.

[ORe(Cp)(BDI)][SnCl$_3$] (3.3a) Diethyl ether (12 mL) was added to a solid mixture of $OReCl_2$(BDI) (250 mg, 0.363 mmol), $SnCp_2$ (90.1 mg, 1 equiv., 0.362 mmol), and anhydrous $SnCl_2$ (34.2 mg, 0.5 equiv., 0.181 mmol) to give a dark green suspension. This suspension was stirred at room temperature for 2 days after which time a copious amount of dark red, crystalline precipitate was observed along with a clear, green supernatant. The supernatant was removed carefully by pipette, and the solids were washed with 2x10 mL of diethyl ether before being dried in vacuo to give **3.3a** (261 mg, 79% yield). Large (5 mm) single crystals suitable for X-ray diffraction were obtained by vapor diffusion of benzene into a concentrated THF solution of **3.3a** at room temperature. m.p.: 204-206 °C. ^{1}H NMR (600 MHz, $CDCl_3$, 298 K): 7.43 (dd, 2H, BDI Ar, *J* = 7.6, 1.4 Hz), 7.37 (t, 2H, BDI Ar, *J* = 7.7 Hz), 7.33 (dd, 2H, BDI Ar, *J* = 7.6, 1.4 Hz), 6.03 (s, 5H, Cp), 5.87 (s, 1H, *H*C[MeC(NAr)]$_2$), 2.89 (sept, 2H, BDI C*H*(Me)$_2$, *J* = 6.7 Hz), 2.51 (sept, 2H, BDI C*H*(Me)$_2$, *J* = 6.8 Hz), 2.04 (s, 6H, HC[*Me*C(NAr)]$_2$), 1.36 (d, 6H, BDI CH(*Me*)$_2$, *J* = 6.9 Hz), 1.32 (d, 6H, BDI CH(*Me*)$_2$, *J* = 6.7 Hz), 1.25 (d, 6H, BDI CH(*Me*)$_2$, *J* = 6.8 Hz), 1.21 (d, 6H, BDI CH(*Me*)$_2$, *J* = 6.7 Hz). ^{13}C NMR (151 MHz, $CDCl_3$, 298 K): 171.99 (HC[Me*C*(NAr)]$_2$), 154.74 (BDI Ar), 141.79 (BDI Ar), 140.36 (BDI Ar), 130.15 (BDI Ar), 127.31 (BDI Ar), 124.78 (BDI Ar), 118.35 (H*C*[MeC(NAr)]$_2$), 107.76 (Cp), 28.76 (BDI *C*H(Me)$_2$), 27.87 (BDI *C*H(Me)$_2$), 25.74 (BDI CH(*Me*)$_2$), 25.36 (BDI CH(*Me*)$_2$), 25.22 (HC[*Me*C(NAr)]$_2$), 24.70 (BDI CH(*Me*)$_2$), 24.52 (BDI CH(*Me*)$_2$). Anal. Cald for $C_{34}H_{46}N_2OReSnCl_3$ (**3.3a**): C, 44.87; H, 5.09; N, 3.08%. Found: C, 44.48; H, 5.25; N, 2.90%.

[ORe(Cp)(BDI)][PF_6] (3.3b): Solid $AgPF_6$ (27.8 mg, 0.110 mmol) was added to a stirred solution of **3.3a** (100 mg, 0.100 mmol) in THF (5 mL) at ambient temperature. A pale precipitate formed immediately. After the reaction mixture was stirred for 15 minutes, the solution component of the reaction mixture was decanted by pipette and filtered through diatomaceous earth. The solids remaining in the reaction vial were further extracted with an additional 20 mL of THF, and these extracts were also filtered through diatomaceous earth. The two filtered solutions were concentrated in vacuo and combined to give a final volume of ca. 8 mL. This concentrated solution was stored at -40 ºC to yield red, needle-shaped crystals of **3.3b** (57 mg, 62% yield). m.p.: decomp. above 100 ºC. ^{1}H NMR (600 MHz, $CDCl_3$, 298 K): 7.42 (dd, 2H, BDI Ar, J = 7.6, 1.1 Hz), 7.35 (t, 2H, BDI Ar, J = 7.6 Hz), 7.32 (dd, 2H, BDI Ar, J = 7.6, 1.1 Hz), 5.97 (s, 5H, Cp), 5.81 (s, 1H, *H*C[MeC(NAr)]$_2$), 2.87 (sept, 2H, BDI C*H*(Me)$_2$, J = 6.7 Hz), 2.49 (sept, 2H, BDI C*H*(Me)$_2$, J = 6.8 Hz), 1.99 (s, 6H, HC[*Me*C(NAr)]$_2$), 1.34 (d, 6H, BDI CH(*Me*)$_2$, J = 6.9 Hz), 1.30 (d, 6H, BDI CH(*Me*)$_2$, J = 6.6 Hz), 1.23 (d, 6H, BDI CH(*Me*)$_2$, J = 6.7 Hz), 1.19 (d, 6H, BDI CH(*Me*)$_2$, J = 6.7 Hz). ^{13}C NMR (151 MHz, $CDCl_3$, 298 K): 172.10 (HC[Me*C*(NAr)]$_2$), 154.77 (BDI Ar), 141.77 (BDI Ar), 140.41 (BDI Ar), 130.11 (BDI Ar), 127.22 (BDI Ar), 124.73 (BDI Ar), 118.14 (H*C*[MeC(NAr)]$_2$), 107.64 (Cp), 28.71 (BDI *C*H(Me)$_2$), 27.84 (BDI *C*H(Me)$_2$), 25.57 (BDI CH(*Me*)$_2$), 25.16 (BDI CH(*Me*)$_2$), 25.03 (HC[*Me*C(NAr)]$_2$), 24.57 (BDI CH(*Me*)$_2$), 24.35 (BDI CH(*Me*)$_2$). Anal. Cald for $C_{36}H_{50}N_2O_{1.50}F_6PRe$ (**3.3b** • 0.5 THF): C, 49.93; H, 5.82; N, 3.23%. Found: C, 49.71; H, 5.55; N, 3.54%.

[ORe(Cp)(BDI)][OTf] (3.3c): THF (3 mL) was added to a solid mixture of $OReCl_2$(BDI) (500 mg, 0.724 mmol) and silver trifluoromethanesulfonate (186 mg, 0.724 mmol). The resulting dark orange solution and pale precipitate (AgCl) was allowed to stir for 5 minutes at room temperature. This solution was then filtered through diatomaceous earth to remove AgCl. The filtrate was then added to solid $SnCp_2$ (180 mg, 0.724 mmol), and the solution was stirred at room temperature. After 2 days, a dark red solution with substantial amounts of red crystalline precipitate was observed. The volatile components of the reaction mixture were removed in vacuo. The resulting residue was then washed with diethyl ether (2 x 8mL) to give dark red, microcrystalline **3.3c** (431 mg, 69%). m.p.: 229-232 ºC. ^{1}H NMR (600 MHz, $CDCl_3$, 298 K): 7.43 (dd, 2H, BDI Ar, J = 7.6, 1.6 Hz), 7.36 (t, 2H, BDI Ar, J = 7.7 Hz), 7.32 (dd, 2H, BDI Ar, J = 7.7, 1.5 Hz), 5.99 (s, 5H, Cp), 5.90 (s, 1H, *H*C[MeC(NAr)]$_2$), 2.88 (sept, 2H, BDI C*H*(Me)$_2$, J = 6.7 Hz), 2.50 (sept, 2H, BDI C*H*(Me)$_2$, J = 6.8 Hz), 2.01 (s, 6H, HC[*Me*C(NAr)]$_2$), 1.34 (d, 6H, BDI CH(*Me*)$_2$, J = 6.9 Hz), 1.31 (d, 6H, BDI CH(*Me*)$_2$, J = 6.7 Hz), 1.24 (d, 6H, BDI CH(*Me*)$_2$, J = 6.8 Hz), 1.20 (d, 6H, BDI CH(*Me*)$_2$, J = 6.7 Hz). ^{13}C NMR (151 MHz, $CDCl_3$, 298 K): 172.14 (HC[Me*C*(NAr)]$_2$), 154.78 (BDI Ar), 141.84 (BDI Ar), 140.35 (BDI Ar), 130.14 (BDI Ar), 127.29 (BDI Ar), 124.72 (BDI Ar), 118.24 (H*C*[MeC(NAr)]$_2$), 107.68 (Cp), 28.73 (BDI *C*H(Me)$_2$), 27.85 (BDI *C*H(Me)$_2$), 25.60 (BDI CH(*Me*)$_2$), 25.17 (BDI CH(*Me*)$_2$), 25.12 (HC[*Me*C(NAr)]$_2$), 24.62 (BDI CH(*Me*)$_2$), 24.41 (BDI CH(*Me*)$_2$). Anal. Cald for $C_{39}H_{54}N_2O_4F_3SRe$ (**3.3c** • THF): C, 51.69; H, 6.01; N, 3.09%. Found: C, 51.94; H, 5.73; N, 3.13%.

ORe(Cp-Fl)(BDI) (3.4): To a solution of **3.3c** (50.0 mg, 0.0583 mmol) in THF (6 mL) was added a solution of fluorenyl potassium (11.9 mg, 0.0583 mmol) in THF (2 mL) at room temperature. A color change from dark red to a dark orange-green was observed in seconds. The reaction mixture was stirred for 2 minutes, and then exposed to vacuum to remove volatile components. The residue

was triturated with 2 mL of hexane, and then extracted with 10 mL of Et_2O. The dark green extracts were filtered through diatomaceous earth, concentrated in vacuo, and stored at -40 °C to give **3.4** as dark green crystals (35 mg, 71%). Single crystals suitable for X-ray diffraction were obtained by the slow evaporation of a benzene solution of **3.4** at room temperature. m.p.: 190-193 °C (decomp.). ^{1}H NMR (600 MHz, C_6D_6, 298 K): 7.57 (d, 2H, Fl Ar, J = 7.5 Hz), 7.47 (br s, 2H, Fl Ar), 7.25-7.18 (m, 4H, BDI Ar), 7.13 (t, 2H, BDI Ar, J = 7.4 Hz), 7.04 (br s, 4H, Fl Ar), 5.65 (br s, 1H, Cp), 5.30 (s, 1H, *H*C[MeC(NAr)]$_2$), 4.91 (br s, 1H, Cp), 3.89 (s, 1H, Fl methine), 3.85 (br s, 1H, Cp), 3.76 (d, 1H, Cp methine, J = 2.4 Hz), 3.63 (br s, 2H, BDI C*H*Me$_2$), 3.21 (br s, 1H, Cp), 1.89 (s, 6H, HC[*Me*C(NAr)]$_2$), 1.45 (br s, 8H, BDI C*H*Me$_2$ and BDI CH*Me$_2$*), 1.26 (d, 6H, BDI CH*Me$_2$*, J = 6.7 Hz), 0.95 (br s, 6H, BDI CH*Me$_2$*), 0.84 (d, 6H, BDI CH*Me$_2$*, J = 6.7 Hz). ^{13}C NMR (151 MHz, C_6D_6, 298 K): 146.28 (Fl Ar), 141.83 (BDI Ar), 140.29 (BDI Ar), 127.12 (Fl Ar), 127.00 (BDI Ar), 126.88 (Fl Ar), 125.75 (Fl Ar), 124.89 (BDI Ar), 119.69 (Fl Ar), 107.33 (H*C*[MeC(NAr)]$_2$), 60.59 (Fl methine), 54.43 (Cp methine), 28.55 (BDI *C*HMe$_2$), 27.96 (BDI *C*HMe$_2$), 25.23 (BDI CH*Me$_2$*), 24.83 (BDI CH*Me$_2$*), 24.68 (BDI CH*Me$_2$*), 24.48 (BDI CH*Me$_2$*), 24.27 (HC[*Me*C(NAr)]$_2$). Anal. Cald for $C_{47}H_{55}N_2ORe$ (**3.4**): C, 66.40; H, 6.52; N, 3.29%. Found: C, 66.24; H, 6.39; N, 3.35%.

ORe(Cp-Cp*)(BDI) (3.5): A suspension of KCp* (10.2 mg, 0.0583 mmol) in THF (3 mL) was added to a stirred solution of **3.3c** (50.0 mg, 0.0583 mmol) in THF (4 mL) at room temperature. The reaction mixture was observed to slowly change in color from dark red to dark green. After 2 hours, the volatile components of the reaction mixture were removed in vacuo, and the resulting dark residue was triturated with 1 mL of HMDSO, which was removed in vacuo along with residual THF. The solid residue was then extracted with 6 mL of HMDSO. The dark green extracts were filtered through diatomaceous earth and concentrated to ca. 1 mL. Storage of the concentrated filtrate at room temperature yielded a small amount (ca. 8 mg) of dark green crystals that were primarily composed of **3.5** with a significant portion of **3.2**. It was possible to obtain structural characterization of **3.5** by selecting a single crystal from the product mixture for analysis by X-ray diffraction.

[ORe(Cp-PMe$_3$)(BDI)][OTf] (3.6): To a stirred suspension of **3.3c** (50.0 mg, 0.0583 mmol) in THF (3 mL) in a 50 mL Schlenk tube, was added a 1.0 M solution of PMe_3 in toluene (0.50 mL, 0.50 mmol, 8.6 eq.). A clear, dark brown solution formed immediately, and after 10 minutes the volatile components of the reaction mixture were removed in vacuo. Following trituration of the resulting residue with 2 mL of diethyl ether to remove remaining toluene and PMe_3, the beige solids were dissolved in 2 mL of THF. These extracts were filtered through diatomaceous earth and concentrated in vacuo to ca. 0.5 mL in volume. Approximately 4 volumes of hexane were then added to the dark solution, resulting in the immediate formation of crystals. Following storage of this mixture at -40 °C for several hours, **3.6** was isolated as brown crystals (48 mg, 89%). Crystals suitable for X-ray diffraction were grown by the room temperature vapor diffusion of hexane into a benzene solution of **3.6**. m.p.: 136-138 °C. ^{1}H NMR (600 MHz, C_6D_6, 298 K): 7.53 (br s, 1H, BDI Ar), 7.22 (br s, 3H, BDI Ar), 7.03 (br s, 2H, BDI Ar), 5.67 (br s, 1H, Cp), 5.24 (s, 1H, *H*C[MeC(NAr)]$_2$), 4.45, (br s, 1H, Cp), 3.52 (br s, 1H, BDI C*H*(Me)$_2$), 3.44 (br s, 1H, Cp), 3.25 (d and br s, 2H, Cp and Cp C*H*-PMe$_3$, J = 4.7 Hz), 2.88 (br s, 1H, BDI C*H*(Me)$_2$), 1.80 (s, 6H, HC[*Me*C(NAr)]$_2$), 1.52 (d, 9H, PMe$_3$, J = 13.8 Hz), 1.47 (br s, 6H, BDI CH(*Me*)$_2$), 1.34 (br s, 2H,

C*H*(Me)$_2$), 1.23 (d, 6H, BDI CH(*Me*)$_2$, *J* = 6.7 Hz), 0.86 (br s, 6H, BDI CH(*Me*)$_2$), 0.79 (d, 6H, BDI CH(*Me*)$_2$, *J* = 6.7 Hz). ^{13}C NMR (151 MHz, C_6D_6, 298 K): 150.38 (BDI Ar), 141.26 (BDI Ar), 140.41 (BDI Ar), 128.21 (BDI Ar), 123.61 (BDI Ar), 108.13 (H*C*[MeC(NAr)]$_2$), 52.02 (d, Cp *C*H-PMe$_3$, *J* = 40.0 Hz), 28.42 (BDI *C*H(Me)$_2$), 28.01 (BDI *C*H(Me)$_2$), 25.83 (BDI CH(*Me*)$_2$), 25.29 (BDI CH(*Me*)$_2$), 24.74 (BDI CH(*Me*)$_2$), 24.53 (HC[*Me*C(NAr)]$_2$), 5.11 (d, PMe$_3$, *J* = 52.9 Hz). Due to the instability of **3.6** in solution or under vacuum for extended periods (loss of PMe$_3$ and reformation of **3.3c**), satisfactory elemental analysis could not be obtained.

[Re(Cp)(^{t}BuNC)(BDI)][OTf] (3.7): To a suspension of **3.3c** (50.0 mg, 0.0583 mmol) in THF (4 mL) was added neat *tert*-butylisocyanide (0.10 mL, 0.89 mmol, 15 eq.), which immediately gave a dark orange solution. After the reaction mixture was stirred for 5 minutes, its volatile components were removed in vacuo. The orange solids were redissolved in 5 mL of THF, and the extracts were filtered through diatomaceous earth. To these filtered extracts was added an equal volume of diethyl ether, which initiated the formation of crystals. This mixture was stored at -40 ºC overnight to yield **3.7** as orange crystals (41 mg, 78%). Single crystals suitable for X-ray diffraction were grown by the slow evaporation of THF solution of **3.7**. The production of *tert*-butylisocyanate (^{t}BuNCO) in the reaction was confirmed by an NMR scale experiment where **3.3c** was combined with ca. 1.6 eq. of ^{t}BuNC in $CDCl_3$, producing equal amounts of **3.7** as well as a singlet at 1.35 ppm in the ^{1}H NMR spectrum that integrated to 9 protons, which aligns to the reported chemical shift of ^{t}BuNCO.[45] m.p.: 214-216 ºC. ^{1}H NMR (600 MHz, $CDCl_3$, 298 K): 7.31 (s, 1H, *H*C[MeC(NAr)]$_2$), 7.13 (t, 2H, BDI Ar, *J* = 7.6 Hz), 7.09 (dd, 2H, BDI Ar, *J* = 7.7, 1.5 Hz), 7.01 (dd, 2H, BDI Ar, *J* = 7.5, 1.4 Hz), 6.79 (s, 5H, Cp), 3.99 (s, 6H, HC[*Me*C(NAr)]$_2$), 2.68 (sept, 2H, BDI C*H*(Me)$_2$, *J* = 6.8 Hz), 1.90 (sept, 2H, BDI C*H*(Me)$_2$, *J* = 6.8 Hz), 1.42 (s, 9H, ^{t}BuNC), 1.21 (dd overlapped, 12H, BDI CH(*Me*)$_2$, *J* = 6.8 Hz), 1.06 (d, 6H, BDI CH(*Me*)$_2$, *J* = 6.7 Hz), 1.02 (d, 6H, BDI CH(*Me*)$_2$, *J* = 6.9 Hz). ^{13}C NMR (151 MHz, $CDCl_3$, 298 K): 177.39 (HC[Me*C*(NAr)]$_2$), 157.79 (Me$_3$CN*C*), 141.15 (BDI Ar), 137.75 (BDI Ar), 130.12 (H*C*[MeC(NAr)]$_2$), 128.13 (BDI Ar), 125.02 (BDI Ar), 124.12 (BDI Ar), 99.61 (Cp), 57.66 (Me$_3$*C*NC), 35.40 (*Me$_3$*CNC), 29.79 (BDI *C*H(Me)$_2$), 27.74 (BDI *C*H(Me)$_2$), 25.34 (BDI CH(*Me*)$_2$), 25.27 (BDI CH(*Me*)$_2$), 24.54 (BDI CH(*Me*)$_2$), 23.65 (BDI CH(*Me*)$_2$), 22.58 (HC[*Me*C(NAr)]$_2$). IR (Nujol): 2109 cm^{-1} (νN≡C). Anal. Cald for $C_{40}H_{53}N_3O_3F_3SRe$ (**3.7**): C, 53.43; H, 5.94; N, 4.67%. Found: C, 53.16; H, 5.96; N, 4.67%.

X-Ray Crystallographic Details: X-ray diffraction data for **3.1**, **3.2**, **3.3a**, **3.3c**, **3.4**, **3.6**, and **3.7** were collected at CheXray, Berkeley, CA, using a Bruker SMART APEX (**3.2**, **3.3a**, **3.4**) or Bruker APEX II QUAZAR (**3.1**, **3.3c**, **3.6**, **3.7**) instrument outfitted with a monochromated Mo-K$_\alpha$ radiation source (λ = 0.71073 Å). Diffraction data for **3.5** were obtained at the Advanced Light Source (ALS), (Lawrence Berkeley National Laboratory, Berkeley, CA) station 11.3.1 using a silicon monochromated beam of 16 keV (λ = 0.7749 Å) radiation. All data collections were conducted in a 100 K stream of dry nitrogen. Absorption corrections were carried out by a multi-scan method, utilizing the SADABS program.[46] Bruker APEX3 software were used for the data collection and the associated Bruker SAINT V8.37A program conducted the cell refinement and data reduction procedures.[46] Initial structure solutions were found using SHELXT and refinements were conducted by SHELXL-2014.[47] All main residue (**3.1**) and solvent (**3.3c**) disorder was adequately resolved into two components. Publication materials were made using WinGX.[48] Thermal ellipsoid plots were made using Mercury.[49] All structures have been deposited to the

CCDC, with deposition numbers 1565563 (**3.1**), 1565564 (**3.2**), 1565565 (**3.3a**), 1565566 (**3.3c**), 1565567 (**3.4**), 1565568 (**3.5**), 1565569 (**3.6**), and 1565570 (**3.7**).

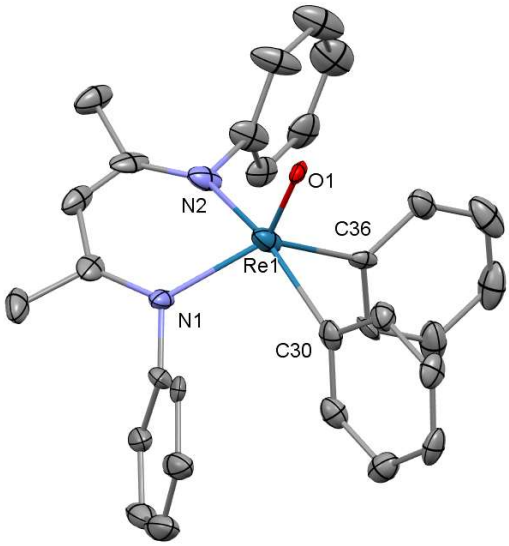

Figure 3.6 Crystal structure of **3.1** with 50% probability ellipsoids. BDI isopropyl groups and H atoms have been excluded for clarity. Selected distances (Å) and angles (°): Re1-O1 = 1.598(10), Re1-N1 = 2.088(5), Re1-N2 = 2.116(5), Re1-C30 = 2.130(5), Re1-C36 = 2.253(13), N1-Re1-N2 = 85.55(19).

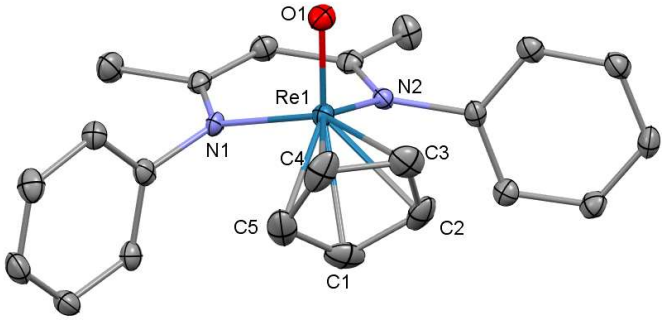

Figure 3.7 Crystal structure of the cationic portion of **3.3c** with 50% probability ellipsoids. Anion, solvent, BDI isopropyl, and H atoms have been excluded for clarity. Selected distances (Å) and angles (°): Re1-O1 = 1.692(2), Re1-N1 = 2.044(3), Re1-N2 = 2.026(3), Re1-Cp(centroid) = 2.0199(18), N1-Re1-N2 = 85.41(11).

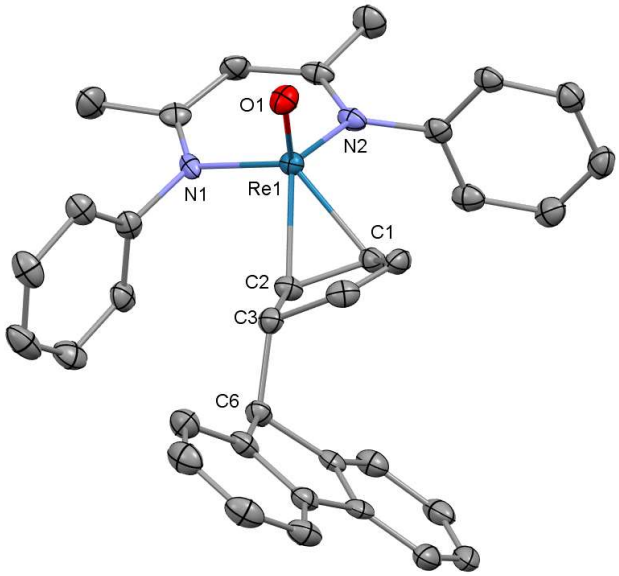

Figure 3.8 Crystal structure of **3.4** with 50% probability ellipsoids. BDI isopropyl groups and H atoms have been excluded for clarity. Selected distances (Å) and angles (°): Re1-O1 = 1.686(2), Re1-N1 = 2.070(3), Re1-N2 = 2.035(3), Re1-C1 = 2.113(4), Re1-C2 = 2.105(4), C1-C2 = 1.469(6), C2-C3 = 1.528(5), C3-C6 = 1.560(5), N1-Re1-N2 = 87.42(11).

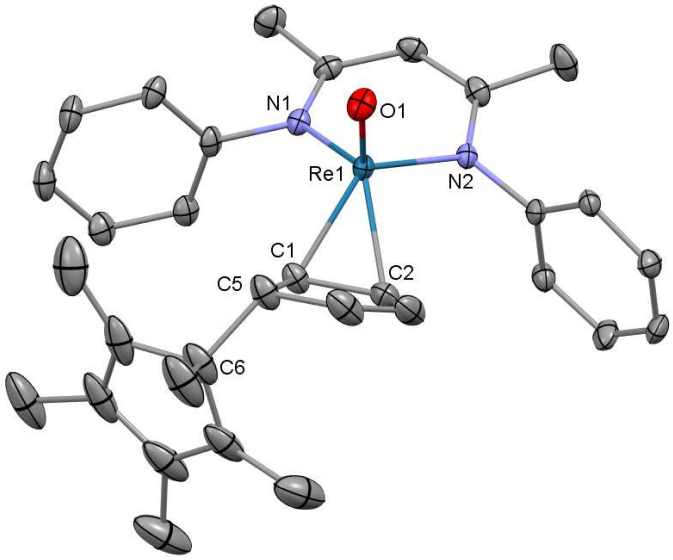

Figure 3.9 Crystal structure of **3.5** with 50% probability ellipsoids. BDI isopropyl groups and H atoms have been excluded for clarity. Selected distances (Å) and angles (°): Re1-O1 = 1.693(2), Re1-N1 = 2.028(3), Re1-N2 = 2.048(2), Re1-C1 = 2.116(3), Re1-C2 = 2.106(3), C1-C2 = 1.459(4), C2-C5 = 1.549(4), C5-C6 = 1.563(4), N1-Re1-N2 = 86.75(8).

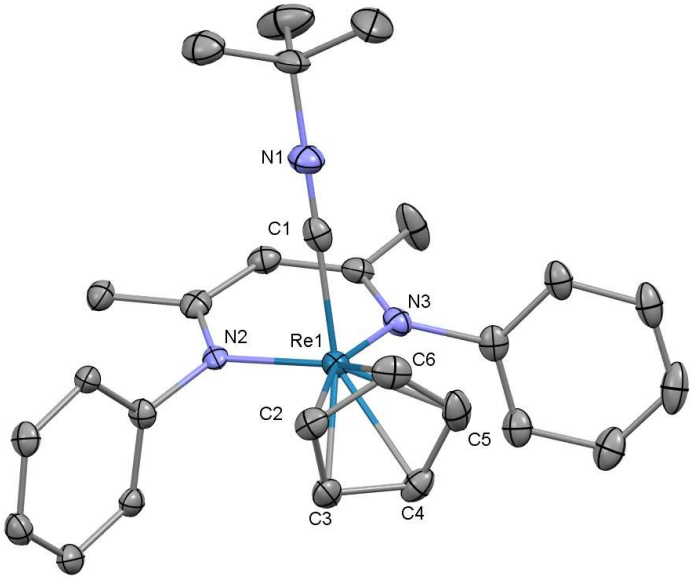

Figure 3.10 Crystal structure of one of the two crystallographically-independent cationic portions of **3.7** with 50% probability ellipsoids. Anion, solvent, BDI isopropyl, and H atoms have been excluded for clarity. Selected distances (Å) and angles (°): Re1-C1 = 1.982(6), Re1-N1 = 2.014(4), Re1-N2 = 2.024(3), Re1-Cp(centroid) = 1.931(2), N1-Re1-N2 = 89.66(14).

Table 3.1. Crystallographic details for compounds **3.1**, **3.2**, **3.3a**, and **3.3c**.

	3.1	**3.2**	**3.3a**	**3.3c• 0.5 Tol**
Chemical formula	$C_{41}H_{51}N_2ORe$	$C_{39}H_{51}N_2ORe$	$C_{34}H_{46}N_2ORe$ Sn	$C_{38.50}H_{50}F_3N_2O_4ReS$
Formula weight	774.03	750.02	909.97	880.06
Color, habit	Orange, plate	Green, rod	Red, lath	Red, plate
Temperature (K)	100(2)	100(2)	100(2)	100(2)
Crystal system	Triclinic	Triclinic	Monoclinic	Monoclinic
Space group	P -1	P -1	P $2_1/n$	P $2_1/n$
a (Å)	8.9276(4)	11.9092(4)	10.7631(5)	10.1761(3)
b (Å)	10.0088(4)	12.1245(4)	19.7494(9)	21.6910(7)
c (Å)	22.2322(8)	12.9056(5)	17.1630(7)	17.1400(6)
α (°)	87.064(2)	86.2610(10)	90	90
β (°)	80.901(2)	77.7500(10)	102.4450(10)	100.4260(10)
γ (°)	64.838(2)	68.8620(10)	90	90
V ($Å^3$)	1775.13(13)	1698.39(10)	3562.5(3)	3720.8(2)
Z	2	2	4	4
Density (Mg m^{-3})	1.448	1.467	1.697	1.571
F(000)	788	764	1792	1780
Radiation Type	MoK_α	MoK_α	MoK_α	MoK_α
μ (mm^{-1})	3.456	3.610	4.349	3.379
Crystal size	0.06 x 0.04 x 0.01	0.08 x 0.04 x 0.02	0.20 x 0.10 x 0.04	0.10 x 0.10 x 0.01
Meas. Refl.	22208	48269	93857	57061
Indep. Refl.	6450	6205	6524	6849
R(int)	0.0708	0.0609	0.0377	0.0371
Final R indices	R = 0.0452	R = 0.0349	R = 0.0263	R = 0.0278
[I > 2σ(I)]	R_w = 0.0828	R_w = 0.0670	R_w = 0.626	R_w = 0.0622
Goodness-of-fit	1.027	1.087	1.154	1.086
$\Delta\rho_{max}$, $\Delta\rho_{min}$ (e $Å^{-3}$)	1.616, -1.937	4.371, -1.684	2.907, -0.630	2.615, -0.900

Table 3.2 Crystallographic details for compounds **3.4**, **3.5**, **3.6**, and **3.7**.

	3.4	**3.5**	**3.6 · 0.25 *n*-hexane**	**3.7 · 0.5 THF**
Chemical formula	$C_{47}H_{55}N_2ORe$	$C_{44}H_{61}N_2ORe$	$C_{39.50}H_{58.50}F_3N_2O_4PReS$	$C_{42}H_{59}F_3N_3O_{3.50}ReS$
Formula weight	850.13	820.14	931.61	937.18
Color, habit	Green, shard	Green, shard	Orange, lath	Orange, plate
Temperature (K)	100(2)	100(2)	100(2)	100(2)
Crystal system	Monoclinic	Monoclinic	Monoclinic	Triclinic
Space group	P 2_1/n	P 2_1/n	P 2_1/n	P -1
a (Å)	12.9408(18)	10.179(5)	21.2352(9)	12.4703(6)
b (Å)	22.116(3)	17.536(10)	9.6042(4)	18.6139(9)
c (Å)	13.8371(19)	21.913(12)	22.9845(10)	19.5750(9)
α (°)	90	90	90	103.176(2)
β (°)	97.435(3)	101.404(4)	113.483(2)	96.488(2)
γ (°)	90	90	90	105.810(2)
V (Å^3)	3926.9(9)	3834(4)	4299.4(3)	4181.8(3)
Z	4	4	4	4
Density (Mg m^{-3})	1.438	1.421	1.439	1.489
F(000)	1736	1688	1898	1912
Radiation Type	MoK$_\alpha$	Synchrotron	MoK$_\alpha$	MoK$_\alpha$
μ (mm^{-1})	3.132	3.852	2.964	3.011
Crystal size	0.16 x 0.10 x 0.08	0.07 x 0.05 x 0.03	0.11 x 0.02 x 0.01	0.10 x 0.06 x 0.01
Meas. Refl.	56530	54579	71230	64961
Indep. Refl.	7234	7906	7889	15099
R(int)	0.0442	0.0362	0.0619	0.0453
Final R indices	R = 0.0269	R = 0.0193	R = 0.0440	R = 0.0357
[I > 2σ(I)]	R_w = 0.0562	R_w = 0.0349	R_w = 0.1052	R_w = 0.0759
Goodness-of-fit	1.059	1.021	1.055	1.073
$\Delta\rho_{max}$, $\Delta\rho_{min}$ (e Å^{-3})	0.962, -0.817	0.818, -0.769	2.426, -1.414	3.105, -0.897

DFT Calculations: The structures and energies of complexes **3.2** and **3.3**$^+$ were calculated using the *Gaussian09* suite of programs.[12] Self-consistent field calculations were performed with tight convergence criteria on fine grids, while geometry optimizations were converged to tight geometric convergence criteria. Frequencies were calculated analytically at 298.15 K and 1 atm. The optimized structures were considered a true minima by virtue of their lack of imaginary vibrational modes. The B3LYP hybrid functional was used, along with the 6-31G(d,p) basis for light atoms (C, N, O, H) while the Re atom was treated with a Stuttgart/Dresden ECP pseudopotential (SDD).

Notes and References

(1) Que Jr., L. *Acc. Chem. Res.* **2007**, *40*, 493.
(2) Newcomb, M.; Zhang, R.; Chandrasena, R. E. P.; Halgrimson, J. A.; Horner, J. H.; Makris. T. M.; Sligar, S. G. *J. Am. Chem. Soc.* **2006**, *128*, 4580.
(3) Nam, W. *Acc. Chem. Res.* **2007**, *40*, 522.
(4) Hohenberger, J.; Ray, K.; Meyer, K. *Nat. Commun.* **2012**, *3*, 720.
(5) Rohde, J.-U.; In, J.-H.; Lim, M. H.; Brennessel, W. W.; Bukowski, M. R.; Stubna, A.; Münck, E.; Nam, W.; Que Jr., L. *Science* **2003**, *299*, 1037.
(6) Moyer B. A.; Meyer, T. J. *Inorg. Chem.* **1981**, *20*, 436.
(7) Che, C.-M.; Lai, T.-F.; Lin, K.-Y. *Inorg. Chem.* **1987**, *26*, 2289.
(8) de Oliveira, F. T.; Chanda, A.; Banerjee, D.; Shan, X.; Mondal, S.; Que Jr., L.; Bominaar, E. L.; Münck, E.; Collins, T. J. *Science* **2007**, *315*, 835.
(9) Chen, J.; Lee, Y.-M.; Davis, K. M.; Wu, X.; Seo, M. S.; Cho, K.-B.; Yoon, H.; Park, Y. J.; Fukuzumi, S.; Pushkar, Y. N.; Nam, W. *J. Am Chem. Soc.* **2013**, *135*, 6388.
(10) Leto, D. F.; Ingram, R.; Day, V. W.; Jackson, T. A. *Chem. Commun.* **2013**, *49*, 5378.
(11) Mayer, J. M.; Tulip, T. H. *J. Am. Chem. Soc.* **1984**, *106*, 3878.
(12) Mayer, J. M.; Thorn, D. L.; Tulip, T. H. *J. Am. Chem. Soc.* **1985**, *107*, 7454.
(13) Mayer, J. M.; Tulip, T. H.; Calabrese, J. C.; Valencia, E. *J. Am. Chem. Soc.* **1987**, *109*, 157.
(14) Valencia, E.; Santarsiero, B. D.; Geib, S. J.; Rheingold, A. L.; Mayer, J. M. *J. Am. Chem. Soc.* **1987**, *109*, 6896.
(15) Erikson, T. K. G.; Mayer, J. M. *Angew. Chem., Int. Ed.* **1988**, *27*, 1527.
(16) Spaltenstein, E.; Erikson, T. K. G.; Critchlow, S. C.; Mayer, J. M. *J. Am. Chem. Soc.* **1989**, *111*, 617.
(17) Spaltenstein, E.; Conry, R. C.; Critchlow, S. C.; Mayer, J. M. *J. Am. Chem. Soc.* **1989**, *111*, 8741.
(18) de Boer, E. J. M.; de With, J. *J. Am. Chem. Soc.* **1986**, *108*, 8271.
(19) Herrmann, W. A.; Fischer, R. A.; Herdtweck, E. *J. Organomet. Chem.* **1987**, *329*, C1.
(20) Lohrey, T. D.; Bergman, R. G.; Arnold, J. *Inorg. Chem.* **2016**, *55*, 11993.
(21) Ziegler, J. A.; Bergman, R. G.; Arnold, J. *Dalton Trans.* **2016**, *45*, 12661.
(22) Su, F.-M.; Cooper, C.; Geib, S. J.; Rheingold, A. L.; Mayer, J. M. *J. Am. Chem. Soc.* **1986**, *108*, 3545.
(23) Su, F.-M.; Bryan, J. C.; Jang, S.; Mayer, J. M. *Polyhedron* **1989**, *8*, 1261.
(24) Brock, S. L.; Mayer, J. M. *Inorg. Chem.* **1991**, *30*, 2138.
(25) de la Mata, F. J.; Grubbs, R. H. *Organometallics* **1996**, *15*, 577.
(26) Fischer, E. O.; Fellmann, W.; Herberich, G. E.; *Chem. Ber.* **1962**, *95*, 2254.
(27) Cheung, K. K.; Cross, R. J.; Forrest, K. P.; Wardle, R. J. *J. Chem. Soc., Chem. Commun.* **1971**, *15*, 875.
(28) Wilkinson, G.; Birmingham, G. M. *J. Am. Chem. Soc.* **1955**, *77*, 3421.
(29) A. Escher, W. Rutsch and M. Neuenschwander, *Helv. Chim. Acta* **1986**, *69*, 1644.
(30) Gaussian 09, Revision D.01, M. J. Frisch, G. W. Trucks, H. B. Schlegel, G. E. Scuseria, M. A. Robb, J. R. Cheeseman, G. Scalmani, V. Barone, B. Mennucci, G. A. Petersson, H. Nakatsuji, M. Caricato, X. Li, H. P. Hratchian, A. F. Izmaylov, J. Bloino, G. Zheng, J. L. Sonnenberg, M. Hada, M. Ehara, K. Toyota, R. Fukuda, J. Hasegawa, M. Ishida, T.

Nakajima, Y. Honda, O. Kitao, H. Nakai, T. Vreven, J. A. Montgomery, Jr., J. E. Peralta, F. Ogliaro, M. Bearpark, J. J. Heyd, E. Brothers, K. N. Kudin, V. N. Staroverov, T. Keith, R. Kobayashi, J. Normand, K. Raghavachari, A. Rendell, J. C. Burant, S. S. Iyengar, J. Tomasi, M. Cossi, N. Rega, J. M. Millam, M. Klene, J. E. Knox, J. B. Cross, V. Bakken, C. Adamo, J. Jaramillo, R. Gomperts, R. E. Stratmann, O. Yazyev, A. J. Austin, R. Cammi, C. Pomelli, J. W. Ochterski, R. L. Martin, K. Morokuma, V. G. Zakrzewski, G. A. Voth, P. Salvador, J. J. Dannenberg, S. Dapprich, A. D. Daniels, O. Farkas, J. B. Foresman, J. V. Ortiz, J. Cioslowski, and D. J. Fox, Gaussian, Inc., Wallingford CT, 2013.

(31) de Azevedo, C. G.; Calhorda, M. J.; Carrondo, M. A. A. F. de C. T.; Dias, A. R.; Duarte, M. T.; Galvão, A. M.; Gamelas, C. A.; Gonçalves, I. S.; da Piedade, F. M.; Romão, C. C. *J. Organomet. Chem.* **1997**, *544*, 257.

(32) Davies, S. G.; Green, M. L. H.; Mingos, D. M. P. *Tetrahedron* **1978**, *34*, 3047.

(33) Yonke, B. L.; Reeds, J. P.; Zavalij. P. Y.; Sita, L. R. *Angew. Chem. Int. Ed.* **2011**, *50*, 12342.

(34) Chao, Y.-W.; Rogers, P. M.; Wigley, D. E.; Alexander, S. J.; Rheingold, A. L. *J. Am. Chem. Soc.* **1991**, *113*, 6326.

(35) Tomson, N. C.; Arnold, J.; Bergman, R. G. *Organometallics* **2010**, *29*, 2926.

(36) La Pierre, H. S.; Arnold, J.; Toste, F. D. *Angew. Chem. Int. Ed.* **2011**, *50*, 3900.

(37) La Pierre, H. S.; Arnold, J.; Bergman, R. G.; Toste, F. D. *Inorg. Chem.* **2012**, *51*, 13334.

(38) Kriegel, B. M.; Bergman, R. G.; Arnold, J. *J. Am. Chem. Soc.* **2016**, *138*, 52.

(39) Panda, T. K.; Gamer, M. T.; Roesky, P. W. *Organometallics*, **2003**, *22*, 877.

(40) Janiak, C. *Z. Anorg. Allg. Chem.*, **2010**, *636*, 2387.

(41) $MgPh_2$ was made by the addition of dry 1,4-dioxane to a commercially available phenylmagnesium bromide solution and removing the volatile components of the resulting solution following its filtration away from the precipitate $MgCl_2$.

(42) Brown, C. A. *J. Org. Chem.*, **1974**, *39*, 3913.

(43) Manriquez, J. M.; Fagan, P. J.; Schertz, L. D.; Marks, T. J.; Bercaw, J.; Mcgrady, N. *Inorg. Synth.*, **2007**, *28*, 317.

(44) Monreal, M. J.; Thomson, R. K.; Cantat, T.; Travia, N. E.; Scott, B. L.; Kiplinger, J. L. *Organometallics*, **2011**, *30*, 2031.

(45) Spectral Database for Organic Compounds, SDBS. http://sdbs.db.aist.go.jp (National Institute of Advanced Industrial Science and Technology, accessed 8/22/17)

(46) Bruker. SADABS, APEX3, and SAINT. Bruker AXS, Madison, Wisconsin, USA.

(47) Sheldrick, G. M. *Acta Cryst. **2008**, A**64**, 112.*

(48) Farrugia, L. J. *J. Appl. Cryst.* **2012**, *45*, 849.

(49) Macrae, C. F.; Bruno, I. J.; Chisholm, J. A.; Edgington, P. R.; McCabe, P.; Pidcock, E.; Rodriguez-Monge, L.; Taylor, R.; van de Streek, J.; Wood, P. A. *J. Appl. Cryst.*, **2008**, *41*, 466.

Chapter 4

Reductions of a Rhenium(III) Terminal Oxo Complex by Isocyanides and Carbon Monoxide

Introduction

Transition metal oxo complexes have played a central role in the development of our understanding of metal-ligand multiple bonds.[1] In early metal systems (i.e. those containing electron-deficient transition metals with electronic configurations of d^2 or less) oxo moieties are generally quite robust, as the lack of valence electrons on the metal center allows for extensive electron donation from the oxo ligand.[2] However, in the handful of known oxo complexes where the metal center is occupied by a greater number of valence electrons, a unique range of stabilities, geometries, and reactivities has been observed.[2-14] The relative lack of well-defined examples of these atypical metal oxo species, coupled with their unpredictable behavior, makes the study of new low-valent metal oxo systems a promising area of research.

We recently reported the synthesis of the d^4 terminal oxo species ORe(η^2-DHF)(BDI) (DHF = dihydrofulvalene, BDI = N,N'-bis(2,6-diisopropylphenyl)-2,4-dimethyl-β-diketiminate), which was the unexpected reaction product of $OReCl_2$(BDI) and NaCp (Cp = cyclopentadienide).[15] Studies by Mayer and coworkers of Re(III) oxo complexes found that this multiply-bonded Re-O metal-ligand fragment was quite robust when supported by two highly electron-accepting acetylene moieties, as it remained intact upon exposure to a variety of reagents and conditions, including reduction to a formally Re(I) oxo species.[9-14] Considering there have been no similar studies of any Re(III) oxo compounds reported since, we wished to determine the relative reactivity of the oxo moiety in ORe(η^2-DHF)(BDI) as a means of comparison. Herein, we present the reactivity of ORe(η^2-DHF)(BDI) with isocyanides and carbon monoxide, whereby the oxo moiety of this complex will readily undergo transfer to these substrates under mild conditions. We rationalize these results in the context of previously reported examples of Re(III) terminal oxo complexes and demonstrate that the oxo moiety of ORe(η^2-DHF)(BDI) can be understood as solely nucleophilic, as opposed to electrophilic, in character by virtue of its inertness to trimethylphosphine (PMe_3).

Results and Discussion

Our preliminary studies of ORe(η^2-DHF)(BDI) attempted to exchange the DHF ligand with other unsaturated hydrocarbons, as well as strong σ-donors. We found no evidence for ligand exchange or any other mode of reactivity of ORe(η^2-DHF)(BDI) with ethylene, various alkynes (*e.g.* diphenylacetylene and 3-hexyne), or 4-dimethylaminopyridine (DMAP). Upon the addition of excess aryl or alkyl isocyanide, however, a color change or the formation of a precipitate was observed within minutes. Specifically, the addition of excess (ca. 7 eq.) of *tert*-butyl isocyanide (^{t}BuNC) to a solution of ORe(η^2-DHF)(BDI) in diethyl ether gave an emerald green solution, while the addition of 2,6-xylyl isocyanide (XylNC) under similar conditions resulted in the formation of a yellow-orange precipitate (Scheme 4.1). The C_{2v} solution symmetry of each of the new products, as observed by ^{1}H NMR spectroscopy, indicated the incorporation of four equivalents of isocyanide in two distinct chemical environments. The *in situ* production of one equivalent of the appropriate isocyanate was also observed in both cases. Broad absorbance bands spanning ca. 1750-2150 cm^{-1} were also measured in the FT-IR spectra of both compounds. Based on the spectroscopic evidence, the products of these reactions were assigned as the Re(I) tetrakis(isocyanide) complexes, $(RNC)_4$Re(BDI) (**4.1**, R = ^{t}Bu; **4.2**, R = Xyl). (Scheme 4.1).

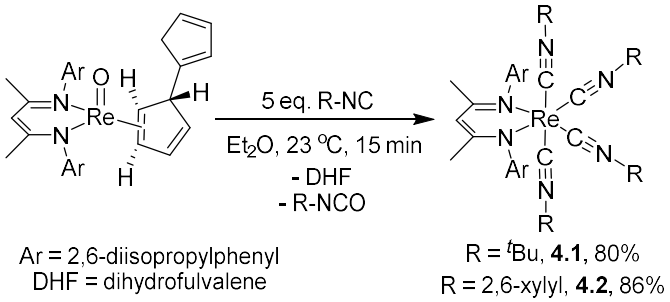

Scheme 4.1 Reduction and trapping of a rhenium(III) oxo complex by isocyanides yields complexes **4.1** and **4.2**.

Complexes **4.1** and **4.2** have vastly differing solubilities: while **4.1** is highly soluble in HMDSO, **4.2** was found to be completely insoluble in diethyl ether and hydrocarbon solvents, but moderately soluble in THF. Complex **4.2** is soluble enough in chloroform-*d* to facilitate its characterization by NMR spectroscopy, but these samples visibly darken and degrade upon standing overnight at room temperature, giving a complicated mixture of products. The ^{1}H NMR spectrum of **4.2** displays broadened peaks for the BDI backbone methyl and C-H groups, while all of the resonances for the XylNC ligands are sharp and well-defined.

Single crystals of **4.2** suitable for X-ray diffraction studies could be grown by vapor diffusion of *n*-hexane into a THF solution of the isolated compound. The complex crystallizes along a 2-fold rotational axis in the monoclinic space group *C*2/*c*, with the two chemically equivalent sets of XylNC ligands being related by symmetry (Figure 4.1). In the solid state, there is an observable torsion to the BDI ligand, with the backbone methyl groups displaced approximately 21° from co-planarity. The BDI nitrogen atoms also lie 2.220(3) Å from the metal, which is ca. 0.1 Å longer than is generally observed in our studies of Re complexes of this ligand.[15,16] This distal binding of the BDI ligand, which is likely due to the steric and electronic influence of the isocyanide ligands, appears to lead to a decrease in conjugation of the BDI π-system: Compared to other Re BDI complexes the C^{imine}-N bond lengths (1.324(3) Å) are shortened and the C^{imine}-C^{α} bond lengths (1.411(3) Å) are elongated. This indicates a buildup of negative charge on the backbone CH group, explaining the observable torsion in the BDI ligand backbone in the solid state and the corresponding fluxionality of this moiety in solution.

The reactivity observed with isocyanides prompted us to investigate the reaction of ORe(η^2-DHF)(BDI) with carbon monoxide, with the intention of forming a tetracarbonyl complex analogous to **4.1** and **4.2**. Observation of the reaction by ^{1}H NMR spectroscopy revealed the formation of several new products within minutes. One of the products identified is protonated BDI ligand, along with two or more rhenium-containing BDI species. When the reaction mixture was heated at 80 °C, the conversion to protonated BDI species was complete within 3 hours. When the reaction was conducted on a larger scale at room temperature, only an intractable mixture of products could be isolated. On the basis of these experiments, we concluded that if the intended tetracarbonyl complex $(CO)_4$Re(BDI) was being formed, its lifetime in solution was markedly shorter than the time needed for the reaction to go to completion.

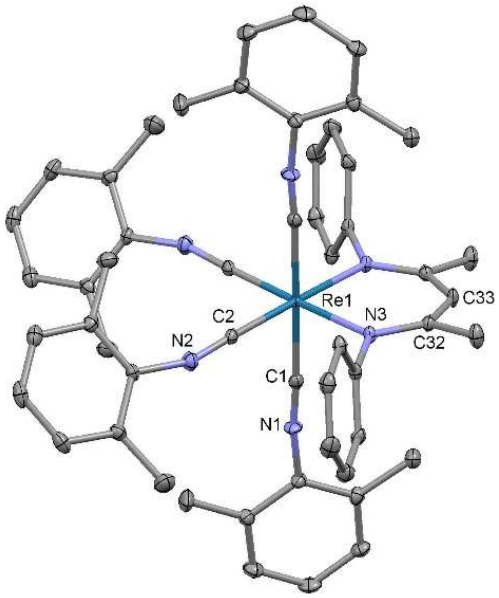

Figure 4.1 X-ray crystal structure of **4.2** with 50% probability ellipsoids. BDI isopropyl groups and H atoms are excluded for clarity. Labels are reserved for select, crystallographically independent atoms. Selected bond distances (Å) and angles (°): C1-Re1 = 2.034(4), C2-Re1 = 1.937(3), N3-Re1 = 2.220(3), C1-N1 = 1.155(4), C2-N2 = 1.188(3), N3-C32 = 1.324(3), C32-C33 = 1.411(3), C1-Re1-C2 = 86.82(10), C1-Re1-N3 = 89.26(9), C2-Re1-N3 = 92.94(13), N1-C1-Re1 = 176.44(18), N2-C2-Re1 = 173.7(2).

An analogous Re(I) tetracarbonyl complex containing a less encumbering and less electron-donating BDI derivative (with 2,6-dichlorophenyl substituents on the binding nitrogens) has been reported.[17] This complex could be isolated as crystalline material, yet it expelled one equivalent of CO within minutes in the presence of nitriles or amines to give *fac*-tricarbonyl adducts of the added σ-donor. Therefore, it is likely that either the increased steric profile or increased donor properties of the BDI ligand used in this study increases the lability of the tetracarbonyl complex $(CO)_4Re(BDI)$, generating coordinately unsaturated species in solution that contribute to the degradative pathways leading to protonated BDI. It is also possible the presence of free DHF as generated in the reaction mixture may contribute to the degradation of $(CO)_4Re(BDI)$.

Taking inspiration from the reactivity of the previously reported rhenium tetracarbonyl complex, we repeated the reaction of $ORe(\eta^2\text{-DHF})(BDI)$ with CO in the presence of one equivalent of DMAP. Upon workup, the product *fac*-$(CO)_3Re(DMAP)(BDI)$ (**4.3**) was isolated as light-yellow crystals in moderate yield (Scheme 4.2). The IR absorbance of spectrum displayed metal carbonyl stretches at 2004 and 1878 cm^{-1}. The solid state structure of **4.3** was determined by X-ray crystallography, which confirmed the facial arrangement of the three carbonyl ligands (Figure 4.2). When the same reaction was conducted by adding CO to a solution of $ORe(\eta^2\text{-DHF})(BDI)$, followed by the addition of DMAP after consumption of the Re starting material, the isolated yield of **4.3** was markedly lower. This result supports the hypothesis that the reaction of $ORe(\eta^2\text{-DHF})(BDI)$ likely generates a monomeric tetracarbonyl complex that can bind DMAP and

release one equivalent of CO to form **4.3**. In all, the isolation of **4.3** in these experiments indicates that OAT from ORe(η^2-DHF)(BDI) to CO takes place quickly under mild conditions, as was observed with isocyanides.

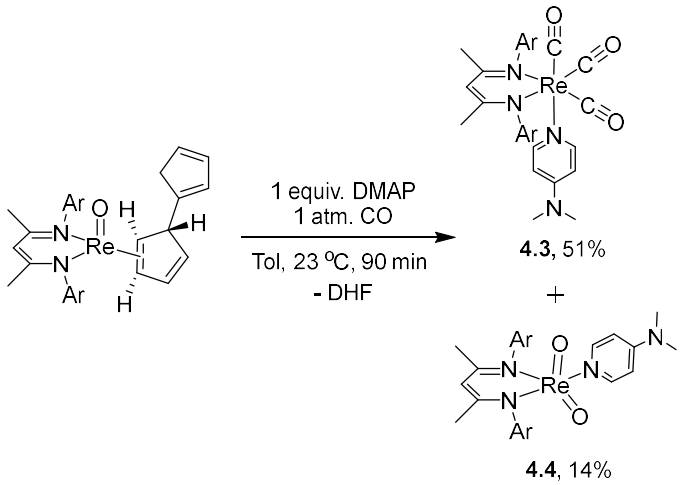

Scheme 4.2 The reduced rhenium(I) complex **4.3** and the oxidized *cis*-dioxo complex **4.4** are generated upon exposure of the rhenium(III) terminal oxo complex to CO in the presence of DMAP.

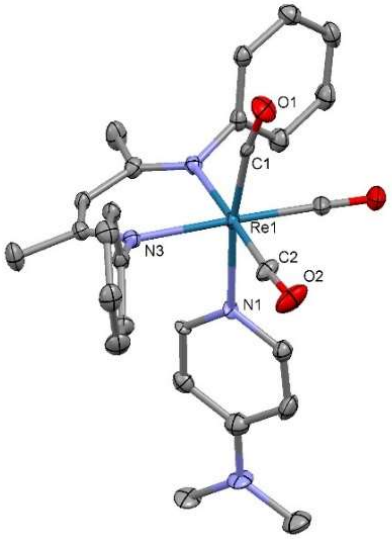

Figure 4.2 X-ray crystal structure of one of the two crystallographically independent molecules of **4.3** with 50% probability ellipsoids. BDI isopropyl groups, solvent molecules, and H atoms are excluded for clarity. Labels are reserved for select, crystallographically independent atoms. Selected bond distances (Å) and angles (º): C1-Re1 = 1.910(9), C2-Re1 = 1.920(6), N1-Re1 = 2.267(9), N3-Re1 = 2.192(6), C1-O1 = 1.175(8), C2-O2 = 1.157(6), C1-Re1-C2 = 83.80(19), C1-Re1-N1 = 171.3(2), C1-Re1-N3 = 97.99(17), C2-Re1-N1 = 89.80(17), C2-Re1-N3 = 94.4(3), O1-C1-Re1 = 171.4(6), O2-C2-Re1 = 175.8(5).

In all of our reactions to form **4.3**, a minor product was also isolated as a green powder, with its separation and purification eased by its insolubility in diethyl ether and hydrocarbon solvents (Scheme 4.2). The IR absorbance spectrum of this green product indicated it did not contain any carbonyl ligands or unsaturated C-O bonds. X-ray structural determination of the recrystallized product revealed that it was a rhenium(V) *cis*-dioxo compound, $(O)_2Re(DMAP)(BDI)$ (**4.4**) (Figure 4.3). The geometry of this complex is distorted trigonal bipyramidal with the oxo ligands occupying equatorial positions, and the DMAP ligand being situated in an axial positon *trans* to one of the bound nitrogen atoms of the BDI ligand, which occupies both axial and equatorial sites around the metal. This geometry is analogous to that of the well-known Re(V) *cis*-dioxo compound $(O)_2ReI(PPh_3)_2$,[18-20] as well as Lewis base adducts of niobium(V) bis(imido) complexes studied by our groups that also contain the BDI ancillary ligand.[21,22]

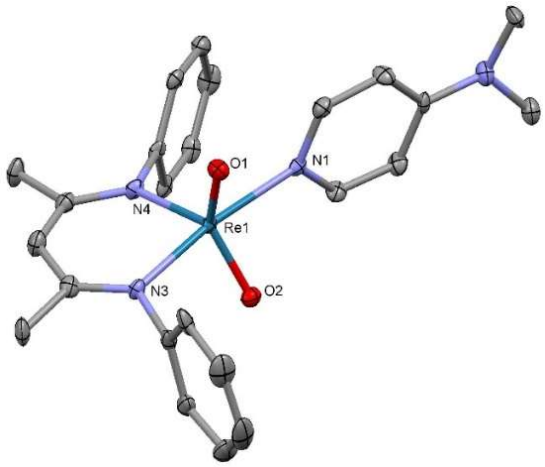

Figure 4.3 X-ray crystal structure of **4.4** with 50% probability ellipsoids. BDI isopropyl groups and H atoms are excluded for clarity. Selected bond distances (Å) and angles (°): O1-Re1 = 1.742(5), O2-Re2 = 1.732(5), N1-Re1 = 2.184(6), N3-Re1 = 2.099(6), N4-Re1 = 2.019(6), O1-Re1-O2 = 137.0(2), O1-Re1-N4 = 111.0(2), O2-Re1-N4 = 111.8(2), N1-Re1-N3 = 170.7(2), N3-Re1-N4 = 90.0(2).

While the isolated yields of **4.4** were consistently low (12-14%), the fact that an oxidized product was generated under reducing reaction conditions was at first, unintuitive. We tested whether the CO_2 generated *in situ* by OAT was capable of oxidizing the starting material $ORe(\eta^2$-DHF)(BDI) or **4.3** to form **4.4** (or an analog of **4.4** free of the dative DMAP ligand). We found no evidence of any reaction between CO_2 and these complexes, either as isolated species, or following the simultaneous exposure of $ORe(\eta^2$-DHF)(BDI) to both CO and CO_2 gases. By excluding CO_2 as potential means for the formation of **4.4**, we were left with the following hypothesis: an intermediate along the pathway between $ORe(\eta^2$-DHF)(BDI) and **4.3**, perhaps a species of the formulation "$ORe(CO)_2$(BDI)" or similar, where the DHF ligand has been displaced by CO ligands, is capable of transferring its oxo ligand to an equivalent of the starting material or exchanging oxo ligands between itself. OAT between metal species has been observed in several systems,[23-25] including between identical or closely related species containing the same metal.[26-29] This proposed OAT-mediated disproportionation, a subset of such metal-centered OAT reactions,

aligns with the fact that the oxidized product **4.4** is only isolated when CO is used as an OAT acceptor; its steric profile is much smaller than those of either ^{t}BuNC or XylNC, increasing the feasibility of an intermetallic OAT. The generation of Re dioxo compounds and other oxidized products from ORe(η^2-DHF)(BDI) by more efficient and selective routes will be a topic of future studies.

Considering the mild conditions necessary for OAT between ORe(η^2-DHF)(BDI) and isocyanides or CO, it was expected that OAT from this Re(III) oxo complex to PMe_3 would be similarly facile. Trialkylphosphines are considered to be excellent OAT acceptors, owing to their electron-rich phosphorus centers. PMe_3 is particularly potent in this regard: it is reducing enough to require handling under inert conditions to prevent its rapid decomposition when combined with atmospheric oxygen. Therefore, we were surprised to find that ORe(η^2-DHF)(BDI) did not show any signs of reactivity with PMe_3, even when the complex was heated for several days in the presence of excess phosphine. This indicates that the rhenium oxo moiety of ORe(η^2-DHF)(BDI) does not have demonstrable electrophilic character, and therefore must be the nucleophilic agent in the observed OAT reactions with isocyanides and CO. In conventional transition metal terminal oxo complexes, the oxo ligand tends to display electrophilic character as a result of extensive electron donation to the metal through one σ-bond and two equivalent, orthogonal π-bonds.[1,2] Many other examples of nucleophilic metal oxo moieties have been known,[30-36] including, relevantly, a Re(V) oxo complex that displays ambiphilic character.[37] We attempted to demonstrate the nucleophilic character of the oxo moiety in ORe(η^2-DHF)(BDI) by making an adduct with the Lewis acid $B(C_6F_5)_3$. We found that this reaction led to the decomposition of the starting material, and no products could be isolated from the resulting mixture.

The OAT reactivity of ORe(η^2-DHF)(BDI) deviates from the chemistry of the Re(III) terminal oxo complexes originally studied by Mayer. This difference can be rationalized in terms of the ancillary ligands in both complexes. Namely, Mayer's Re(III) oxo complexes were invariably supported by two highly electron-accepting alkyne ligands,[10-14] whereas ORe(η^2-DHF)(BDI) is supported by a less electron-accepting olefin group and a sterically encumbering, electron-donating BDI ligand.[14] The expected impact on the rhenium oxo moiety in ORe(η^2-DHF)(BDI) as compared to those in Mayer's complexes thus aligns with our experimental observations, whereby a decrease in backbonding from the d^4 Re(III) center leads to increased electron density on the oxo moiety, which, as demonstrated by this study, manifests as nucleophilicity and a corresponding selectivity for electrophilic OAT acceptors.

Summary and Conclusions

We have described the oxygen atom transfer reactivity of the d^4 terminal oxo complex ORe(η^2-DHF)(BDI), yielding several Re(I) isocyanide and carbonyl complexes containing the BDI ligand. While the tetrakis(isocyanide) complexes proved to be stable at room temperature, the inclusion of a trapping agent was necessary to obtain an isolable product from the reduction of ORe(η^2-DHF)(BDI) by CO. Unexpectedly, in addition to the DMAP-trapped *fac*-tricarbonyl complex **4.3**, the oxidation product **4.4** was also isolated, indicating that under the reaction conditions OAT also occurs between reactive, transient Re species as well as from Re to CO. The lack of reactivity of ORe(η^2-DHF)(BDI) with PMe_3 indicated that the oxo moiety of this low-

valent species can be typified as a nucleophile, which explains its facile OAT reactivity with CO and isocyanides. Future work will continue to explore the use of ORe(η^2-DHF)(BDI) as a convenient synthetic source of the Re(III) oxo fragment.

Experimental

General Considerations: All manipulations were carried out under a dry nitrogen atmosphere, either in an MBraun LabStar glovebox or on a Schlenk line using standard techniques. Toluene, diethyl ether, and *n*-hexane were dried by passage through a basic alumina column and were handled and stored under a dry nitrogen atmosphere in standard Strauss flasks or in the glovebox. Hexamethyldisiloxane (HMDSO) was dried over Na/benzophenone, distilled under N_2, and stored in the glovebox prior to use. Deuterated benzene and chloroform were obtained from Cambridge Isotope Labs, dried over an appropriate reagent (Na/benzophenone for C_6D_6, CaH_2 for $CDCl_3$), and transferred under reduced pressure prior to storage in the glovebox over 4 Å molecular sieves. Celite was dried in a 150 ºC oven for 24 hours prior to storage in the glovebox. 2,6-Xylyl isocyanide, *tert*-butylisocyanide, 4-dimethylaminopyridine, and CO gas were obtained from commercial sources. Solid reagents were dried under high vacuum and liquid reagents were degassed prior to use. The reported compound ORe(η^2-DHF)(BDI) was synthesized using known procedures.[6] NMR spectroscopy data were obtained on Bruker AV-500 and AV-600 instruments. All ^{1}H and ^{13}C spectra were referenced to the residual peak of the solvent used. Select peak assignments were corroborated with ^{1}H-^{13}C HSQC experiments as necessary. Unless noted otherwise, "room temperature" and "ambient temperature" both refer to approx. 23 ºC. Infrared absorption data were obtained using a Thermo Scientific Nicolet iS10 instrument, with the sample chamber under ambient atmosphere. Samples were prepared as Nujol mulls pressed between KBr plates in the glovebox. A background IR spectrum was obtained immediately prior to data acquisition for each sample.

(^{t}BuNC)$_4$Re(BDI) (4.1): A solution of *tert*-butyl isocyanide (39.1 mg, 0.470 mmol, 7 equiv.) in Et_2O (3 mL) was added to a stirred solution of ORe(η^2-DHF)(BDI) (50.0 mg, 0.0667 mmol) in Et_2O (5 mL) at ambient temperature. Within minutes, a color change from dark forest green to a lighter emerald green was observed. After the reaction mixture was stirred for 15 minutes, its volatile components were removed *in vacuo*. The dry residue was extracted into HMDSO (5 mL), and these extracts were filtered through Celite. The volatile components of the filtered extracts were removed *in vacuo*, and the resulting residue was further exposed to high vacuum for ca. 3 h to give **1** (50 mg, 80% yield) as an emerald green powder. m.p.: decomp. above 117 ºC. ^{1}H NMR (600 MHz, C_6D_6, 298 K): 7.27 (d, 4H, BDI Ar, J = 7.6 Hz), 7.15 (t, 2H, BDI Ar, J = 7.6 Hz), 4.75 (s, 1H, *H*C[MeC(NAr)]$_2$), 3.71 (sept, 4H, BDI C*H*(Me)$_2$, J = 6.8 Hz), 1.72 (s, 6H, HC[*Me*C(NAr)]$_2$), 1.69 (d, 12H, BDI CH(*Me*)$_2$, J = 6.7 Hz), 1.35 (d, 12H, BDI CH(*Me*)$_2$, J = 6.8 Hz), 1.23 (s, 18H, *Me$_3$*CNC), 1.19 (s, 18H, *Me$_3$*CNC). ^{13}C NMR (151 MHz, C_6D_6, 298 K): 183.70 (HC[Me*C*(NAr)]$_2$), 162.60 (BDI Ar), 153.81 (BDI Ar), 142.94 (BDI Ar), 124.30 (BDI Ar), 123.71 (BDI Ar), 98.73 (H*C*[MeC(NAr)]$_2$), 55.99 (Me$_3$*C*NC), 55.64 (Me$_3$*C*NC), 33.05 (BDI *C*H(Me)$_2$), 31.73 (HC[*Me*C(NAr)]$_2$), 27.77 (BDI CH(*Me*)$_2$), 25.89 (*Me$_3$*CNC), 25.83 (*Me$_3$*CNC), 24.90 (BDI CH(*Me*)$_2$). IR (Nujol/KBr, cm^{-1}): 2117 (^{t}BuNC), 1967 (^{t}BuNC), 1836 (^{t}BuNC), 1774 (^{t}BuNC). Elemental analysis was not obtained for this compound, as its extreme solubility prevented its

purification by crystallization or washing. A detectable, variable amount of HMDSO remained in isolated **1** even after prolonged exposure to vacuum at room temperature. The instability of **1** to heat also precluded its purification by heating under vacuum.

(XylNC)$_4$Re(BDI) (4.2): A solution of 2,6-xylyl isocyanide (43.7 mg, 0.333 mmol, 5 equiv.) in Et_2O (5 mL) was added to a stirred solution of ORe(η^2-DHF)(BDI) (50.0 mg, 0.0667 mmol) in Et_2O (5 mL) at ambient temperature. Within minutes, a color change from dark forest green to orange was observed, quickly followed by the formation of a yellow-orange precipitate. After the reaction mixture was stirred for 15 minutes, its volatile components were removed *in vacuo*. The resulting residue was washed with hexane (2 x 6 mL), and the residual volatiles were removed *in vacuo* to give **2** as a yellow-orange powder (67 mg, 86% yield). Single crystals suitable for structural determination by X-ray crystallography were grown by the vapor diffusion of *n*-hexane into a filtered, saturated solution of **2** in THF. m.p.: decomp. above 190 ºC. ^{1}H NMR (600 MHz, $CDCl_3$, 298 K): 7.08-7.04 (m, 6H, BDI Ar), 6.98 (d, 4H, Xyl Ar, J = 7.6 Hz), 6.90 (t, 2H, Xyl Ar), 6.80 (d, 4H, Xyl Ar), 6.71 (t, 2H, Xyl Ar), 4.71 (bs, 1H, *H*C[MeC(NAr)]$_2$), 3.71 (sept, 4H, BDI C*H*(Me)$_2$, J = 6.8 Hz), 2.42 (s, 12H, Xyl Me), 1.92 (s, 12H, Xyl Me), 1.62 (bs, 6H, HC[*Me*C(NAr)]$_2$), 1.03 (d, 12H, BDI CH(*Me*)$_2$, J = 6.7 Hz), 0.93 (d, 12H, BDI CH(*Me*)$_2$, J = 6.8 Hz). ^{13}C NMR (151 MHz, $CDCl_3$, 298 K): 134.76 (XylNC Ar), 130.27 (XylNC Ar), 127.97 (BDI Ar), 126.88 (XylNC Ar), 126.44 (XylNC Ar), 123.84 (XylNC Ar), 123.42 (XylNC Ar), 123.42 (BDI Ar), 100.16 (H*C*[MeC(NAr)]$_2$), 27.64 (BDI *C*H(Me)$_2$), 25.73 (HC[*Me*C(NAr)]$_2$), 25.16 (XylNC Me), 24.92 (XylNC Me), 19.43 (BDI CH(*Me*)$_2$), 18.86 (BDI C(*Me*)$_2$). IR (Nujol/KBr, cm^{-1}): 2023 (XylNC), 1996 (XylNC), 1921 (XylNC). Anal. Cald. for $ReN_6C_{65}H_{77}$ (**2**): C, 69.18; H, 6.88; N, 7.45 %. Found: C, 68.93; H, 7.02; N, 7.62 %.

***fac*-(CO)$_3$Re(DMAP)(BDI) (4.3):** A solid mixture of ORe(η^2-DHF)(BDI) (150 mg, 0.200 mmol) and DMAP (24.4. mg, 0.200 mmol, 1 eq.) were dissolved in toluene (ca. 7 mL), and this solution was added to a 25 mL Schlenk flask, which was then sealed. The room temperature solution was degassed under vacuum for ca. 15 seconds, the headspace of the flask was refilled with CO gas (ca. 1 atm.) via the Schlenk line, and the flask was again sealed. The reaction mixture was stirred at room temperature for 90 minutes, yielding a dark, turbid green-yellow solution. The volatile components of the reaction mixture were removed *in vacuo* and the flask was returned to the glovebox. The reaction residue was extracted with 15 mL Et_2O, and these extracts were filtered through Celite to give a dark yellow solution, which was concentrated in vacuo and stored at -40ºC to give **3** as light yellow crystals (82 mg, 51%). X-ray quality crystals were obtained by recrystallizing isolated **3** from Et_2O at -40 ºC. m.p.: decomp. above 252 ºC. ^{1}H NMR (500 MHz, C_6D_6, 298 K): 8.75 (bs, 1H, DMAP Ar), 8.49 (bs, 1H, DMAP Ar), 7.27 (dd, 2H, BDI Ar, J = 6.9, 2.2 Hz), 7.20-7.14 (m, 4H, BDI Ar), 5.95 (bs, 1H, DMAP Ar), 5.55 (bs, 1H, DMAP Ar), 5.00 (s, 1H, *H*C[MeC(NAr)]$_2$), 3.78 (sept, 2H, BDI C*H*(Me)$_2$, J = 6.7 Hz), 2.72 (sept, 2H, BDI C*H*(Me)$_2$, J = 6.8 Hz), 2.06 (s, 6H, DMAP Me), 1.79 (s, 6H, HC[*Me*C(NAr)]$_2$), 1.71 (d, 6H, BDI CH(*Me*)$_2$, J = 6.7 Hz), 1.32 (d, 6H, BDI CH(*Me*)$_2$, J = 6.7 Hz), 1.01 (d, 6H, BDI CH(*Me*)$_2$, J = 6.8 Hz), 0.98 (d, 6H, BDI CH(*Me*)$_2$, J = 6.8 Hz). ^{13}C NMR (151 MHz, C_6D_6, 298 K): 163.22 (HC[Me*C*(NAr)]$_2$), 154.05 (DMAP Ar), 152.83 (DMAP Ar),143.35 (BDI Ar) 140.91 (BDI Ar), 126.13 (BDI Ar), 124.60 (BDI Ar), 123.87 (BDI Ar), 106.94 (DMAP Ar), 96.52 (H*C*[MeC(NAr)]$_2$), 38.28 (DMAP Me), 28.59 (BDI *C*H(Me)$_2$), 27.94 (BDI *C*H(Me)$_2$), 25.65 (BDI CH(*Me*)$_2$), 25.63 (BDI CH(*Me*)$_2$),

25.49 (BDI CH(*Me*)$_2$), 25.11 (HC[*Me*C(NAr)]$_2$), 24.09 (BDI CH(*Me*)$_2$). IR (Nujol/KBr, cm^{-1}): 2004 (CO), 1878 (CO). Anal. Cald. for $ReO_3N_4C_{39}H_{51}$ (**3**): C, 57.83; H, 6.35; N, 6.92 %. Found: C, 57.95; H, 6.19; N, 7.02 %.

(O)$_2$Re(DMAP)(BDI) (4.4): Following the above synthetic procedure for **3**, extraction of the dry reaction residue with Et_2O (to dissolve and separate **3**) left behind kelly green solids. These solids were dissolved into THF (ca. 6 mL), and the resulting green solution was filtered through Celite. The volatile components of the filtered solution were removed *in vacuo*. The resulting solids were washed with 2 x 3 mL Et_2O, and the residual volatiles were removed *in vacuo* to give **4** as kelly green solids (21 mg, 14%). X-ray quality crystals were obtained by the vapor diffusion of *n*-hexane into a filtered solution of **4** in THF. m.p.: decomp. above 114 ºC. ^{1}H NMR (600 MHz, $CDCl_3$, 298 K): 7.47-7.39 (m, 2H, DMAP Ar), 7.13-7.04 (m, 3H, BDI Ar), 6.93 (bs, 3H, BDI Ar), 6.01 (d, 2H, DMAP Ar, J = 6.6 Hz), 5.04 (s, 1H, *H*C[MeC(NAr)]$_2$), 3.35 (bs, 2H, BDI C*H*(Me)$_2$), 3.27 (bs, 2H, BDI C*H*(Me)$_2$), 2.90 (s, 6H, DMAP Me), 1.93 (bs, 3H, HC[*Me*C(NAr)]$_2$), 1.83 (bs, 3H, HC[*Me*C(NAr)]$_2$), 1.43 (bs, 6H, BDI CH(*Me*)$_2$), 1.14 (bs, 18H, BDI CH(*Me*)$_2$). ^{13}C NMR (151 MHz, $CDCl_3$, 298 K): 170.59 (HC[Me*C*(NAr)]$_2$), 155.20 (DMAP Ar), 150.04 (DMAP Ar),143.35 (BDI Ar) 140.91 (BDI Ar), 126.54 (BDI Ar), 123.90 (BDI Ar), 105.61 (DMAP Ar), 103.42 (H*C*[MeC(NAr)]$_2$), 39.12 (DMAP Me), 28.47 (BDI *C*H(Me)$_2$), 27.39 (BDI *C*H(Me)$_2$), 25.77 (BDI CH(*Me*)$_2$), 25.32 (BDI CH(*Me*)$_2$), 25.23 (BDI CH(*Me*)$_2$), 23.64 (HC[*Me*C(NAr)]$_2$). Anal. Cald. for $ReO_2N_4C_{36}H_{51}$ (**4**): C, 57.04; H, 6.78; N, 7.39 %. Found: C, 57.23; H, 6.66; N, 7.31 %.

X-Ray Crystallographic Details: X-ray crystallographic measurements were conducted at the Advanced Light Source (ALS), Lawrence Berkeley National Laboratory (LBNL), beam line 12.2.1, using a Bruker diffractometer equipped with a PHOTON100 CMOS detector and a silicon-monochromated beam of 17 keV (0.7288 Å) synchrotron radiation. Diffraction data was collected, reduced, and corrected for absorption using the Bruker APEX3 software package and its associated programs (SAINT, SADABS, TWINABS).[38] Structure solutions were obtained by direct methods using SHELXT and refined against F^2 using SHELXL-2014, as implemented by the WinGX shell program.[39,40] Thermal ellipsoid plots as presented in this report were generated using Mercury.[41] CCDC 1834897 (**4.2**), 1834898 (**4.3**), and 1834899 (**4.4**) contain the supplementary crystallographic information for this paper. These data can be obtained free-of-charge from the Cambridge Crystallographic Data Centre.

Table 4.1 Unit Cell and and Refinement Metrics for the Crystal Structures of **4.2**, **4.3**, and **4.4**.

	4.2	**4.3**	**4.4**
Chemical formula	$C_{65}H_{77}N_6Re$	$C_{43}H_{61}N_4O_4Re$	$C_{36}H_{51}N_4O_2Re$
Formula weight	1128.52	844.15	758.00
Color, habit	Orange, block	Yellow, block	Green, blade
Temperature (K)	100(2)	100(2)	100(2)
Crystal system	Monoclinic	Monoclinic	Triclinic
Space group	C 2/c	P 2_1/m	P-1
a (Å)	17.210(17)	13.79(4)	9.0737(6)
b (Å)	16.719(16)	17.25(5)	11.6586(8)
c (Å)	19.140(18)	17.98(6)	16.9664(12)
α (°)	90	90	73.799(5)
β (°)	90.651(8)	94.494(17)	88.041(5)
γ (°)	90	90	75.883(4)
V (Å^3)	5507(9)	4265(22)	1670.4(2)
Z	4	4	2
Density (Mg m^{-3})	1.361	1.377	1.507
F(000)	2336	1816	772
Radiation Type	Synchrotron	Synchrotron	Synchrotron
μ (mm^{-1})	2.341	3.456	3.675
Crystal size (mm^3)	0.020 x 0.020 x 0.015	0.020 x 0.020 x 0.010	0.050 x 0.020 x 0.005
Meas. Refl.	46796	85554	17967
Indep. Refl.	8421	10278	7706
R(int)	0.0502	0.0665	0.0542
Final R indices	R = 0.0323	R = 0.0319	R = 0.0556
[I > 2σ(I)]	R_w = 0.1129	R_w = 0.0610	R_w = 0.1338
Goodness-of-fit	1.076	1.172	1.091
$\Delta\rho_{max}$, $\Delta\rho_{min}$ (e Å^{-3})	1.189, -3.221	1.310, -1.330	9.764, -3.702

Notes and References

(1) Nugent, W. A.; Mayer, J. M. *Metal-ligand Multiple bonds*. John Wiley & Sons: New York, 1988.

(2) Winkler, J. R.; Gray, H. B. Electronic Structures of Oxo-Metal Ions. In: *Molecular Electronic Structures of Transition Metal Complexes I. Structure and Bonding*; Mingos, D.; Day, P.; Dahl, J., Ed.; Springer: Berlin, Heidelberg, 2011; Vol. 142; p 17-28.

(3) Hay-Motherwell, R. S.; Wilkinson, G.; Hussain-Bates, B.; Hursthouse, M. B. Synthesis and X-ray Crystal Structure of Oxotrimesityliridium(V). *Polyhedron* **1993**, *12*, 2009-2012.

(4) MacBeth, C. E.; Golombek, A. P.; Young Jr., V. G.; Yang, C.; Kuczera, K.; Hendrich, M. P.; Borovik, A. S. O_2 Activation by Nonheme Iron Complexes: A Monomeric Fe(III)-Oxo Complex Derived From O_2. *Science*, **2000**, *289*, 938-941.

(5) Poverenov, E.; Efremenko, I.; Frenkel, A. I.; Ben-David, Y.; Shimon, L. J. W.; Leitus, G.; Konstantinovski, L.; Martin, J. M. L.; Milstein, D. Evidence for a terminal Pt(IV)-oxo complex exhibiting diverse reactivity. *Nature* **2008**, *455*, 1093-1096.

(6) Hong, S.; Lee, Y.-M.; Sankaralingam, M.; Vardhaman, A. K.; Park, Y. J.; Cho, K.-B.; Ogura, T.; Sarangi, R.; Fukuzumi, S.; Nam, W. A Manganese(V)–Oxo Complex: Synthesis by Dioxygen Activation and Enhancement of Its Oxidizing Power by Binding Scandium Ion. *J. Am. Chem. Soc.* **2016**, *138*, 8523-8532.

(7) Herrmann, W. A.; Fischer, R. A.; Herdtweck, E. Mehrfachbindungen zwischen Hauptgruppenelementen und Übergangsmetallen: XLIX. Reduktive Enthalogenierung von Organorhenium(V)-Komplexen als geradliniger Syntheseweg zu niedervalenten Rhenium-Derivaten. *J. Organomet. Chem.* **1987**, *329*, C1-C6.

(8) Esteruelas, M. A.; Modrego, F. J.; Oñate, E.; Royo, E. Dioxygen Activation by an Osmium-dihydride: Preparation and Characterization of a d^4 Square-Planar Complex. *J. Am. Chem. Soc.* **2003**, *125*, 13344-13345.

(9) Spaltenstein, E.; Conry, R. R.; Critchlow, S. C.; Mayer, J. M. Synthesis, Characterization, and Reactivity of a Formally Rhenium(I) Terminal Oxo Complex, $NaRe(O)(RC{\equiv}CR)_2$. *J. Am. Chem. Soc.* **1989**, *111*, 8741-8742.

(10) Mayer, J. M.; Tulip, T. H. Synthesis, Reactivity, and Crystal and Molecular Structure of $Re(O)I(MeC{\equiv}CMe)_2$. *J. Am. Chem. Soc.* **1984**, *106*, 3878-3879.

(11) Mayer, J. M.; Thorn, D. L.; Tulip, T. H. Synthesis, Reactions, and Electronic Structure of Low-Valent Rhenium-Oxo Compounds. Crystal and Molecular Structure of $Re(O)I(MeC{\equiv}CMe)_2$. *J. Am. Chem. Soc.* **1985**, *107*, 7454-7462.

(12) Mayer, J. M.; Tulip, T. H.; Calabrese, J. C.; Valencia, E. Associative Ligand Substitution Reactions of Low-Valent Rhenium-Oxo Compounds. Crystal and Molecular Structures of $[ReO(MeC{\equiv}CMe)_2L]SbF_6$, L = Pyridine and 4,4'-Dimethyl-2,2'-bipyridine. *J. Am. Chem. Soc.* **1987**, *109*, 157-163.

(13) Valencia, E.; Santarsiero, B. D.; Geib, S. J.; Rheingold, A. L.; Mayer, J. M. Synthesis and Characterization of Symmetrical and Unsymmetrical Low-Valent Rhenium-Oxo Dimers, $Re_2O_2(RC{\equiv}CR)_4$. *J. Am. Chem. Soc.* **1987**, *109*, 6896-6898.

(14) Spaltenstein, E.; Erikson, T. K. G.; Critchlow, S. C.; Mayer, J. M. Low-Valent Rhenium-Oxo Alkyl and -Oxo Hydride Complexes. The Stabilizing Influence of the Oxo Ligand. *J. Am. Chem. Soc.* **1989**, *111*, 617-623.

(15) Lohrey, T. D.; Bergman, R. G.; Arnold, J. Olefin-Supported Rhenium(III) Terminal Oxo Complexes Generated by Nucleophilic Addition to a Cyclopentadienyl Ligand. *Angew. Chem. Int. Ed.* **2017**, *56*, 14241-14245.
(16) Lohrey, T. D.; Bergman, R. G.; Arnold, J. Oxygen Atom Transfer and Intramolecular Nitrene Transfer in a Rhenium β-Diketiminate Complex. *Inorg. Chem.* **2016**, *55*, 11993-12000.
(17) Yempally, V.; Fan, Y. P.; Arndtsen, B. A.; Bengali, A. A. Intramolecular C–C Bond Coupling of Nitriles to a Diimine Ligand in Group 7 Metal Tricarbonyl Complexes. *Inorg. Chem.* **2015**, *54*, 11441-11449.
(18) Freni, M.; Giusto, D.; Romiti, P.; Minghetti, G. Hydrolysis products of dihalo(oxo)(ethoxy)bis(triphenylphosphine)rhenium(V) compounds and their reactions. *Gazz. Chim. It.* **1969**, *99*, 286-299.
(19) Ciani, G.; D'Alfonso, G.; Romiti, P.; Sironi, A.; Freni, M. Rhenium(V) Oxide Complexes. Crystal and Molecular Structures of the Compounds *trans*-$ReI_2O(OR)(PPh_3)_2$ (R = Et, Me) and of their Hydrolysis Derivative $ReIO_2(PPh_3)_2$. *Inorg. Chim. Acta* **1983**, *72*, 29-37.
(20) Schmid, S.; Strahle, J. On the Reaction of $ReO_2I(PPh_3)_2$ with Phenyl Isocyanate. Synthesis and Crystal Structures of $ReO_2I(PPh3)_2.CHCl_3$, $[ORe(OCONPh)I(PPh_3)]_3$, $Re(NPh)(NH_2Ph)I_2(PPh_3)(OCONHPh)$, and $Re(NPh)(NH_2Ph)I_2(PPh_3)(OReO_3)$. *Z. Naturforsch., B: Chem. Sci.* **1991**, *46*, 235-244.
(21) Tomson, N. C.; Arnold, J.; Bergman, R. G. Halo, Alkyl, Aryl, and Bis(imido) Complexes of Niobium Supported by the β-Diketiminato Ligand. *Organometallics* **2010**, *29*, 2926-2942.
(22) Kriegel, B. M.; Bergman, R. G.; Arnold, J. Nitrene Metathesis and Catalytic Nitrene Transfer Promoted by Niobium Bis(imido) Complexes. *J. Am. Chem. Soc.* **2016**, *138*, 52-55.
(23) Templeton, J. L.; Ward, B. C.; Chen, G. J.-J.; McDonald, J. W.; Newton, W. E. Oxotungsten(IV)-Acetylene Complexes: Synthesis via Intermetal Oxygen Atom Transfer and Nuclear Magnetic Resonance Studies. *Inorg. Chem.* **1981**, *20*, 1248-1253.
(24) Holm, R. H. Metal-Centered Oxygen Atom Transfer Reactions. *Chem. Rev.* **1987**, *87*, 1401-1449.
(25) Woo, L. K. Intermetal Oxygen, Sulfur, Selenium, and Nitrogen Atom Transfer Reactions. *Chem. Rev.* **1993**, *93*, 1125-1136.
(26) Harlan, E. W.; Berg, J. M.; Holm, R. H. Thermodynamic Fitness of Molybdenum(IV,VI) Complexes for Oxygen Atom Transfer Reactions, Including Those with Enzymatic Substrates. *J. Am. Chem. Soc.* **1986**, *108*, 6992-7000.
(27) Srinivasan, K.; Michaud, P.; Kochi, J. K. Epoxidation of Olefins with Cationic (salen)Mn^{III} Complexes. The Modulation of Catalytic Activity by Substituents. *J. Am. Chem. Soc.* **1986**, *108*, 2309-2320.
(28) Hays, J. A.; Day, C L.; Young, V. G.; Woo, L. K. Intermetal Oxygen Atom Transfer Reactions of Titanium Porphyrins: Complete vs Incomplete Atom Transfer. X-ray Structure of (μ-Oxo)bis[(*meso*-tetra-*p*-tolylporphyrinato)titanium(III)]. *Inorg. Chem.* **1996**, *35*, 7601-7607.
(29) Sastri, C. V.; Oh, K.; Lee, Y. J.; Seo, M. S.; Shin W.; Nam W. Oxygen-Atom Transfer between Mononuclear Nonheme Iron(IV)–Oxo and Iron(II) Complexes. *Angew. Chem. Int. Ed.* **2006**, *45*, 3992-3995.

(30) Carney, M. J.; Walsh, P. J.; Hollander, F. J.; Bergman, R. G. A Reactive Organometallic Oxo Intermediate, $Cp^*_2Zr{=}O$: Generation and Subsequent Trapping Reactions Forming Alkyne and Nitrile Addition Products. *J. Am. Chem. Soc.* **1989**, *111*, 8751-8753.
(31) Carney, M. J.; Walsh, P. J.; Bergman, R. G. Room Temperature Generation of Reactive Intermediates $Cp^*_2Zr{=}O$ and $Cp^*_2Zr{=}S$: Trapping Reactions with Unsaturated Organic Molecules and Dative Ligands. *J. Am. Chem. Soc.* **1990**, *112*, 6426-6428.
(32) Carney, M. J.; Walsh, P. J.; Hollander, F. J.; Bergman, R. G. Generation of the Highly Reactive Intermediates $Cp^*_2Zr{=}O$ and $Cp^*_2Zr{=}S$: Trapping Reactions with Alkynes, Nitriles, and Dative Ligands. *Organometallics* **1992**, *11*, 761-777.
(33) Howard, W. A.; Waters, M.; Parkin, G. Terminal Zirconium Oxo Complexes: Synthesis, Structure, and Reactivity of $(\eta^5\text{-}C_5Me_4R)_2Zr(O)(NC_5H_4R')$. *J. Am. Chem. Soc.* **1993**, *115*, 4917-4918.
(34) Partyka, D. V.; Staples, R. J.; Holm, R. H. Nucleophilic Reactivity and Oxo/Sulfido Substitution Reactions of $M^{VI}O_3$ Groups (M = Mo, W). *Inorg. Chem.* **2003**, *42*, 7877-7886.
(35) Cross, W. B.; Anderson, J. C.; Wilson, C. S. Nucleophilic reactivity of a d^0 molybdenum oxo moiety. *Dalton Trans.* **2009**, *7*, 1201-1205.
(36) Yonke, B. L.; Reeds, J. P.; Zavalij, P. Y.; Sita, L. R. Catalytic Degenerate and Nondegenerate Oxygen Atom Transfers Employing N_2O and CO_2 and a M^{II}/M^{IV} Cycle Mediated by Group 6 M^{IV} Terminal Oxo Complexes. *Angew. Chem. Int. Ed.* **2011**, *50*, 12342-12346.
(37) Smeltz, J. L.; Lilly, C. P.; Boyle, P. D.; Ison, E. A. The Electronic Nature of Terminal Oxo Ligands in Transition-Metal Complexes: Ambiphilic Reactivity of Oxorhenium Species. *J. Am. Chem. Soc.* **2013**, *135*, 9433-9441.
(38) Bruker. *APEX3, SADABS, TWINABS*. Bruker AXS Inc., Madison, Wisconsin, USA.
(39) Sheldrick, G. M. A Short History of *SHELX*. *Acta Cryst.* **2008**, A*64*, 112-122.
(40) Farrugia, L. J. *WinGX* and *ORTEP* for *Windows*: an update. *J. Appl. Cryst.* **2012**, *45*, 849-854.
(41) Macrae, C. F.; Bruno, I. J.; Chisholm, J. A.; Edgington, P. R.; McCabe, P.; Pidcock, E.; Rodriguez-Monge, L.; Taylor, R.; van de Streek J.; Wood, P. A. Mercury CSD 2.0 - New Features for the Visualization and Investigation of Crystal Structures. *J. Appl. Cryst.* **2008**, *41*, 466-470.

Chapter 5

Heterotetrametallic Re-Zn-Zn-Re Complex Generated by an Anionic Rhenium(I) β-Diketiminate

Introduction

The controlled introduction and removal of electrons into and out of a molecule can provide critical insights into its structure, bonding, and reactivity. In the cases when a strong reductant is required, chemists typically rely on alkali metals and their derivatives (*e.g.* alkali napthalides, alkali anthrocenides, KC_8), which can be difficult to handle and present a potential safety hazard.[1] This has led to the development of alternative reducing agents that are both safer to handle and provide additional utility as reagents. For example, organic reductants have been developed that can be used in place of alkali metals and also avoid the subsequent generation of alkali halides as side products.[2-4] Consistent developments have also been made in photoredox catalysis, where a strong reductant is generated by the photoexcitation of an organic compound or a transition metal complex (such as Ru(2,2'-bipyridine)$_3^{2+}$ or Ir(2,2'-phenylpyridine)$_3$).[5,6] Additionally, there have been a number of studies into the use of low valent metal coordination complexes as strong reductants, a class that includes magnesium(I) compounds[7-9] and gallium(I)[10-12] and aluminum(I)[13-15] species. Conveniently, these low valent complexes are soluble in common organic solvents and can subsequently provide kinetic stabilization to the reduced species they generate. This last point is of particular note, as canonical examples of strongly reducing homogeneous metal complexes are largely precluded from forming complexes with reduced species due to their saturated coordination environment (such as in the 19-electron reductants Cp*$_2$Co and Cp*(η^6-C_6Me_6)Fe, Cp* = pentamethylcyclopentadienyl).[1] Consequently, developing the chemistry of coordinately unsaturated, strongly reducing metal coordination compounds has facilitated the isolation of many uncommon or previously unknown inorganic fragments[16-25] as well as the direct activation of a variety of C-F bonds.[8,26,27] Here, we report the synthesis of an anionic rhenium(I) complex free of any electron accepting substituents that can behave as both a strong reductant and a supporting ligand. This behavior is exemplified in the reactivity of the rhenium(I) anion with divalent zinc, which leads to a zinc(I) compound containing both Re-Zn and Zn-Zn bonds. We have also found that this anionic rhenium(I) reagent can be oxidized or protonated to give well defined compounds, including a rare example of a rhenium(II) complex.

Results and Discussion

Following our initial report of the oxo rhenium(V) cation ORe(η^5-Cp)(BDI)$^+$ (Cp = cyclopentadienyl, BDI = N,N'-bis(2,6-diisopropylphenyl)-3,5-dimethyl-β-diketiminate),[28] we developed a reliable method of using this species as a precursor to the rhenium(I) salt Na[Re(η^5-Cp)(BDI)] (**5.1**). This synthesis utilizes the $SnCl_3^-$ salt of the starting cation with excess metallic sodium as the reducing agent, forming **5.1** in good yield (Scheme 5.1). Isolated **5.1** is a highly air-sensitive dark purple, crystalline solid that is very soluble in coordinating solvents. The X-ray crystal structure of **1** confirms its composition and reveals that the Na^+ ion is coordinated by the Cp and BDI moieties of surrounding equivalents of anion, forming polymeric 1-D chains in the solid-state (Figure 5.1). The ^{1}H NMR spectrum of **5.1** in pyridine-*d*5 indicates the expected C_{2v} solution-state symmetry for the BDI ligand.

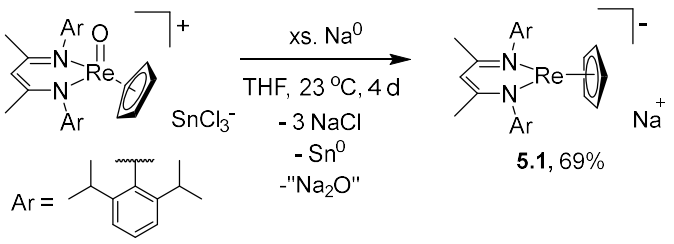

Scheme 1. The scalable synthesis of **5.1** using metallic sodium as a reductant.

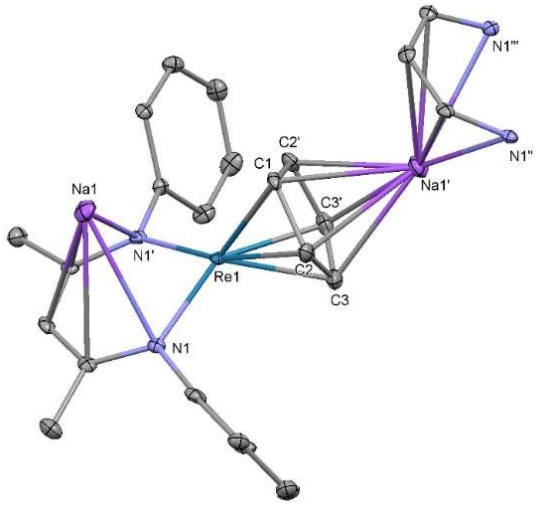

Figure 5.1 X-ray crystal structure of **5.1** with 50% probability ellipsoids. The structure is extended to display the full coordination environment of the Na atom. H atoms and BDI isopropyl groups are excluded for clarity. Selected distances (Å) and angles (°): Re1-N1 = 2.031(3), Re1-Cp(centroid) = 1.816(2), Na1-N1 = 2.869(4), Na1-Cp(centroid) = 2.348(3), N1-Re1-N1' = 87.16(17).

We expected **5.1** to be both basic and reducing; as such, we began to explore its oxidation and protonation to form neutral species. We found that oxidation of **5.1** with silver(I) trifluoromethanesulfonate (AgOTf) gives the neutral species Re(η^5-Cp)(BDI) (**5.2**), a rare example of a formally rhenium(II) compound (Scheme 5.2). The ^{1}H NMR spectrum of paramagnetic **5.2** is too broad to discern its composition, but X-ray crystallography reveals that it is structurally analogous to the rhenium(I) anion in **5.1** (see Experimental). By the Evans NMR method, the magnetic moment of **5.2** is 1.67 μ_B, indicating that there is one unpaired electron in this d^5 species. Reported examples of isolated rhenium(II) species have often contained linear nitrosyl ligands.[29-31] Also, a thermally unstable rhenium(II) pincer compound has previously been found to bind, reduce, and cleave dinitrogen to form rhenium(V) nitride compounds.[32,33]

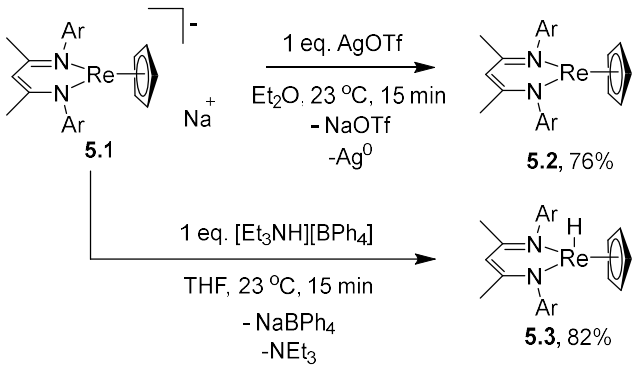

Scheme 5.2. Oxidation and protonation of **5.1** to form **5.2** and **5.3**, respectively.

Protonation of **5.1** with triethylammonium tetraphenylborate gives the rhenium(III) hydride complex Re(H)(η^5-Cp)(BDI) (**5.3**, Scheme 5.2). Compound **5.3** is identified as a metal hydride complex based on a distinct peak in the IR absorbance spectrum at 2028 cm^{-1}, and a singlet at -27.95 ppm in the ^{1}H NMR spectrum in C_6D_6. Single crystal X-ray diffraction studies of **5.3** also allowed for the metal hydride to be located and freely refined (see Experimental).

Based on the observation that the rhenium center of **5.1** is the site of protonation, we hypothesized that we might be able to employ this anionic fragment as a metalloligand for other metal centers. Influenced by literature examples of divalent zinc compounds supported by anionic metalloligands,[34,35] we combined **5.1** with zinc(II) chloride in THF. Based on ^{1}H NMR spectra of crude material, we discerned that significant quantities of **5.2** were formed by the reaction, in addition to another, presumably reduced species. This hypothesis was confirmed upon the purification and structural characterization of the second product, identified as the zinc(I) compound [ZnRe(η^5-Cp)(BDI)]$_2$ (**5.4**, Scheme 5.3). Complex **5.4** is thermally stable in solution up to 120 °C, decomposing over several days to form a grey precipitate (presumably Zn^0) and a mixture of diamagnetic products, including a small amount of **5.3**. While several examples of zinc(I) compounds have been reported,[21,36-45] **5.4** is the first example of such a compound to be supported by bonding exclusively to other metal centers. Furthermore, the structural assignment of **5.4** allowed us to conclude that in a single reaction, **5.1** had demonstrated utility as both a reducing agent and a metalloligand.

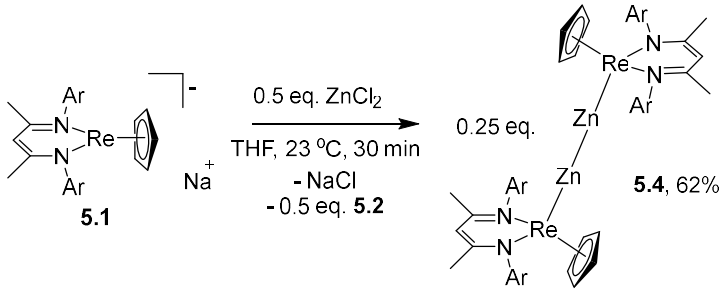

Scheme 5.3 The formation and trapping of **5.4**, a heterotetrametallic Re-Zn-Zn-Re complex, facilitated by **5.1**.

The X-ray crystal structure of **5.4** shows a Zn_2^{2+} core flanked on each side by an anionic Re(η^5-Cp)(BDI)$^-$ fragment bound to Zn through the rhenium(I) center (Figure 5.2). The nearly linear tetrametallic Re-Zn-Zn-Re linkage in **5.4** (Re-Zn-Zn = 173.563(16)° and 173.371(15)°) has two closely related examples, containing Co-Hg-Hg-Co and Ga-Sb=Sb-Ga motifs, where a central metal homodimer is bonded exclusively to the terminal metal centers.[46,47] The Zn-Zn distance in **5.4** is 2.3938(4) Å, in line with other Zn-Zn bonds (though ca. 0.1 Å longer than the Zn-Zn bond in $Cp^*_2Zn_2$).[36] The Re-Zn distances in **5.4** are 2.4681(3) Å and 2.4711(3) Å, which are substantially shorter (by ca. 0.15 Å) than the two other crystallographically characterized examples of Re-Zn interactions.[48,49]

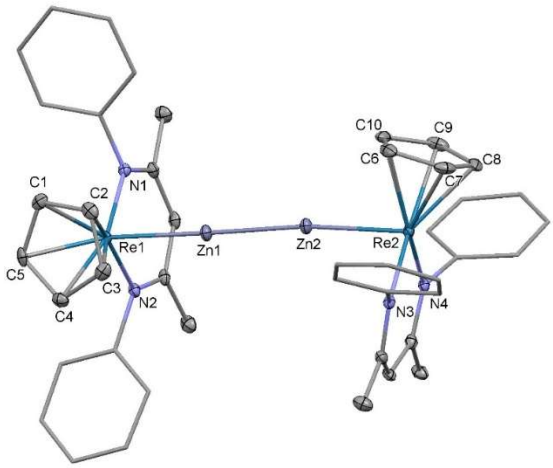

Figure 5.2 X-ray crystal structure of **5.4** with 50% probability ellipsoids. H atoms and BDI isopropyl groups are removed, and the BDI aryl rings are displayed as capped sticks for clarity. Selected distances (Å) and angles (°): Zn1-Zn2 = 2.3938(4), Re1-Zn1 = 2.4681(3), Re1-N1 = 2.031(2), Re1-N2 = 2.028(2), Re1-Cp(centroid) = 1.8986(12), Re2-Zn2 = 2.4711(3), Re2-N3 = 2.022(2), Re2-N4 = 2.025(2), Re2-Cp(centroid) = 1.8938(16), Re1-Zn1-Zn2 = 173.563(16), Re2-Zn2-Zn1 = 173.371(15), N1-Re1-N2 = 87.11(9), N3-Re2-N4 = 87.46(8).

A structural optimization and subsequent frequency calculation of **5.4** was carried out using density functional theory (DFT) with a correction applied for dispersion forces (B3PW91-GD3BJ,[50-52] see Experimental), and the results have provided some insights into the nature of the metal-metal interactions and frontier orbitals in this compound (Figure 5.3). According to a second-order Natural Bond Orbital (NBO) analysis, the Re-Zn interaction is formed by the dative donation of a Re-based lone pair housed in a 5d orbital into an empty Zn-based 4p orbital. This assignment is further supported by the calculated Wiberg Bond Index (WBI) between Re and Zn of 0.37, which is indicative of a dative interaction. The Zn-Zn bonding orbital was found to lie lower in energy than the Re-Zn bonding orbital, and based on a first-order NBO analysis the Zn-Zn bond is entirely composed of Zn 4s orbitals, with a corresponding WBI of 0.77, which is in line with similar computational studies of zinc(I) compounds.[21,41-45] Overall, these calculations support the assignment that **5.4** is composed of a covalently bonded Zn_2^{2+} core with datively bound, anionic rhenium(I) centers. Additionally, the calculations indicated that the frontier orbitals of **4** are

composed almost entirely of linear combinations of 5d orbitals on the rhenium centers, with no significant contributions from the zinc centers.

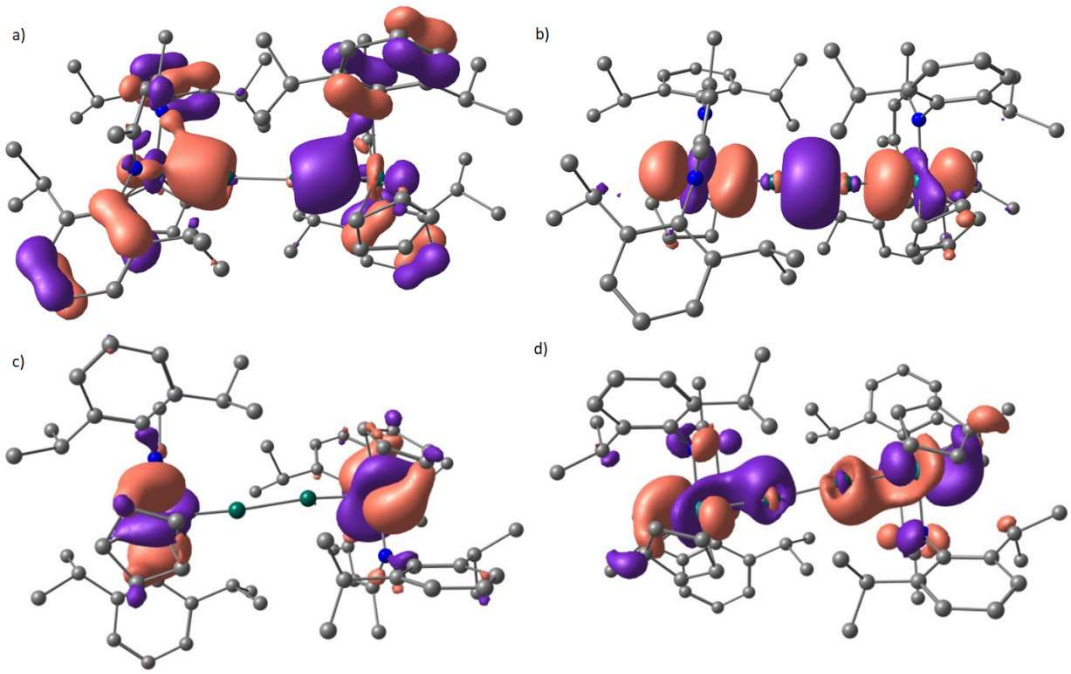

Figure 5.3 Renderings of select calculated molecular orbitals of **5.4**, featuring a) the Re-Zn bonding orbital (HOMO-5), b) the Zn-Zn bonding orbital (HOMO-10), c) the HOMO, and d) the LUMO.

Inspired by our computational results and previous reactivity studies of zinc(I) compounds we investigated the behavior of **5.4** upon oxidation. We found that combining 1 equiv. of AgOTf with **5.4** led to the formation of two identifiable species, namely **5.2** and the dimeric complex [(μ-OTf)ZnRe(η^5-Cp)(BDI)]$_2$ (**5.5**, Scheme 5.4). The X-ray crystal structure of **5.5** shows the Re-Zn distance of 2.4418(3) Å is slightly shorter than those in **4**. While the structure of **5.5** (Figure 5.4) initially appeared to result from direct oxidative cleavage of the Zn-Zn bond, further investigation revealed that this is likely not the case. When the oxidation of **5.4** was carried out using 2 equiv. of AgOTf, the only identifiable product by NMR spectroscopy was **5.2**, with no **5.5** observed. We also confirmed that only a half equiv. of **5.5** is produced from the quantity of **4** consumed when less than 1 equiv. of AgOTf is added. We thus propose that the oxidation of **4** leads directly to the formation of stoichiometric amounts of **5.2**, followed by disproportionation of the Zn-Zn bond to give metallic zinc and zinc(II). Therefore, we propose **5.5** is a dimer of zinc(II) species formed by this disproportionation mechanism, rather than a product of the direct oxidative schism of the Zn-Zn bond in **5.4**. This hypothesis aligns with the computational results, which indicate that the HOMO of **5.4** (the orbital from which a chemical oxidant will remove an electron) is mainly composed of rhenium 5d orbitals.

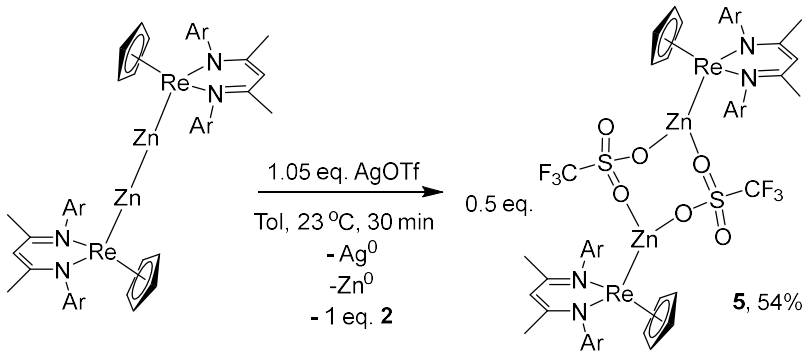

Scheme 5.4 Oxidation of **5.4** leads to the isolation of the triflate-bridged heterotetrametallic complex **5.5**.

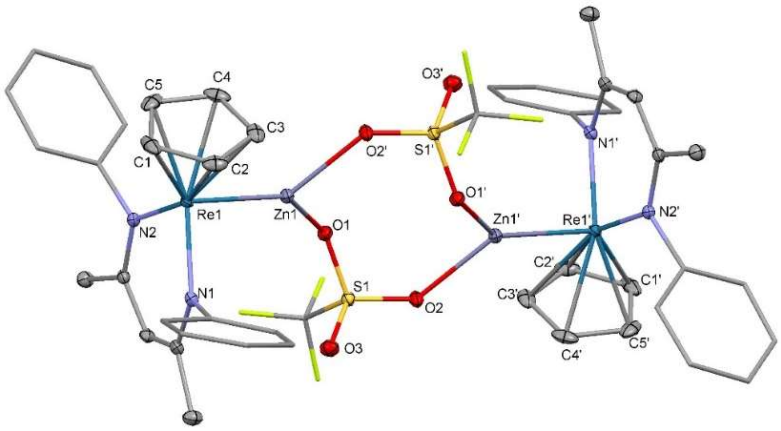

Figure 5.4 X-ray crystal structure of **5.5** with 50% probability ellipsoids. H atoms, BDI isopropyl groups, and outer sphere solvent have been removed, and the triflate CF_3 groups and BDI aryl rings are displayed as capped sticks for clarity. Selected distances (Å) and angles (°): Zn1-O1 = 2.0346(13), Zn1-O2' = 2.0835(16), Re1-Zn1 = 2.4418(3), Re1-N1 = 2.024(2), Re1-N2 = 2.020(2), Re1-Cp(centroid) = 1.9107(10), N1-Re1-N2 = 87.37(8).

Summary and Conclusions

In conclusion, we have presented the synthesis of the rhenium(I) salt Na[Re(η^5-Cp)(BDI)] (**5.1**), and demonstrated its use as a reducing agent and ancillary metalloligand by preparing the tetrametallic zinc(I) compound [ZnRe(η^5-Cp)(BDI)]$_2$ (**5.4**) from $ZnCl_2$. By studying the oxidation and protonation products derived from **5.1**, we were able to access a rare example of a formally rhenium(II) complex Re(η^5-Cp)(BDI) (**5.2**), as well as the rhenium(III) hydride complex Re(H)(η^5-Cp)(BDI) (**3**). We also isolated an oxidation product derived from **5.4**, the triflate-bridged zinc(II) dimer [(μ-OTf)ZnRe(η^5-Cp)(BDI)]$_2$ (**5.5**). Based on reactivity and computational studies of **5.4**, we determined **5.5** likely forms as the result of oxidation of a rhenium(I) center to form an equivalent of **5.2**, followed by disproportionation of the Zn-Zn bond to yield equal amounts of zinc(II) species and metallic zinc. Future reports will continue to explore the synthetic utility of **5.1** as a reducing agent and metalloligand, and will include reactivity studies and further spectroscopic characterization of the rhenium(II) complex **5.2**.

Experimental

General Considerations: All manipulations were carried out under a dry nitrogen atmosphere, either in an MBraun LabStar glovebox or on a Schlenk line using standard techniques. Toluene, diethyl ether, tetrahydrofuran, *n*-pentane, and *n*-hexane were dried by passage through a basic alumina column and were handled and stored under a dry nitrogen atmosphere in standard Strauss flasks or in the glovebox. Hexamethyldisiloxane (HMDSO) was dried over Na/benzophenone, distilled under N_2, and stored in the glovebox prior to use. Deuterated benzene and pyridine were obtained commercially, dried over an appropriate reagent (Na/benzophenone for C_6D_6, CaH_2 for pyridine-d5), and distilled prior to storage in the glovebox over 4 Å molecular sieves. Celite was dried in a 150 ºC oven for 24 hours prior to storage in the glovebox. Sodium metal, silver(I) trifluoromethanesulfonate, and anhydrous zinc(II) chloride were obtained from commercial sources and stored in the glovebox. The reported compounds [ORe(η^5-Cp)(BDI)][$SnCl_3$][28] and triethylammonium tetraphenylborate[53] were synthesized using known procedures. NMR spectroscopy data were obtained on Bruker AVQ-400, AVB-400, AV-500 and AV-600 instruments. All ^{1}H and ^{13}C spectra were referenced to the residual peak of the solvent used. Select peak assignments were corroborated with ^{1}H-^{13}C HSQC experiments as necessary. Unless noted otherwise, "room temperature" and "ambient temperature" both refer to approx. 23 ºC. Infrared absorption data were obtained using a Thermo Scientific Nicolet iS10 instrument, with the sample chamber under ambient atmosphere. Samples were prepared as Nujol mulls pressed between KBr plates in the glovebox.

Na[Re(η^5-Cp)(BDI)] (5.1): In the glovebox, [ORe(η^5-Cp)(BDI)][$SnCl_3$] (2.60 g, 2.86 mmol), a pre-weighed quantity of metallic sodium (800 mg, 34.8 mmol, 12.2 eq.) cut into approximately 20 equal sized pieces, and an egg-shaped Teflon-coated stir bar were added to a 100 mL pear-shaped Schlenk flask. The flask was sealed, removed from the glovebox, and transferred onto a Schlenk line, where THF (80 mL) was added, ensuring all of the rhenium starting material was dissolved. The reaction mixture, sealed under N_2, was stirred vigorously at ambient temperature for 4 days, with an observable change in color from dark red to a deep maroon-purple color. The volatile components of the reaction mixture were removed in vacuo, and the resulting solids were extracted with 200 mL of diethyl ether. These extracts were filtered through Celite, and concentrated in vacuo to one quarter of their original volume. Hexane (100 mL) was then added, and the solution was concentrated in vacuo to half of its volume (to remove most of the remaining diethyl ether) and crystalline solids were observed. An additional aliquot of hexane (50 mL) was added to this mixture, and the diluted mother liquor was then decanted by cannula transfer. The remaining deep purple crystalline solids were washed with hexane (2 x 50 mL) and dried in vacuo to give **1** (1.36 g, 69% yield). m.p.: 161-168 ºC (decomp.). ^{1}H NMR (300 MHz, C_6D_6, 298 K): 7.19 (d, 4H, BDI Ar, J = 7.5 Hz), 6.81 (t, 2H, BDI Ar, J = 7.5 Hz), 6.13 (bs, 1H, *H*C[MeC(NAr)]$_2$), 4.51 (bs, 5H, Cp), 3.74 (bs, 4H, BDI C*H*(Me)$_2$), 1.60 (bs, 6H, HC[*Me*C(NAr)]$_2$), 1.50-0.88 (m, 24H, BDI CH(*Me*)$_2$). ^{13}C NMR (101 MHz, C_6D_6, 298 K): 122.64 (BDI Ar), 120.51 (BDI Ar), 79.08 (Cp), 30.01 (HC[*Me*C(NAr)]$_2$), 29.42 (BDI *C*H(Me)$_2$), 25.78 (BDI CH(*Me*)$_2$), 25.59 (BDI CH(*Me*)$_2$). Due to the fluxional behavior of **1** in solution and the correspondingly low signal-to-noise ratio, we could not observe a ^{13}C NMR signal for the BDI backbone C-H group, as well as several BDI

aryl signals typically observed in other Re BDI compounds. Anal. Calcd. for $ReC_{34}H_{46}N_2Na$ (**1**): C, 59.00; H, 6.70; N, 4.05 %. Found: C, 58.70; H, 7.00; N, 3.75 %.

Re(η^5-Cp)(BDI) (5.2): In the glovebox, solid **1** (100 mg, 0.144 mmol) ,and silver(I) trifluoromethanesulfonate (37.1 mg, 0.144 mmol) were separately dissolved in diethyl ether (5 mL and 3 mL, respectively). The solution of AgOTf was then added to the solution of **1** with magnetic stirring. The formation of a dark grey precipitate was observed in seconds, and the dark solution became bright red in color. After being stirred for 15 min, the volatile components of the reaction mixture were removed in vacuo. The red residue was extracted with pentane (6 mL). These extracts were filtered through Celite and concentrated in vacuo prior to storage at -40 ºC. The following day, **2** was isolated as red crystals (63 mg). Concentration of the mother liquor and storage at -40 ºC yielded a second crop (10 mg) of similar purity. Total yield: 73 mg, 76%. m.p.: 137-141 ºC (decomp.). ^{1}H NMR (400 MHz, C_6D_6, 298 K): 69.0 (bs), 38.8 (bs), 34.3 (bs), -1.5 (bs), -13.5 (bs), -22.8 (bs), -29.1 (bs). Anal. Calcd. for $ReC_{34}H_{46}N_2$ (**2**): C, 61.03; H, 6.93; N, 4.19 %. Found: C, 60.92; H, 6.91; N, 4.22 %.

Re(H)(η^5-Cp)(BDI) (5.3): In the glovebox, solid **1** (100 mg, 0.144 mmol) was dissolved in THF (5 mL) and this solution was set to stir. Separately, solid triethylammonium tetraphenylborate (60.8 mg, 0.144 mmol) was dissolved in THF (4 mL), and this colorless solution was added to the stirred solution of **1**. In seconds, an emerald green solution was observed. After 15 minutes, the volatile components of the reaction mixture were removed in vacuo, giving a tacky solid residue that was triturated with 2 mL of HMDSO. The residue was then extracted with 7 mL HMDSO, and these extracts were filtered through Celite. The filtered extracts were concentrated in vacuo and stored at -40 ºC to give **3** as green crystals (79 mg, 82%). m.p.: 125-128 ºC. ^{1}H NMR (600 MHz, C_6D_6, 298 K): 7.11 (bs, 2H, BDI Ar), 6.95 (bs, 2H, BDI Ar), 6.93 (t, 2H, BDI Ar, J = 7.7 Hz), 6.40 (s, 1H, *H*C[MeC(NAr)]$_2$), 4.80 (s, 5H, Cp), 3.44 (bs, 2H, BDI C*H*(Me)$_2$), 2.80 (s, 6H, HC[*Me*C(NAr)]$_2$), 1.95 (bs, 2H, BDI C*H*(Me)$_2$), 1.22-1.00 (m, 18H, BDI CH(*Me*)$_2$), 0.91 (bs, 6H, BDI CH(*Me*)$_2$), -27.95 (s, 1H, Re-*H*). ^{13}C NMR (151 MHz, C_6D_6, 298 K): 165.42 (HC[Me*C*(NAr)]$_2$), 158.85 (BDI Ar), 139.51 (BDI Ar), 138.55 (BDI Ar), 124.94 (BDI Ar), 123.81 (BDI Ar), 122.42 (BDI Ar), 105.44 (H*C*[MeC(NAr)]$_2$), 78.67 (Cp), 29.40 (BDI *C*H(Me)$_2$), 28.15 (BDI *C*H(Me)$_2$), 25.19 (BDI CH(*Me*)$_2$), 24.74 (BDI CH(*Me*)$_2$), 24.46 (BDI CH(*Me*)$_2$), 24.16 (BDI CH(*Me*)$_2$), 23.28 (HC[*Me*C(NAr)]$_2$). FT-IR (Nujol): 2028 cm^{-1} (Re-H). Anal. Calcd. for $ReC_{34}H_{47}N_2$ (**3**): C, 60.93; H, 7.07; N, 4.18 %. Found: C, 60.79; H, 7.24; N, 4.12 %.

[ZnRe(η^5-Cp)(BDI)]$_2$ (5.4): In the glovebox, solid **1** (250 mg, 0.361 mmol) was dissolved in THF (6 mL). To this stirred solution was added $ZnCl_2$ (24.6 mg, 0.181 mmol) dissolved in 4 mL THF. This mixture was stirred at ambient temperature for 30 minutes, and then its volatile components were removed in vacuo. The residue was triturated with hexane (2 x 2 mL) to remove residual THF. The dry, dark red residue was then extracted with toluene (8 mL), and these extracts were filtered through Celite. The volatile components of the filtered extracts were removed in vacuo, and then hexane (10 mL) was added to give a dark red-brown, homogeneous solution that was left to sit at room temperature. Over the course of several days, large, block-shaped green crystals formed. These crystals were isolated, washed with pentane (2 mL), and dried in vacuo to give **4**

(72 mg). A second crop of **4** of similar purity (10 mg) could be isolated by a similar method, using half the volume of hexane (ca. 5 mL) in the crystallization conditions. Total yield: 82 mg, 62%. m.p.: 181-186 °C (decomp.). ^{1}H NMR (600 MHz, C_6D_6, 298 K): 7.18 (dd, 2H, BDI Ar, J = 7.1, 2.2 Hz), 7.06 (dd, 2H, BDI Ar, J = 7.5, 1.6 Hz), 7.03-6.97 (m, 6H, BDI Ar), 6.95 (t, 2H, BDI Ar, J = 7.6 Hz), 6.31 (s, 2H, *H*C[MeC(NAr)]$_2$), 4.51 (s, 10H, Cp), 3.79 (sept, 2H, BDI C*H*(Me)$_2$, J = 6.8 Hz), 3.61 (sept, 2H, BDI C*H*(Me)$_2$, J = 6.8 Hz), 2.46 (s, 6H, HC[*Me*C(NAr)]$_2$), 2.42 (s, 6H, HC[*Me*C(NAr)]$_2$), 1.99-1.91 (m, 4H, BDI C*H*(Me)$_2$), 1.40 (d, 6H, BDI CH(*Me*)$_2$, J = 6.7 Hz), 1.28 (d, 6H, BDI CH(*Me*)$_2$, J z= 6.7 Hz), 1.23-1.19 (m, 12H, BDI CH(*Me*)$_2$), 1.03-1.01 (m, 12H, BDI CH(*Me*)$_2$), 0.99-0.95 (m, 12H, BDI CH(*Me*)$_2$). ^{13}C NMR (151 MHz, C_6D_6, 298 K): 159.68 (HC[Me*C*(NAr)]$_2$), 159.40 (HC[Me*C*(NAr)]$_2$), 158.22 (BDI Ar), 158.15 (BDI Ar), 140.45 (BDI Ar), 140.40 (BDI Ar), 136.91 (BDI Ar), 136.88 (BDI Ar), 124.70 (BDI Ar), 124.67 (BDI Ar), 123.96 (BDI Ar), 123.94 (BDI Ar), 122.64 (BDI Ar), 122.62 (BDI Ar), 105.10 (H*C*[MeC(NAr)]$_2$), 72.03 (Cp), 30.02 (BDI *C*H(Me)$_2$), 29.98 (BDI *C*H(Me)$_2$), 27.95 (BDI *C*H(Me)$_2$), 27.72 (BDI *C*H(Me)$_2$), 25.35 (BDI CH(*Me*)$_2$), 25.08 (BDI CH(*Me*)$_2$), 24.93 (BDI CH(*Me*)$_2$), 24.30 (BDI CH(*Me*)$_2$), 24.25 (BDI CH(*Me*)$_2$), 24.22 (BDI CH(*Me*)$_2$), 24.09 (BDI CH(*Me*)$_2$), 23.94 (HC[*Me*C(NAr)]$_2$). Anal. Calcd. for $Re_2Zn_2C_{68}H_{92}N_4$ (**4**): C, 55.59; H, 6.32; N, 3.82 %. Found: C, 55.81; H, 6.47; N, 3.59 %.

[(μ-OTf)ZnRe(η^5-Cp)(BDI)]$_2$ (5.5): Solid **4** (50.0 mg, 0.0340 mmol) was dissolved in toluene (6 mL) and set to stir. Solid silver(I) trifluoromethanesulfonate (9.2 mg, 0.036 mmol) was added to this solution, and the mixture was stirred for 30 minutes at ambient temperature. The volatile components of the reaction mixture were removed and the residue was triturated with hexane (1 mL), washed with additional hexane (3 x 3 mL) to remove the **2** formed in the reaction, and finally extracted with Et_2O (8 mL). These extracts were filtered through Celite, and their volatile components were removed in vacuo. The resulting solids were washed with pentane (3 x 1 mL) to give **5** as green microcrystalline solids (16 mg, 54 %). m.p.: 153-158 °C (decomp.). ^{1}H NMR (600 MHz, C_6D_6, 298 K): 7.14 (d, 4H, BDI Ar, J = 8.3), 6.95-6.89 (m, 8H, BDI Ar), 6.49 (s, 2H, *H*C[MeC(NAr)]$_2$), 5.08 (s, 10H, Cp), 3.88 (sept, 4H, BDI C*H*(Me)$_2$, J = 6.8 Hz), 2.82 (s, 12H, HC[*Me*C(NAr)]$_2$), 1.75 (sept, 4H, BDI C*H*(Me)$_2$, J = 6.7 Hz), 1.57-1.48 (m, 24H, BDI CH(*Me*)$_2$), 1.01 (d, 12H, BDI CH(*Me*)$_2$, J = 6.7 Hz), 0.90 (d, 12H, BDI CH(*Me*)$_2$, J = 6.7 Hz). ^{13}C NMR (151 MHz, C_6D_6, 298 K): 159.43 (HC[Me*C*(NAr)]$_2$), 139.38 (BDI Ar), 137.95 (BDI Ar), 125.27 (BDI Ar), 124.21 (BDI Ar), 122.78 (BDI Ar), 106.88 (H*C*[MeC(NAr)]$_2$), 76.26 (Cp), 30.10 (BDI *C*H(Me)$_2$), 28.63 (BDI *C*H(Me)$_2$), 25.82 (BDI *C*H(Me)$_2$), 25.23 (BDI *C*H(Me)$_2$), 24.00 (BDI CH(*Me*)$_2$), 23.95 (HC[*Me*C(NAr)]$_2$), 23.24 (BDI CH(*Me*)$_2$). ^{19}F NMR (376 MHz, C_6D_6, 298 K): 77.22 (bs). Despite multiple attempts to obtain a satisfactory elemental analysis for **5**, we consistently observed different, very low (by 6-12%) values for its carbon content. Despite this, we believe our other characterization data supports our assignment of its composition and structure.

X-Ray Crystallographic Details: X-ray diffraction data were collected at CheXray, UC Berkeley (**5.1**, **5.2**, **5.4**, **5.5**) and the Advanced Light Source (ALS), Lawrence Berkeley National Laboratory (**5.3**). At CheXray, measurements for **5.1** were taken using a Rigaku XtalLAB P200 instrument equipped with a rotating-anode Mo X-ray source and a Pilatus 200K detector, and the data was analyzed, reduced, and solved using the CrysAlisPro software package and Olex2 (SHELXT and

SHELXL).[54-56] Measurements for **5.2**, **5.4**, and **5.5** were taken using a Bruker APEXII Quazar diffractometer equipped with a micro-focus Mo X-ray source and a Bruker APEX-II CCD detector, with data analyzed and reduced using either the Bruker APEX2 or APEX3 software package, and solutions and refinements conducted using WinGX (SHELXT and SHELXL-2014).[57,58] Measurements for **5.3** were taken using the ALS beam line 12.2.1, using a monochromated beam of 17 keV synchrotron radiation and a Bruker D8 diffractometer equipped with a Bruker PHOTON II CPAD detector. Diffraction data for **5.3** were analyzed and reduced using the Bruker APEX3 software package, and the structure was solved and refined using SHELXT and SHELXL-2014 as implemented by WinGX. All structures were collected at 100 K in a stream of dry nitrogen. In refining the structure of **5.4**, the SQUEEZE program in PLATON was utilized to remove electron density associated with a highly disordered hexane molecule.[59] All structures have been deposited to the Cambridge Crystallographic Data Centre (CCDC), with deposition numbers 1877453 (**5.1**), 1877454 (**5.2**), 1877455 (**5.3**), 1877456 (**5.4**), and 1877457 (**5.5**).

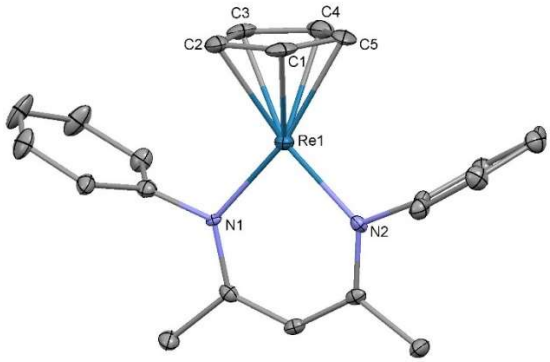

Figure 5.5. X-ray crystal structure of **5.2** with 50% probability ellipsoids. H-atoms and BDI isopropyl groups have been removed for clarity. Selected distances (Å) and angles (º): Re1-N1 = 2.070(3), Re1-N2 = 2.032(3), Re1-Cp(centroid) = 1.890(2), N1-Re1-N2 = 89.15(13).

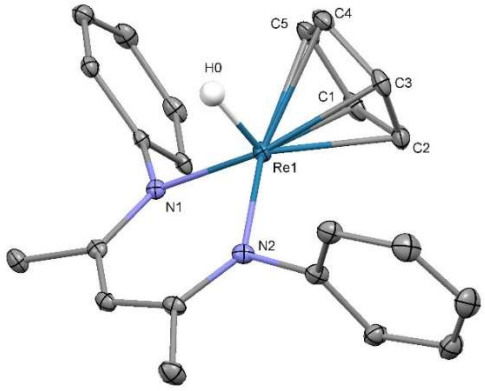

Figure 5.6. X-ray crystal structure of **5.3** with 50% probability ellipsoids. H-atoms (except for the metal hydride) and BDI isopropyl groups have been removed for clarity. Selected distances (Å) and angles (º): Re1-N1 = 2.026(2), Re1-N2 = 2.013(2), Re1-H0 = 1.46(3), Re1-Cp(centroid) = 1.8953(13), N1-Re1-N2 = 86.82(8).

Table 5.1. Crystallographic details and refinement metrics for compounds **5.1**, **5.2**, **5.3**, **5.4**, and **5.5**.

	5.1	**5.2**	**5.3**	**5.4 • *n*-Hexane**	**5.5 • Et_2O**
Chemical formula	$C_{34}H_{46}N_2ORe Na$	$C_{34}H_{46}N_2Re$	$C_{34}H_{47}N_2Re$	$C_{74}H_{106}N_4Re_2Zn_2$	$C_{74}H_{102}N_4O_7F_6S_2Re_2Zn_2$
Formula weight	691.92	668.93	669.93	1554.76	1840.85
Color, habit	Red, plank	Red, tablet	Green, block	Orange, block	Green, block
Temperature (K)	100(2)	100(2)	100(2)	100(2)	100(2)
Crystal system	Orthorhombic	Monoclinic	Triclinic	Triclinic	Triclinic
Space group	Pnma	$P2_1/n$	P-1	P-1	P-1
a (Å)	12.1625(3)	12.5845(6)	9.6137(4)	12.6151(2)	11.9790(3)
b (Å)	21.0519(7)	18.1223(7)	12.4780(6)	12.7440(2)	12.3925(3)
c (Å)	12.4534(4)	13.8772(6)	13.2623(6)	22.8461(4)	13.8937(3)
α (°)	90	90	73.366(2)	88.556(1)	97.317(1)
β (°)	90	106.396(2)	85.413(2)	77.634(1)	109.657(1)
γ (°)	90	90	84.457(2)	73.542(1)	94.520(1)
V ($Å^3$)	3188.61(17)	3036.1(2)	1514.95(12)	3438.22(10)	1910.09(8)
Z	4	4	2	2	1
Density ($Mg\ m^{-3}$)	1.441	1.463	1.469	1.502	1.600
F(000)	1400	1356	680	1578	926
Radiation Type	MoK_α	MoK_α	Synchrotron	MoK_α	MoK_α
μ (mm^{-1})	3.848	4.026	4.271	4.241	3.901
Crystal size (mm^3)	0.430 x 0.070 x 0.060	0.060 x 0.030 x 0.010	0.070 x 0.060 x 0.055	0.300 x 0.200 x 0.060	0.190 x 0.160 x 0.120
Meas. Refl.	34993	48933	16811	51839	33379
Indep. Refl.	3350	5570	6962	14109	7833
R(int)	0.1316	0.0607	0.0348	0.0360	0.0318
Final R indices [$I > 2\sigma(I)$]	$R = 0.0371$ $R_w = 0.0863$	$R = 0.0336$ $R_w = 0.0693$	$R = 0.0223$ $R_w = 0.558$	$R = 0.0218$ $R_w = 0.0462$	$R = 0.0198$ $R_w = 0.0411$
Goodness-of-fit	1.032	1.059	1.095	0.995	1.029
$\Delta\rho_{max}$, $\Delta\rho_{min}$ ($e\ Å^{-3}$)	3.307, -1.997	1.852, -0.754	0.812, -1.695	0.734, -0.728	0.628, -0.539

Computational Details

Calculations were carried out with the *Gaussian09* program[60] with the B3PW91-GD3BJ,[50-51] that includes dispersion effects according to the Grimme's scheme.[52] The Zn and Re atom were treated with the corresponding Stuttgart-Dresden RECP (relativistic effective core potential) in combination with its adapted basis sets,[61-63] and augmented by an extra polarization function.[64] For all the remaining atoms the 6-31G(d,p) basis set was used.[65] Geometry optimizations were carried out without any symmetry restrictions. Natural population analysis (NPA) was performed using Weinhold's methodology.[66,67] Finally, Chemcraft is used for the visualization of the molecular orbitals.[68]

Notes and References

(1) Connelly, N. G.; Geiger, W. E. Chemical Redox Agents for Organometallic Chemistry. *Chem. Rev.* **1996**, *96*, 877-910.

(2) Arteaga-Müller, R.; Tsurugi, H.; Saito, T.; Yanagawa, M.; Oda. S.; Mashima, K. New Tantalum Ligand-Free Catalyst System for Highly Selective Trimerization of Ethylene Affording 1-Hexene: New Evidence of a Metallacycle Mechanism. *J. Am. Chem. Soc.* **2009**, *131*, 5370-5371.

(3) Tsurugi, H.; Saito, T.; Tanahashi, H.; Arnold, J.; Mashima, K. Carbon Radical Generation by d^0 Tantalum Complexes with α-Diimine Ligands through Ligand-Centered Redox Processes. *J. Am. Chem. Soc.* **2011**, *133*, 18673-18683.

(4) Saito, T.; Nishiyama, H.; Tanahashi, H.; Kawakita, K.; Tsurugi, H.; Mashima, K. 1,4-Bis(trimethylsilyl)-1,4-diaza-2,5-cyclohexadienes as Strong Salt-Free Reductants for Generating Low-Valent Early Transition Metals with Electron-Donating Ligands. *J. Am. Chem. Soc.* **2014**, *136*, 5161-5170.

(5) Romero, N. A.; Nicewicz, D. A. Organic Photoredox Catalysis. *Chem. Rev.* **2016**, *116*, 10075-10166.

(6) Prier, C. K.; Rankic, D. A.; MacMillan, D. W. C. Visible Light Photoredox Catalysis with Transition Metal Complexes: Applications in Organic Synthesis. *Chem. Rev.* **2013**, *113*, 5322-5363.

(7) Green, S. P.; Jones, C.; Stasch, A. Stable Magnesium(I) Compounds with Mg-Mg Bonds. *Science* **2007**, *318*, 1754-1757.

(8) Jones, C. Dimeric magnesium(I) β-diketiminates: a new class of quasi-universal reducing agent. *Nat. Chem. Rev.* **2017**, *1*, 0059.

(9) Arras, J.; Kruczyński, T.; Bresien, J.; Schulz, A.; Schnöckel, H. Mg(I) Halide vs. Magnesium Metal: Differences in Reaction Energy and Reactivity Monitored in Reduction Processes of P-Cl Bonds. *Angew. Chem. Int. Ed.* **2018**, Just Accepted, DOI: 10.1002/anie.201811053.

(10) Uhl, W.; Hiller, W.; Layh, M.; Schwarz, W. $[Ga_4\{C(SiMe_3)_3\}_4]$ with a Tetrahedral Ga_4 Skeleton. *Angew. Chem. Int. Ed.* **1992**, *31*, 1364-1366.

(11) Loos, D.; Schnöckel, H. (Cyclopentadienyl)-Gallium(I)-Verbindungen. *J. Organomet. Chem.* **1993**, *463*, 37-40.

(12) Hardman, N. J.; Eichler, B. E.; Power, P. P. Synthesis and characterization of the monomer Ga{(NDippCMe)$_2$CH} (Dipp = $C_6H_3Pr^i_2$-2,6): a low valent gallium(I) carbene analogue. *Chem. Commun.* **2000**, 1991-1992.

(13) Dohmeier, C.; Robl, C.; Tacke, M.; Schnöckel, H. The Tetrameric Aluminum(I) Compound [{Al(η^5-C_5Me_5)}$_4$]. *Angew. Chem. Int. Ed.* **1991**, *30*, 564-565.

(14) Purath, A.; Dohmeier, C.; Ecker, A.; Schnöckel, H. Synthesis and Crystal Structure of the Tetraaluminatetrahedrane Al_4[Si(*t*-Bu)$_3$]$_4$, the Second Al_4R_4 Compound. *Organometallics* **1998**, *17*, 1894-1896.

(15) Cui, C.; Roesky, H. W.; Schmidt, H.-G.; Noltemeyer, M.; Hao, H.; Cimpoesu, F. Synthesis and Structure of a Monomeric Aluminum(I) Compound [{HC(CMeNAr)$_2$}Al] (Ar=2,6–*i*$Pr_2C_6H_3$): A Stable Aluminum Analogue of a Carbene. *Angew. Chem. Int. Ed.* **2000**, *39*, 4274-4276.

(16) Dohmeier, C.; Loos, D.; Schnöckel, H. Aluminum(I) and Gallium(I) Compounds: Syntheses, Structures, and Reactions. *Angew. Chem. Int. Ed.* **1996**, *35*, 129-149.

(17) Kempter, A.; Gemel, C.; Cadenbach, T.; Fischer, R. A. Synthesis and Structure of New Compounds with Zn−Ga Bonds: Insertion of the Gallium(I) Bisimidinate Ga(DDP) into Zn−X (X = CH_3, Cl) and the Homoleptic Complex Cation $[Zn(GaCp^*)_4]^{2+}$. *Inorg. Chem.* **2007**, *46*, 9481-9487.

(18) Weβing, J.; Göbel, C.; Weber, B.; Gemel, C.; Fischer, R. A. Diverse Reactivity of ECp* (E = Al, Ga) toward Low-Coordinate Transition Metal Amides [TM(N($SiMe_3$)$_2$)$_2$] (TM = Fe, Co, Zn): Insertion, Cp* Transfer, and Orthometalation. *Inorg. Chem.* **2017**, *56*, 3517-3525.

(19) Chu, T.; Korobkov, I.; Nikonov, G. I. Oxidative Addition of σ Bonds to an Al(I) Center. *J. Am. Chem. Soc.* **2014**, *136*, 9195-9202.

(20) Weβing, J.; Göbel, C.; Weber, B.; Gemel, C.; Fischer, R. A. Diverse Reactivity of ECp* (E = Al, Ga) toward Low-Coordinate Transition Metal Amides [TM(N($SiMe_3$)$_2$)$_2$] (TM = Fe, Co, Zn): Insertion, Cp* Transfer, and Orthometalation. *Inorg. Chem.* **2017**, *56*, 3517-3525.

(21) Hicks, J.; Underhill, E. J.; Kefalidis, C. E.; Maron, L.; Jones, C. A Mixed-Valence Tri-Zinc Complex, [LZnZnZnL] (L=Bulky Amide), Bearing a Linear Chain of Two-Coordinate Zinc Atoms. *Angew. Chem. Int. Ed.* **2015**, *54*, 10000-10004.

(22) Rit, A.; Campos, J.; Niu, H.; Aldridge, S. A stable heavier group 14 analogue of vinylidene. *Nat. Chem.* **2016**, *8*, 1022-1026.

(23) Braunschweig, H.; Damme, A.; Dewhurst, R. D.; Vargas, A. Bond-strengthening *π* backdonation in a transition-metal *π*-diborene complex. *Nat. Chem.* **2013**, *5*, 115-121.

(24) Lalrempuia, R.; Stasch, A.; Jones, C. The reductive disproportionation of CO_2 using a magnesium(I) complex: analogies with low valent f-block chemistry. *Chem. Sci.* **2013**, *4*, 4383-4388.

(25) Jones, C.; Bonhady, S. J.; Holzmann, N.; Frenking, G., Stasch, A. The preparation, characterization and theoretical analysis of group 14 element(I) dimers: a case study of magnesium(I) compounds as reducing agents in inorganic synthesis. *Inorg. Chem.* **2011**, *50*, 12315-12325.

(26) Bakewell, C.; White, A. J. P.; Crimmin, M. R. Reactions of Fluoroalkenes with an Aluminum(I) Complex. *Angew. Chem. Int. Ed.* **2018**, *57*, 6638-6642.

(27) Bakewell, C.; Ward, B. J.; White, A. J. P.; Crimmin M. R. A combined experimental and computational study on the reaction of fluoroarenes with Mg-Mg, Mg-Zn, Mg-Al, and Al-Zn bonds. *Chem. Sci.* **2018**, *9*, 2348-2356.

(28) Lohrey, T. D.; Bergman, R. G.; Arnold, J. Olefin-Supported Rhenium(III) Terminal Oxo Complexes Generated by Nucleophilic Addition to a Cyclopentadienyl Ligand. *Angew. Chem. Int. Ed.* **2017**, *56*, 14241-14245.

(29) Ciani, G.; Giusto, D.; Manassero, M.; Sansoni, M. Nitrosyl Complexes of Rhenium. Crystal and Molecular Structures of the Tetraethylammonium Salts of Tetrabromo(ethanol)nitrosylrhenate-(II) and of Acetonitriletetrabromonitrosylrhenate(II). *J. Chem. Soc., Dalton Trans.* **1975**, 2156-2161.

(30) Fenske, D.; Mronga, N.; Dehnicke, K. $AsPh_4[ReCl_4(NO)(OC(NH_2)CH_3)]$; Darstellung, IR-Spektrum und Kristallstruktur. *Z. Anorg. Allg. Chem.* **1982**, *482*, 106-112.

(31) Jiang, Y.; Blacque, O.; Fox, T.; Frech, C. M.; Berke, H. Facile Synthetic Access to Rhenium(II) Complexes: Activation of Carbon–Bromine Bonds by Single-Electron Transfer. *Chem. Eur. J.* **2010**, *16*, 2240-2249.

(32) Klopsch, I.; Finger, M.; Würtele, C.; Milde, B.; Werz, D. B.; Schneider, S. Dinitrogen Splitting and Functionalization in the Coordination Sphere of Rhenium. *J. Am. Chem. Soc.* **2014**, *136*, 6881-6883.

(33) Lindley, L.; Alten, R. S. v.; Finger, M.; Schendzielorz, F.; Würtele, C.; Miller, A. J. M.; Siewert, I.; Schneider, S. Mechanism of Chemical and Electrochemical N_2 Splitting by a Rhenium Pincer Complex. *J. Am. Chem. Soc.* **2018**, *140*, 7922-7935.

(34) St. Denis, J.; Butler, W.; Glick, M. D.; Oliver, J. P. Preparation and Structural Characterization of Transition Metal-Zinc Chloride Derivatives. The Crystal and Molecular Structure of $[\pi\text{-}C_5H_5(CO_3)MoZnCl \bullet O(C_2H_5)_2]_2$ and $[\pi\text{-}C_5H_5(CO_3)Mo]_2Zn$. *J. Am. Chem. Soc.* **1974**, *96*, 5427-5436.

(35) Pierpont, C. G.; Shong, R. G.; Sosinsky, B. A. Characterization of a Mixed-Metal Bimetallic with an Unusual Set of Carbonyl Distortions: $[Na(THF)_2]^+_2[Zn(Fe(CO)_4)_2]^{2-}$. *Inorg. Chem.* **1982**, *21*, 3247-3248.

(36) Resa, I.; Carmona, E.; Gutierrez-Puebla, E.; Monge, A. Decamethyldizincocene, a Stable Compound of Zn(I) with a Zn-Zn Bond. *Science* **2004**, *305*, 1136-1138.

(37) Mayer, K.; Jantke, L.-A.; Schulz, S.; Fässler, T. F. Retention of the Zn−Zn bond in $[Ge_9Zn{-}ZnGe_9]^{6-}$ and Formation of $[(Ge_9Zn){-}(Ge_9){-}(ZnGe_9)]^{8-}$ and Polymeric $[{-}(Ge_9Zn)^{2-}{-}]$. *Angew. Chem. Int. Ed.* **2017**, *56*, 2350-2355.

(38) Schulz, S.; Schuchmann, D.; Westphal, U.; Bolte, M. Dizincocene as a Building Block for Novel Zn−Zn-Bonded Compounds? *Organometallics*, **2009**, *28*, 1590-1592.

(39) Nayek, H. P.; Lühl, A.; Schulz, S.; Köppe, R.; Roesky, P. W. Aminotroponiminatozinc(I) Complexes: Syntheses and Spectroscopic Analyses. *Chem. Eur. J.* **2011**, *17*, 1773-1777.

(40) Banh, H.; Dilchert, K.; Schulz, C.; Gemel, C.; Seidel, R. W.; Gautier, R.; Kahlal, S.; Saillard, J.-Y.; Fischer, R. A. Atom-Precise Organometallic Zinc Clusters. *Angew. Chem. Int. Ed.* **2016**, *55*, 3285-3289.

(41) Wang, Y.; Quillian, B.; Wei, P.; Wang, H.; Yang, X.-J.; Xie, Y.; King, R. B.; Schleyer, P. v. R.; Schaefer, H. F.; Robinson, G. H. On the Chemistry of Zn−Zn Bonds, RZn−ZnR (R = [{(2,6-$Pr^i_2C_6H_3$)N(Me)C}$_2$CH]): Synthesis, Structure, and Computations. *J. Am. Chem. Soc.* **2005**, *127*, 11944-11945.

(42) Zhu, Z.; Wright, R. J.; Olmstead, M. M.; Rivard, E.; Brynda, M.; Power, P. P. A Zinc–Zinc-Bonded Compound and Its Derivatives Bridged by One or Two Hydrogen Atoms: A New Type of Zn-Zn Bonding. *Angew. Chem. Int. Ed.* **2006**, *45*, 5807-5810.

(43) Yang, X.-J.; Yu, J.; Liu, Y.; Xie, Y.; Schaefer, H. F.; Liang, Y.; Wu, B. A new zinc–zinc-bonded compound with a dianionic α-diimine ligand: synthesis and structure of $[Na(THF)_2]_2{\cdot}[LZn{-}ZnL]$ (L = $[(2,6\text{-}{}^iPr_2C_6H_3)N(Me)C]_2^{2-}$). *Chem. Commun.* **2007**, 2363-2365.

(44) Tsai, Y.-C.; Lu, D.-Y.; Lin, Y.-M.; Hwang, J.-K.; Yu., J.-S. K. Structural transformations in dinuclear zinc complexes involving Zn–Zn bonds. *Chem. Commun.* **2007**, 4125-4127.

(45) Fedushkin, I. L.; Skatova, A. A.; Ketkov, S. Y.; Eremenko, O. V.; Piskinov, A. V.; Fukin, G. K. [(dpp-bian)Zn-Zn(dpp-bian)]: A Zinc–Zinc-Bonded Compound Supported by Radical-Anionic Ligands. *Angew. Chem. Int. Ed.* **2007**, *46*, 4302-4305.

(46) Cecconi, F.; Ghilardi, C. A.; Midollini, S.; Moneti, S. Synthesis of novel mercury(I) complexes containing a linear chain Co–Hg–Hg–Co. *X*-Ray crystal structure of the complex $[\{Co[N(CH_2CH_2PPh_2)_3]\}_2(\mu\text{-}Hg_2)]{\cdot}$thf. *J. Chem. Soc., Dalton Trans.* **1983**, 349-352.

(47) Tuscher, L.; Ganesamoorthy, C.; Bläser, D.; Wölper, C.; Schulz, S. A Gallium-Substituted Distibene and an Antimony-Analogue Bicyclo[1.1.0]butane: Synthesis and Solid-State Structures. *Angew. Chem. Int. Ed.* **2015**, *54*, 10657-10661.

(48) Wright, C. A.; Shapley, J. R. Carbidoheptarhenate Cluster Complexes of Cadmium and Zinc Units: The Structure of $[PPh_4]_2[Re_7C(CO)_{21}(\mu_3\text{-}ZnCl)]$. *Inorg. Chem.* **2001**, *40*, 6338-6340.

(49) West, N. M.; Labinger, J. A.; Bercaw, J. E. Heterobimetallic Complexes of Rhenium and Zinc: Potential Catalysts for Homogeneous Syngas Conversion. *Organometallics* **2011**, *30*, 2690-2700.

(50) Becke, A. D. *J.* Density-functional thermochemistry. III. The role of exact exchange. *J. Chem. Phys.* **1993**, *98*, 5648.

(51) Perdew, J. P.; Wang, Y. Accurate and simple analytic representation of the electron-gas correlation energy. *Phys. Rev. B* **1992**, *45*, 13244.

(52) Grimme, S.; Ehrlich, S.; Goerigk, L. Effect of the damping function in dispersion corrected density functional theory. *J. Comp. Chem.* **2011**, *32*, 1456-1465.

(53) Dilworth, J. R.; Henderson, R. A. The Chemistry of the Hydrazido(1-)-ligand. Preparations and Crystal Structures of $[Mo(NHNHCO_2Me)(NNCO_2Me)(S_2CNMe_2)_2]$, $[Mo(NHNMePh)(NNMePh)(S_2CNMe_2)_2]BPh_4$, and $[ReCl_2(NHNHCOPh)(NNHCOPh)(PPh_3)_2$. Mechanism of formation of substituted hydrazines from $[Mo(NNRPh)_2(S_2CNMe_2)_2]$(R = Me or Ph). *J. Chem. Soc.*, *Dalton Trans.* **1987**, 529-540.

(54) CrysAlisPro 1.171.39.45f (Rigaku Oxford Diffraction, 2018)

(55) Dolomanov, O.V., Bourhis, L.J., Gildea, R.J, Howard, J.A.K. & Puschmann, H. (2009), J. Appl. Cryst. 42, 339-341.

(56) Sheldrick, G.M. (2015). Acta Cryst. A71, 3-8.

(57) *APEX2, APEX3, SADABS, and SAINT*. Bruker AXS. Madison, WI, USA.

(58) Farrugia, L. J.; *J. Appl. Cryst.* **2012**, *45*, 849-854.

(59) Spek, A. L. *Acta Cryst.* **2009**, **D**65, 148-155.

(60) Gaussian 09, Revision D.01, M. J. Frisch, G. W. Trucks, H. B. Schlegel, G. E. Scuseria, M. A. Robb, J. R. Cheeseman, G. Scalmani, V. Barone, B. Mennucci, G. A. Petersson, H. Nakatsuji, M. Caricato, X. Li, H. P. Hratchian, A. F. Izmaylov, J. Bloino, G. Zheng, J. L. Sonnenberg, M. Hada, M. Ehara, K. Toyota, R. Fukuda, J. Hasegawa, M. Ishida, T. Nakajima, Y. Honda, O. Kitao, H. Nakai, T. Vreven, J. A. Montgomery, Jr., J. E. Peralta, F. Ogliaro, M. Bearpark, J. J. Heyd, E. Brothers, K. N. Kudin, V. N. Staroverov, R. Kobayashi, J. Normand, K. Raghavachari, A. Rendell, J. C. Burant, S. S. Iyengar, J. Tomasi, M. Cossi, N. Rega, J. M. Millam, M. Klene, J. E. Knox, J. B. Cross, V. Bakken, C. Adamo, J. Jaramillo, R. Gomperts, R. E. Stratmann, O. Yazyev, A. J. Austin, R. Cammi, C. Pomelli, J. W. Ochterski, R. L. Martin, K. Morokuma, V. G. Zakrzewski, G. A. Voth, P. Salvador, J. J. Dannenberg, S. Dapprich, A. D. Daniels, Ö. Farkas, J. B. Foresman, J. V. Ortiz, J. Cioslowski, and D. J. Fox, Gaussian, Inc., Wallingford CT, **2009**.

(61) Dolg, M.; Wedig, U.; Stoll, H.; Preuss, H. *J. Chem. Phys.* **1987**, *86*, 866.

(62) Dolg, M. *Modern Methods and Algorithm of Quantum Chemistry, Vol. 1* (Ed.: J. Grotendorst), John von Neuman Institute for Computing, Jülich (Germany), 2000, pp. 479.

(63) Andrae, D.; Haeussermann, U.; Dolg, M.; Stoll, H.; Preuss, H. *Theor. Chim. Acta* **1990**, *77*, 123.

(64) Ehlers, A. W.; Böhme, M.; Dapprich, S.; Gobbi, A.; Höllwarth, A.; Jonas, V.; Köhler, K. F.; Stegmann, R.; Veldkamp, A.; Frenking, G. *Chem. Phys. Lett.* **1993**, *208*, 111.

(65) Hariharan, P. C.; Pople, J. A. *Theor. Chim. Acta* **1973**, *28*, 213.

(66) Reed, A. E.; Agrtiss, L. A.; Weinhold, F. *Chem. Rev.* **1988**, *88*, 899.

(67) Weinhold, F. In the Encyclopedia of Computational Chemistry; P. v. R. Schleyer, Ed., JohnWiley & Sons: Chichester, pp 1792, 1998.

(68) www.chemcraftprog.com